The Scientific World Journal

Mathematical Problems for Complex Systems

Guest Editors: Haijun Jiang, Haibo He, Jianlong Qiu, Qiankun Song, and Jianquan Lu

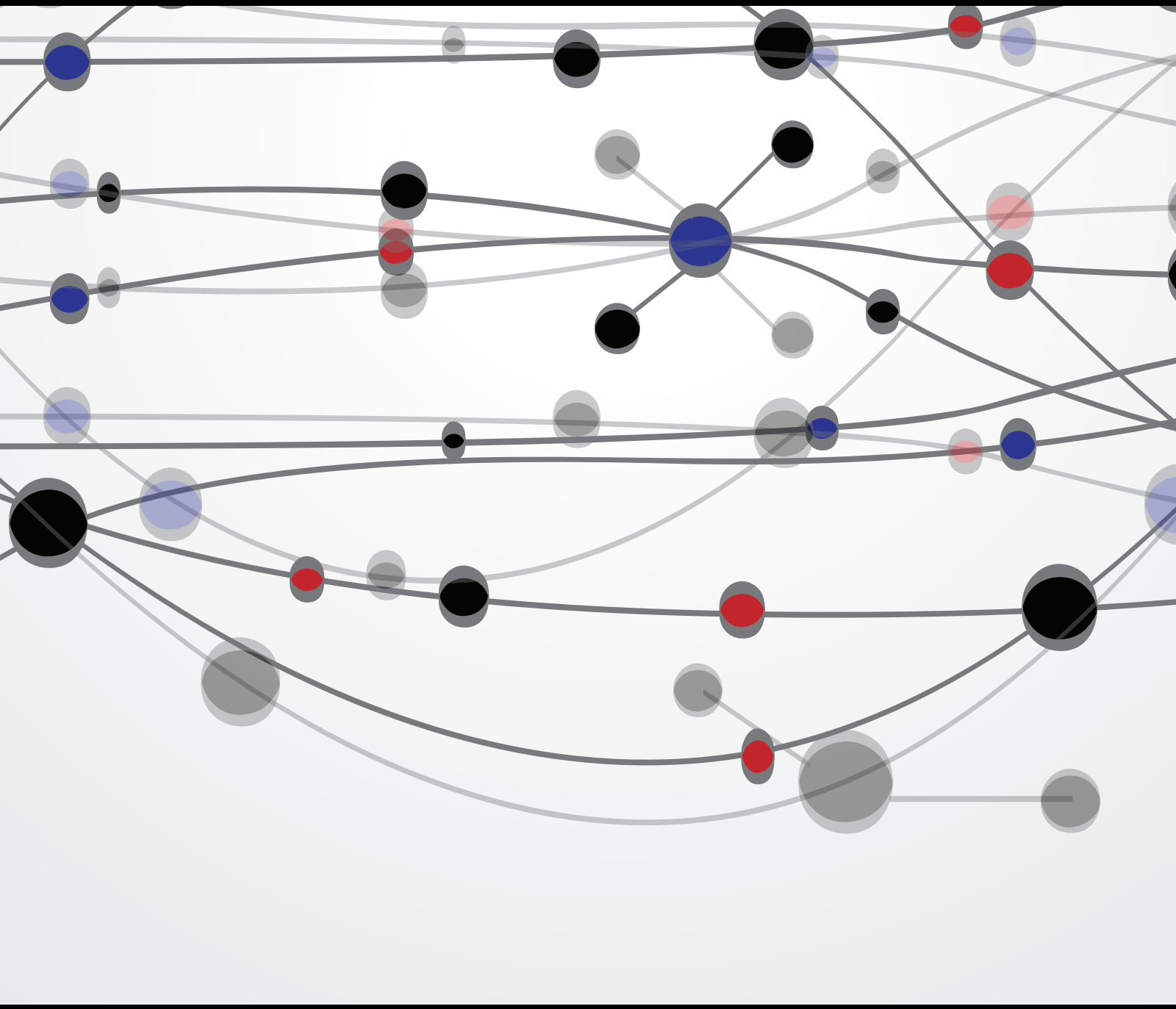

Mathematical Problems for Complex Systems

The Scientific World Journal

Mathematical Problems for Complex Systems

Guest Editors: Haijun Jiang, Haibo He, Jianlong Qiu, Qiankun Song, and Jianquan Lu

Contents

Mathematical Problems for Complex Systems, Haijun Jiang, Haibo He, Jianlong Qiu, Qiankun Song, and Jianquan Lu
Volume 2015, Article ID 605172, 2 pages

Consensus of Nonlinear Complex Systems with Edge Betweenness Centrality Measure under Time-Varying Sampled-Data Protocol, M. J. Park, O. M. Kwon, and E. J. Cha
Volume 2015, Article ID 493907, 11 pages

Results for Two-Level Designs with General Minimum Lower-Order Confounding, Zhi Ming Li and Run Chu Zhang
Volume 2015, Article ID 163234, 9 pages

A Learning Framework of Nonparallel Hyperplanes Classifier, Zhi-Xia Yang, Yuan-Hai Shao, and Yao-Lin Jiang
Volume 2015, Article ID 497617, 12 pages

Description and Application of a Mathematical Method for the Analysis of Harmony, Qiting Zuo, Runfang Jin, Junxia Ma, and Guotao Cui
Volume 2015, Article ID 831396, 9 pages

On the Maximum Estrada Index of 3-Uniform Linear Hypertrees, Faxu Li, Liang Wei, Jinde Cao, Feng Hu, and Haixing Zhao
Volume 2014, Article ID 637865, 7 pages

One Adaptive Synchronization Approach for Fractional-Order Chaotic System with Fractional-Order $1 < q < 2$, Ping Zhou and Rongji Bai
Volume 2014, Article ID 490364, 7 pages

A Novel Chaotic Map and an Improved Chaos-Based Image Encryption Scheme, Xianhan Zhang and Yang Cao
Volume 2014, Article ID 713541, 8 pages

Hindawi Publishing Corporation
The Scientific World Journal
Volume 2015, Article ID 605172, 2 pages
http://dx.doi.org/10.1155/2015/605172

Editorial

Mathematical Problems for Complex Systems

Haijun Jiang,[1] Haibo He,[2] Jianlong Qiu,[3] Qiankun Song,[4] and Jianquan Lu[5]

[1] *College of Mathematics and System Sciences, Xinjiang University, Ürümqi, China*
[2] *University of Rhode Island, Kingston, RI, USA*
[3] *College of Science, Linyi University, Shandong, China*
[4] *Department of Mathematics, Chongqing Jiaotong University, Chongqing 400074, China*
[5] *Department of Mathematics, Southeast University, Nanjing 210096, China*

Correspondence should be addressed to Haijun Jiang; jhj@xju.edu.cn

Received 5 May 2015; Accepted 5 May 2015

As most of practical systems have high complexity, complex systems have become a rapidly growing area of mathematics and attracted many researchers. The study of complex systems not only has an important theoretical interest but also is motivated by problems from applied mathematics including physics, chemistry, astronomy, technology, and natural and social sciences. It should be noted that some major problems have not been fully investigated, such as the behavior of stability, synchronization, bifurcation, and chaos control for complex systems, as well as their applications in, for example, communication and bioinformatics.

The special issue contains seven papers; of these, three of the papers are related to application analysis of complex systems to the real world problems. One paper studies the synchronization of chaotic complex systems with fractional-order. One paper investigates the consensus problem for nonlinear complex systems. Another paper provides an approach to determine the unique 3-uniform linear hypertree with the maximum Estrada index. Finally, a paper provides interior principles to calculate the leading elements of the aliased effect-number pattern.

In the paper "Results for Two-Level Designs with General Minimum Lower-Order Confounding," the authors study the interior principles of calculating the leading elements in ${}^{\#}_{1}C_1$ and ${}^{\#}_{2}C_2$ aliased effect-number pattern. Also, their mathematical formulations are obtained for every lower-order confounding 2^{n-m} design according to the two different cases.

In the paper "On the Maximum Estrada Index of 3-Uniform Linear Hypertrees," authors give some basic definitions on the Estrada index of hypergraph and then formulate an algorism for determining the unique 3-uniform linear hypertree with the maximum Estrada index.

In the paper "Consensus of Nonlinear Complex Systems with Edge Betweenness Centrality Measure under Time-Varying Sampled-Data Protocol," by constructing a suitable Lyapunov-Krasovskii functional and using linear matrix inequality technique, the authors propose a new consensus criterion for nonlinear complex systems with edge betweenness centrality measure. Finally, a numerical example is provided to illustrate the effectiveness of the proposed consensus schemes.

In the paper "One Adaptive Synchronization Approach for Fractional-Order Chaotic System with Fractional-Order $1 < q < 2$," based on a new stability result of equilibrium point in nonlinear fractional-order systems, the authors investigate the adaptive synchronization for the fractional-order Lorenz chaotic system with fractional-order $1 < q < 2$. Numerical simulations show the feasibility of the proposed adaptive synchronization scheme.

In the paper "A New Chaotic Map and Its Application on Image Encryption," the authors present a novel approach to create the new chaotic map and then applied it to image encryption. Compared with traditional classic one-dimensional chaotic map like Logistic Map and Tent Map, this newly created chaotic map demonstrates many better chaotic properties for encryption. The simulation results and security analysis show that such method not only meets the requirement of imagine encryption but also has better security, which is very useful for general applications.

In the paper "Description and Application of a Mathematical Method for the Analysis of Harmony," after briefly

introducing the basic concepts of harmony theory, the authors expound the five essential elements for the quantitative description of harmony issues in water resources management: harmony participant, harmony objective, harmony regulation, harmony factor, and harmony action. Furthermore, a basic mathematical equation for the harmony degree is introduced.

In the paper "A Learning Framework of Nonparallel Hyperplanes Classifier," the authors concerned the learning framework of nonparallel hyperplanes support vector machines (SVM) for binary classification and multiclass classification. The given framework not only includes twin SVM and its many deformation versions but also extends them into multiclass classification problem with loss functions or different parameters. The numerical experiments on several artificial and benchmark datasets indicate that the introduced frameworks not only are fast but also have good generalization.

Acknowledgments

We would like to thank the authors for their excellent contribution and work on choosing the topics, preparing the manuscripts, and going through the revisions in a timely fashion. Furthermore, all reviewers should be congratulated and acknowledged for their essential work and time spent to improve the content of these papers.

Haijun Jiang
Haibo He
Jianlong Qiu
Qiankun Song
Jianquan Lu

Hindawi Publishing Corporation
The Scientific World Journal
Volume 2015, Article ID 493907, 11 pages
http://dx.doi.org/10.1155/2015/493907

Research Article

Consensus of Nonlinear Complex Systems with Edge Betweenness Centrality Measure under Time-Varying Sampled-Data Protocol

M. J. Park,[1] O. M. Kwon,[1] and E. J. Cha[2]

[1] *School of Electrical Engineering, Chungbuk National University, 52 Naesudong-ro, Cheongju 361-763, Republic of Korea*
[2] *Department of Biomedical Engineering, School of Medicine, Chungbuk National University, 52 Naesudong-ro, Cheongju 361-763, Republic of Korea*

Correspondence should be addressed to O. M. Kwon; madwind@chungbuk.ac.kr

Received 22 July 2014; Accepted 3 September 2014

Academic Editor: Qiankun Song

This paper proposes a new consensus criterion for nonlinear complex systems with edge betweenness centrality measure. By construction of a suitable Lyapunov-Krasovskii functional, the consensus criterion for such systems is established in terms of linear matrix inequalities (LMIs) which can be easily solved by various effective optimization algorithms. One numerical example is given to illustrate the effectiveness of the proposed methods.

1. Introduction

During the last few years, complex systems have received increasing attention from the real world such as the social networks, electrical power grids, global economic markets, small-world network, and scale-free network. Complex systems have the information flow which is consisted of a set of interconnected nodes with specific dynamics. For more details, see the literature [1–4] and the references therein. Also, many models has been proposed to describe multiagent systems, various coupled neural network, and so on [5–9].

Nowadays, most systems use microprocessor or microcontrollers, which are called digital computer. But the physical real situation is that the computers are on discrete signals while the plants are on continuous signals. In line with this thinking, in order to analyze the behavior of the plant between sampling instants, it is necessary to consider both the discrete operation of the computer and the continuous response of the plant. A little more to say, the fundamental character of the digital computer is that it takes the computed answers at sampling instants to calculate the control operation of a continuous plant. In addition to this, samples are taken from the continuous physical signals such as position, velocity, or temperature and these samples are used in the computer to calculate the controls to be applied. Systems in which discrete signals appear in some places and continuous signals occur in other parts are called sampled-data systems because continuous data are sampled before being used [10]. For this reason, various sampled-date control problems were investigated in [11–13]. Return to complex systems, this system is also booked for the consensus problem with sampled data [14–16].

However, there is room for further improvements in consensus analysis of complex systems. In most studies on complex systems such as multiagent system, complex dynamical network, and coupled neural network, the Laplacian matrix which is consisted of the adjacency and degree matrices of network is used. Because the foresaid matrices are based on degree centrality measure, the existing works need only the local structural information of network, that is, the degree centrality of node, which is determined by the number of nodes adjacent to it. Hence, by considering some other properties of graph theory, the structural information of network to analyze consensus problem for such system will be advanced. The edge betweenness centrality is selected from a choice among the properties of graph theory. Moreover, the edge betweenness centrality quantifies the average shortest path between two other nodes per each edge. It was

introduced as a measure for quantifying the control of a human on the communication between other humans in a social network by [17, 18]. Thus, the edge between two nodes has strongly an impact on the overall structure of information flow. Sometimes, the nodes with small degree centrality are directly connected through edges with larger betweenness centrality [3]. In this case, such edges should be weighted by the value with proportional to their betweenness centrality. Therefore, through the edge betweenness centrality measure, not only the local structural information but also the global effects of structure of information flow are considered. As a result, the consensus analysis in complex systems will be advanced by weighting each edge to its betweenness centrality.

Motivated by what was mentioned above, in this paper, a consensus criterion for nonlinear complex systems with edge betweenness centrality measure under time-varying sampled-data protocol will be proposed in Theorem 6 with the frame work of LMIs [19]. For comparison, based on the results of Theorem 6, a consensus criterion for such system with degree centrality measure will be introduced in Corollary 7. Through one numerical example, it will be shown that the proposed model can give its usefulness.

Notation 1. $\mathbb{R}^n$ and $\mathbb{R}^{m\times n}$ denote the n-dimensional Euclidean space with vector norm $\|\cdot\|$ and the set of all $m\times n$ real matrices, respectively. $\mathbb{S}^n$ and $\mathbb{S}^n_+$ are the sets of symmetric and positive definite $n\times n$ matrices, respectively. I_n denotes $n\times n$ identity matrix. $X>0\,(<0)$ means symmetric positive (negative) definite matrix. $X^\perp$ stands for a basis for the nullspace of X. $\mathtt{diag}\{\cdots\}$ represents the block diagonal matrix. For any square matrix X and any vectors x_i, respectively, we define $\mathtt{sym}\{X\}=X+X^T$ and $\mathtt{col}\{x_1,x_2,\ldots,x_n\}=[x_1^T\ x_2^T\cdots x_n^T]^T$. The symmetric terms in symmetric matrices and in quadratic forms will be denoted by $\star$ (This is used if necessary.). $X_{[f(t)]}$ means that the elements of matrix $X_{[f(t)]}$ include the scalar value of $f(t)$ affinely.

2. Problem Statements

Consider the model of nonlinear complex systems given by

$$\begin{aligned}\dot{x}_i(t)&=Ax_i(t)+Bf\left(y_i(t)\right)+u_i(t),\\ y_i(t)&=Cx_i(t),\quad i=1,2,\ldots,N,\end{aligned}\tag{1}$$

where N is the number of coupled nodes, n is the number of state of each node, the subscript i means the ith node, $x_i(t)\in\mathbb{R}^n$ is the state vector, $y_i(t)\in\mathbb{R}^{n_y}$ is the output vector, $A\in\mathbb{R}^{n\times n}$, $B\in\mathbb{R}^{n\times n_y}$, and $C\in\mathbb{R}^{n_y\times n}$ are system matrices, and $f(\cdot)\in\mathbb{R}^{n_y}$ denotes the nonlinearity, which satisfies $f_q(0)=0$ $(q=1,\ldots,n_y)$ and

$$l_q^-\le\frac{f_q(u)-f_q(v)}{u-v}\le l_q^+,\quad u\ne v,\ \forall u,v\in R,\tag{2}$$

where l_q^- and l_q^+ are given constants. For simplicity, let us define $L^-=\mathtt{diag}\{l_1^-,\ldots,l_n^-\}$ and $L^+=\mathtt{diag}\{l_1^+,\ldots,l_n^+\}$.

Let us consider the following consensus protocol proposed by [3]:

$$u_i(t)=-\frac{\sigma}{\sum_{j=1,j\ne i}^N\gamma_{ij}}\sum_{j=1,j\ne i}^N\gamma_{ij}\left(x_i(t)-x_j(t)\right),\quad i=1,2,\ldots,N,\tag{3}$$

where σ is a given scalar meaning the coupling strength, γ_{ij} is the edge betweenness centrality between nodes i and j defined by

$$\gamma_{ij}=\sum_{k\ne l}\frac{\mathtt{g}_{kl}\left(\mathtt{e}_{ij}\right)}{\mathtt{g}_{kl}},\tag{4}$$

where $\mathtt{e}_{ij}$ denotes the edge between nodes i and j, $\mathtt{g}_{kl}$ is the number of the shortest paths from nodes k to l in the graph, and $\mathtt{g}_{kl}(\mathtt{e}_{ij})$ is the number of these shortest paths through path $\mathtt{e}_{ij}$.

Remark 1. The consensus protocol (3) with edge betweenness centrality measure will be compared with the common consensus protocol followed by

$$u_i(t)=-\sigma\sum_{j=1,j\ne i}^N d_{ij}\left(x_i(t)-x_j(t)\right),\tag{5}$$

where $d_{ij}=1$ if node i is connected to node j and otherwise, $d_{ij}=0$.

For details, from Figure 1, the thickness of edge is proportional to the edge betweenness centrality, which can be paraphrased as the load of edge. Thus, node 2 has the edge with the largest value of edge betweenness centrality compared to its smallest degree centrality while the degree centrality of node 1 is the largest value. As a guide, the degree centrality of node is determined by the number of nodes adjacent to it, for example, the value of node 1 is $\sum_{j\ne i}d_{1j}=5$, and in this sense, the common protocol (5) considers degree centrality measure. Therefore, in protocol (3), not only the local structural information but also the global effects of structure of information flow can be considered.

In this paper, the following protocol with the sampled-data information flow is proposed:

$$u_i(t_k)=-\frac{\sigma}{\sum_{j=1,j\ne i}^N\gamma_{ij}}\sum_{j=1,j\ne i}^N\gamma_{ij}\left(x_i(t_k)-x_j(t_k)\right),\quad i=1,2,\ldots,N,\tag{6}$$

where t_k are the sampling instants satisfying $0=t_0<t_1<\cdots<t_k<\cdots<\lim_{k\to\infty}t_k=+\infty$. For its analysis, assume that the sampling interval is constant; that is, $t_{k+1}-t_k=h_M$. Then, let us define

$$h(t)=t-t_k,\quad t\in\left[t_k,t_{k+1}\right).\tag{7}$$

Note that $h(t)\le h_M$ and $\dot{h}(t)=1$ for $t\ne t_k$.

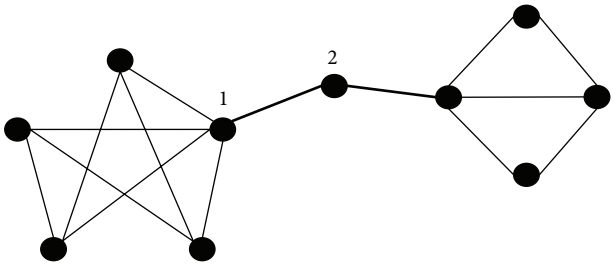

Figure 1: Structure example for information flow.

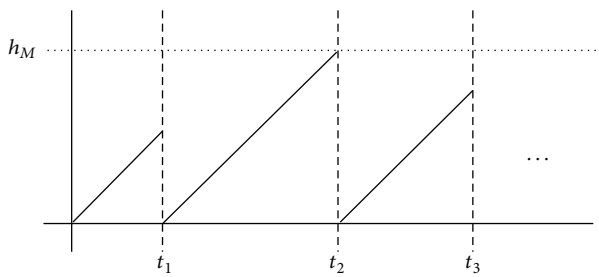

Figure 2: Time-varying sampling.

Remark 2. The consensus protocol (6) is assumed to be generated by using a zero-order-hold function with a sequence of hold times $0 = t_0 < t_1 < \cdots < t_k < \cdots$. Then, the definition (7), $h(t) = t - t_k$, is that the interval between two sampling instants is less than a given bound, $h_M = t_{k+1} - t_k$. Hence, (7) means the time-varying sampling drawn as shown in Figure 2. In addition to the figure, all slopes are 1.

The aim of this paper is to analyze the consensus of the complex systems (1) under the time-varying sampled-data protocol (6) given by

$$\begin{aligned}\dot{x}_i(t) &= Ax_i(t) + Bf\left(Cx_i(t)\right) - \frac{\sigma}{\sum_{j=1,j\neq i}^{N}\gamma_{ij}} \\ &\quad\times \sum_{j\in N_i}^{N}\gamma_{ij}\left(x_i(t_k) - x_j(t_k)\right), \quad i = 1,2,\ldots,N.\end{aligned} \tag{8}$$

This means that the protocol $u_i(t_k)$ solves the consensus problem, if and only if the states of each node satisfy

$$\lim_{t\to\infty}\left\|x_i(t) - x_j(t)\right\| = 0, \quad i,j = 1,2,\ldots,N. \tag{9}$$

The following lemmas will be used to derive the main result.

Lemma 3 (see [6]). *Let $U = [u_{ij}]_{N\times N}$, $P \in \mathbb{R}^{n\times n}$, $x = \mathtt{col}\{x_1, x_2, \ldots, x_n\}$, and $y = \mathtt{col}\{y_1, y_2, \ldots, y_n\}$. If $U = U^T$ and each row sum of U is zero, then*

$$x^T(U\otimes P)\,y = -\sum_{1\le i<j\le N} u_{ij}\left(x_i - x_j\right)^T P\left(y_i - y_j\right). \tag{10}$$

Lemma 4 (see [20]). *Let $x \in \mathbb{R}^n$, $A = A^T \in \mathbb{R}^{n\times n}$, and $B \in \mathbb{R}^{m\times n}$ such that $\mathtt{rank}\{B\} < n$. The following statements are equivalent:*

(i) $x^T Ax < 0$, *for all* $Bx = 0$, $x \neq 0$,

(ii) ${B^{\perp}}^T AB^{\perp} < 0$,

(iii) $\exists X \in \mathbb{R}^{n\times m}$: $A + \mathtt{sym}\{XB\} < 0$.

For convenient analysis, with the Kronecker product [21], the system (8) can be expressed as

$$\begin{aligned}\dot{x}(t) &= \left(I_N\otimes A\right)x(t) + \left(I_N\otimes B\right)F\left(\left(I_N\otimes C\right)x(t)\right) \\ &\quad - \overline{\sigma}\left(\Gamma_e\otimes I_n\right)x\left(t - h(t)\right), \quad t\in\left[t_k, t_{k+1}\right),\end{aligned} \tag{11}$$

which imply

$$\begin{aligned}\underbrace{\begin{bmatrix}\dot{x}_1(t)\\ \vdots\\ \dot{x}_N(t)\end{bmatrix}}_{\dot{x}(t)} &= \underbrace{\mathtt{diag}\{A,\ldots,A\}}_{I_N\otimes A}\underbrace{\begin{bmatrix}x_1(t)\\ \vdots\\ x_N(t)\end{bmatrix}}_{x(t)} \\ &\quad + \underbrace{\mathtt{diag}\{B,\ldots,B\}}_{I_N\otimes B}\underbrace{\begin{bmatrix}f\left(y_1(t)\right)\\ \vdots\\ f\left(y_N(t)\right)\end{bmatrix}}_{F(y(t))} \\ &\quad - \overline{\sigma}\underbrace{\begin{bmatrix}\gamma_{11}I_n & -\gamma_{12}I_n & \cdots\\ -\gamma_{21}I_n & \ddots & \ddots\\ \vdots & \ddots & \gamma_{NN}I_n\end{bmatrix}}_{\Gamma_e\otimes I_n} \\ &\quad\times\begin{bmatrix}x_1\left(t - h(t)\right)\\ \vdots\\ x_N\left(t - h(t)\right)\end{bmatrix}\underbrace{\begin{bmatrix}y_1(t)\\ \vdots\\ y_N(t)\end{bmatrix}}_{y(t)} \\ &= \underbrace{\mathtt{diag}\{C,\ldots,C\}}_{I_N\otimes C}\begin{bmatrix}x_1(t)\\ \vdots\\ x_N(t)\end{bmatrix},\end{aligned} \tag{12}$$

where $\overline{\sigma} = \sigma/\sum_{j=1,j\neq i}^{N}\gamma_{ij}$ and $\Gamma_e = \begin{bmatrix}\gamma_{11} & -\gamma_{12} & \cdots\\ -\gamma_{21} & \ddots & \ddots\\ \vdots & \ddots & \gamma_{NN}\end{bmatrix}$ with $\gamma_{ii} = \sum_{j\neq i}\gamma_{ij}$.

Remark 5. With the Kronecker product, the transformation from (8) to (11) has two advantages in the consensus analysis for the system (8): the first is the ease of mathematical representation, and the second is, in construction of the Lyapunov-Krasovskii functional, the applicability of the relation between the use of the Kronecker product with the matrix U defined in Lemma 3 and the term $\|x_i(t) - x_j(t)\|$ stated in the condition (9) (see the equality (10)). As a result, based on the Kronecker product and Lemma 3, the consensus problem of the system (8) is converted into the Lyapunov stability problem of the transformed system (11).

3. Main Results

For simplicity of matrix and vector notations in Theorem 6, the following scalars and matrices are defined as

$$\begin{aligned}
\nu_1(t) &= \frac{1}{t_k - t + h_M}\int_{t-h_M}^{t_k} x(s)\,ds,\\
\nu_2(t) &= \frac{1}{t - t_k}\int_{t_k}^{t} x(s)\,ds,\\
\varpi(t) &= \frac{1}{t - t_k}\int_{t_k}^{t} \dot{x}(s)\,ds,\\
\zeta(t) &= \mathtt{col}\{x(t), x(t_k), x(t-h_M), \dot{x}(t), \nu_1(t),\\
&\qquad \nu_2(t), \varpi(t), f(Cx(t))\},\\
\Upsilon &= [I_N\otimes A \mid -\overline{\sigma}(\Gamma_e\otimes I_n) \mid 0 \mid -(I_N\otimes I_n) \mid 0 \mid 0 \mid 0 \mid I_N\otimes B]\\
x_{ij}(t) &= x_i(t) - x_j(t),\\
f(Cx_{ij}(t)) &= f(Cx_i(t)) - f(Cx_j(t)),\\
\zeta_{ij}(t) &= \mathtt{col}\{x_{ij}(t), x_{ij}(t_k), x_{ij}(t-h_M), \dot{x}_{ij}(t),\\
&\qquad \nu_{1ij}(t), \nu_{2ij}(t), \varpi_{ij}(t), f(Cx_{ij}(t))\},\\
\Upsilon_{ij} &= [A \mid \overline{\sigma}\gamma_{ij}NI_n \mid 0 \mid -I_n \mid 0 \mid 0 \mid 0 \mid B],\\
\Pi_{1,1[h(t)]} &= \left[\, e_1 \;\middle|\; \underbrace{(t_k - t + h_M)}_{h_M - h(t)} e_5 \;\middle|\; \underbrace{(t - t_k)}_{h(t)} e_6 \,\right],\\
\Pi_{1,2} &= [e_4 \mid -e_3 \mid e_1],\\
\Xi_{1[h(t)]} &= \mathtt{sym}\{\Pi_{1,1[h(t)]}\mathscr{P}\Pi_{1,2}^T\} + e_1Qe_2^T\\
&\quad - e_3Q_3^T + h_M^2 e_4 R e_4^T - \begin{bmatrix} e_2^T - e_3^T \\ \hline e_2^T + e_3^T - 2e_5^T \\ \hline e_1^T - e_2^T \\ \hline e_1^T + e_2^T - 2e_6^T \end{bmatrix}^T\\
&\quad \times \underbrace{\left[\begin{array}{c|c} \mathtt{diag}\{R, 3R\} & \mathscr{M} \\ \hline \star & \mathtt{diag}\{R, 3R\} \end{array}\right]}_{\Omega}\\
&\quad \times \begin{bmatrix} e_2^T - e_3^T \\ \hline e_2^T + e_3^T - 2e_5^T \\ \hline e_1^T - e_2^T \\ \hline e_1^T + e_2^T - 2e_6^T \end{bmatrix},\\
\Xi_{2[h(t)]} &= \underbrace{(t_k - t + h_M)}_{h_M - h(t)} e_4 S e_4^T - \underbrace{(t - t_k)}_{h(t)} e_7 S e_7^T,\\
\Xi_3 &= -\mathtt{sym}\left\{\left(e_8 - e_1C^TL^-\right)D\left(e_8 - e_1C^TL^+\right)^T\right\},\\
\Xi_{[h(t)]} &= \Xi_{1[h(t)]} + \Xi_{2[h(t)]} + \Xi_3,
\end{aligned} \tag{13}$$

where $e_i \in \mathbb{R}^{(7n+n_y)\times n}$ $(i = 1, 2, \ldots, 8)$ are the block entry matrices; for example, $e_2^T\zeta_{ij}(k) = x_{ij}(t_k)$ and $e_8^T\zeta_{ij}(t) = f(Cx_{ij}(t))$.

Theorem 6. *For a given positive scalar h_M, the node in the system (8) is consented, if there exist matrices $\mathscr{P} = [P_{ij}] \in \mathbb{S}_+^{3n}$, $Q \in \mathbb{S}_+^n$, $R \in \mathbb{S}_+^n$, $S \in \mathbb{S}_+^n$, $\mathscr{M} = [M_{ij}] \in \mathbb{R}^{2n\times 2n}$, and diagonal matrix $D \in \mathbb{S}_+^{n_y}$ satisfying the following LMIs for $1 \le i < j \le N$:*

$$\left[(j-i)\Upsilon_{ij}^{\perp}\right]^T \Xi_k \left[(j-i)\Upsilon_{ij}^{\perp}\right] < 0 \quad (k = 1, 2), \tag{14}$$

$$\Omega > 0, \tag{15}$$

where Ξ_i is the two vertices of $\Xi_{[h(t)]}$ with the bounds of $h(t)$, that is, 0 if $k = 1$ and h_M if $k = 2$.

Proof. Define a matrix U as $U = [u_{ij}]_{N\times N}$ with $u_{ij} = N - 1$ if $i = j$, and otherwise, $u_{ij} = -1$. Then, consider the Lyapunov-Krasovskii functional candidate given by

$$V = V_1 + V_2, \tag{16}$$

where

$$\begin{aligned}
V_1 &= \begin{bmatrix} x(t) \\ \hline \int_{t-h_M}^{t_k} x(s)\,ds \\ \hline \int_{t_k}^{t} x(s)\,ds \end{bmatrix}^T \left[\begin{array}{c|c|c} U\otimes P_{11} & U\otimes P_{12} & U\otimes P_{13} \\ \hline \star & U\otimes P_{22} & U\otimes P_{23} \\ \hline \star & \star & U\otimes P_{33} \end{array}\right]\\
&\quad \times \begin{bmatrix} x(t) \\ \hline \int_{t-h_M}^{t_k} x(s)\,ds \\ \hline \int_{t_k}^{t} x(s)\,ds \end{bmatrix} + \int_{t-h_M}^{t} x^T(s)(U\otimes Q)x(s)\,ds\\
&\quad + h_M\int_{t-h_M}^{t}\int_{s}^{t} \dot{x}^T(u)(U\otimes R)\dot{x}(u)\,du\,ds,\\
V_2 &= (t_{k+1} - t)\int_{t_k}^{t} \dot{x}^T(s)(U\otimes S)\dot{x}(s)\,ds.
\end{aligned} \tag{17}$$

Time-differentiating V_1 leads to

$$\begin{aligned}
\dot{V}_1 &= 2\begin{bmatrix} x(t) \\ \hline \int_{t-h_M}^{t_k} x(s)\,ds \\ \hline \int_{t_k}^{t} x(s)\,ds \end{bmatrix}^T \left[\begin{array}{c|c|c} U\otimes P_{11} & U\otimes P_{12} & U\otimes P_{13} \\ \hline \star & U\otimes P_{22} & U\otimes P_{23} \\ \hline \star & \star & U\otimes P_{33} \end{array}\right]\\
&\quad \times \begin{bmatrix} \dot{x}(t) \\ \hline -x(t-h_M) \\ \hline x(t) \end{bmatrix} + x^T(t)(U\otimes Q)x(t)\\
&\quad - x^T(t-h_M)(U\otimes Q)x(t-h_M)
\end{aligned}$$

$$+ h_M^2 \dot{x}^T(t)(U \otimes R)\dot{x}(t) - h_M \int_{t_k}^{t} \dot{x}^T(s)(U \otimes R)\dot{x}(s)\,ds. \tag{18}$$

By Wirtinger-based inequality [22] and reciprocally convex approach [23], the integral term is bounded as

$$\begin{aligned}
&- h_M \int_{t-h_M}^{t} \dot{x}^T(s)(U \otimes R)\dot{x}(s)\,ds \\
&= -h_M \int_{t-h_M}^{t_k} \dot{x}^T(s)(U \otimes R)\dot{x}(s)\,ds \\
&\quad - h_M \int_{t_k}^{t} \dot{x}^T(s)(U \otimes R)\dot{x}(s)\,ds \\
&\le -\frac{h_M}{t_k - t + h_M} \\
&\quad \times \left\{\phi_{1,1}^T(t)(U \otimes R)\phi_{1,1}(t) + \phi_{1,2}^T(t)(U \otimes 3R)\phi_{1,2}(t)\right\} \\
&\quad - \frac{h_M}{t - t_k} \\
&\quad \times \left\{\phi_{2,1}^T(t)(U \otimes R)\phi_{2,1}(t) + \phi_{2,2}^T(t)(U \otimes 3R)\phi_{2,2}(t)\right\} \\
&\le -\begin{bmatrix}\phi_{1,1}(t)\\ \phi_{1,2}(t)\end{bmatrix}^T \\
&\quad \times \left[\begin{array}{c|c} \mathtt{diag}\{U \otimes R, U \otimes 3R\} & \left[\begin{array}{c|c} U \otimes M_{11} & U \otimes M_{12} \\ \hline U \otimes M_{21} & U \otimes M_{22}\end{array}\right] \\ \hline \star & \mathtt{diag}\{U \otimes R, U \otimes 3R\}\end{array}\right] \\
&\quad \times \begin{bmatrix}\phi_{1,1}(t)\\ \phi_{1,2}(t)\end{bmatrix},
\end{aligned} \tag{19}$$

where $\phi_{1,1}(t) = x(t_k) - x(t - h_M)$, $\phi_{1,2}(t) = x(t_k) + x(t - h_M) - (2/(t_k - t + h_M)) \int_{t-h_M}^{t_k} x(s)ds$, $\phi_{2,1}(t) = x(t) - x(t_k)$, and $\phi_{2,2}(t) = x(t) + x(t_k) - (2/(t - t_k)) \int_{t_k}^{t} x(s)ds$.

From Lemma 3, $\dot{V}_1$ can be bounded as

$$\dot{V}_1 \le \sum_{1 \le i < j \le N} \zeta_{ij}^T(t)\,\Xi_{1[h(t)]}\zeta_{ij}(t). \tag{20}$$

By Jensen inequality [24] and Lemma 3, an upper bound of $\dot{V}_2$ is obtained as

$$\begin{aligned}
\dot{V}_2 &= (t_{k+1} - t)\dot{x}^T(t)(U \otimes S)\dot{x}(t) \\
&\quad - \int_{t_k}^{t} \dot{x}^T(s)(U \otimes S)\dot{x}(s)\,ds \\
&\le (t_{k+1} - t)\dot{x}^T(t)(U \otimes S)\dot{x}(t) \\
&\quad - \frac{1}{t - t_k}\left(\int_{t_k}^{t} \dot{x}(s)\,ds\right)^T (U \otimes S)\left(\int_{t_k}^{t} \dot{x}(s)\,ds\right) \\
&= (t_{k+1} - t)\dot{x}^T(t)(U \otimes S)\dot{x}(t) \\
&\quad - (t - t_k)\varpi^T(t)(U \otimes S)\varpi(t) \\
&= \sum_{1 \le i < j \le N} \zeta_{ij}^T(t)\,\Xi_{2[h(t)]}\zeta_{ij}(t).
\end{aligned} \tag{21}$$

In addition, the following inequality holds for any positive diagonal matrix D:

$$\begin{aligned}
0 &\le -2\left[f((I_N \otimes C)x(t)) - (I_N \otimes L^-)(I_N \otimes C)x(t)\right]^T \\
&\quad \times (U \otimes D)\left[f((I_N \otimes C)x(t)) - (I_N \otimes L^+)(I_N \otimes C)x(t)\right] \\
&= -2\left[f((I_N \otimes C)x(t)) - (I_N \otimes L^- C)x(t)\right]^T \\
&\quad \times (U \otimes D)\left[f((I_N \otimes C)x(t)) - (I_N \otimes L^+ C)x(t)\right] \\
&= \sum_{1 \le i < j \le N} \zeta_{ij}^T(t) \\
&\qquad \times \underbrace{\mathtt{sym}\left\{-\left(e_8 - e_1 C^T L^-\right) D \left(e_8 - e_1 C^T L^+\right)^T\right\}}_{\Xi_3} \zeta_{ij}(t).
\end{aligned} \tag{22}$$

Therefore, from (20) to (22), an upper bound of $\dot{V}$ is

$$\dot{V} \le \sum_{1 \le i < j \le N} \zeta_{ij}^T(t)\,\underbrace{\left(\Xi_{1[h(t)]} + \Xi_{2[h(t)]} + \Xi_3\right)}_{\Xi_{[h(t)]}}\zeta_{ij}(t). \tag{23}$$

Then, for $h(t) \to 0$ and $h(t) \to h_M$, the following conditions hold

$$\begin{aligned}
&\sum_{1 \le i < j \le N} \zeta_{ij}^T(t)\,\Xi_{[h(t)]}\zeta_{ij}(t) < 0 \\
&\iff \alpha \sum_{1 \le i < j \le N} \zeta_{ij}^T(t)\,\Xi_{[0]}\zeta_{ij}(t) + (1 - \alpha) \\
&\qquad \times \sum_{1 \le i < j \le N} \zeta_{ij}^T(t)\,\Xi_{[h_M]}\zeta_{ij}(t) < 0,
\end{aligned} \tag{24}$$

where $\alpha = (h_M - h(t))/h_M$. □

Applying (i) and (iii) of Lemma 4 with the following equality:

$$\sum_{1 \le i < j \le N} (j - i)\,\Upsilon_{ij}\zeta_{ij}(t) = 0 \tag{25}$$

leads to the following two conditions:

$$\begin{aligned}
&\sum_{1 \le i < j \le N} \zeta_{ij}^T(t)\left(\Xi_{[0]} + \mathtt{sym}\left\{X\Upsilon_{ij}\right\}\right)\zeta_{ij}(t) < 0, \\
&\sum_{1 \le i < j \le N} \zeta_{ij}^T(t)\left(\Xi_{[h_M]} + \mathtt{sym}\left\{X\Upsilon_{ij}\right\}\right)\zeta_{ij}(t) < 0.
\end{aligned} \tag{26}$$

Here, if the inequality $\Xi_{[h(t)]} + \mathtt{sym}\{X\Upsilon_{ij}\} < 0$ holds, then there exist positive scalars ε_1 and ε_2 such that

$$\begin{aligned}
\Xi_{[0]} + \mathtt{sym}\left\{X\Upsilon_{ij}\right\} &< -\varepsilon_1 I_{8n}, \\
\Xi_{[h_M]} + \mathtt{sym}\left\{X\Upsilon_{ij}\right\} &< -\varepsilon_2 I_{8n}.
\end{aligned} \tag{27}$$

From (25), (26), and (27), we have

$$\begin{aligned}\dot{V} &\leq \sum_{1\leq i<j\leq N} \zeta_{ij}^{T}(t)\left(\Xi_{[h(t)]} + \mathtt{sym}\left\{X\Upsilon_{ij}\right\}\right)\zeta_{ij}(t)\\ &< \sum_{1\leq i<j\leq N} \zeta_{ij}^{T}(t)\left(-\min\{\varepsilon_1,\varepsilon_2\} I_{8n}\right)\zeta_{ij}(t)\\ &< \sum_{1\leq i<j\leq N} x_{ij}^{T}(t)\left(-\min\{\varepsilon_1,\varepsilon_2\} I_{n}\right)x_{ij}(t)\\ &= \sum_{1\leq i<j\leq N}\left(-\min\{\varepsilon_1,\varepsilon_2\}\left\|x_{ij}(t)\right\|^2\right)\\ &= \sum_{1\leq i<j\leq N}\left(-\min\{\varepsilon_1,\varepsilon_2\}\left\|x_{i}(t)-x_{j}(t)\right\|^2\right).\end{aligned} \tag{28}$$

By Lyapunov theorem and the definition for consensus (9), it can be guaranteed that the nodes in the nonlinear complex systems (8) are asymptotically consented.

In addition to this, in order to illustrate the process of obtaining (25), let us define

$$\Lambda = \left[\Lambda_1, \Lambda_2, \ldots, \Lambda_N\right] = [N, N-1, \ldots, 1] \otimes I_n \in \mathbb{R}^{n\times nN}, \tag{29}$$

where $\Lambda_k \in \mathbb{R}^{n\times n}$ $(k = 1, \ldots, N)$.

Then, according to the proof of Theorem 1 in [9], we have the following zero equality:

$$\begin{aligned}0 &= \Lambda\left(U\otimes I_n\right)\Upsilon\zeta(t)\\ &= \Lambda\left(U\otimes I_n\right)\left[\ I_N\otimes A \mid -\overline{\sigma}\left(\Gamma_e\otimes I_n\right)\mid 0\mid -\left(I_N\otimes I_n\right)\mid 0\mid 0\mid 0\mid I_N\otimes B\ \right]\zeta(t)\\ &= \Lambda\left[\ U\otimes A \mid -\overline{\sigma}\left(U\Gamma_e\otimes I_n\right)\mid 0\mid -\left(U\otimes I_n\right)\mid 0\mid 0\mid 0\mid U\otimes B\ \right]\zeta(t)\\ &= \Lambda\left(U\otimes A\right)x(t) - \overline{\sigma}\Lambda\left(U\Gamma_e\otimes I_n\right)x\left(t_k\right)\\ &\quad - \Lambda\left(U\otimes I_n\right)\dot{x}(t) + \Lambda\left(U\otimes B\right)f\left(Cx(t)\right).\end{aligned} \tag{30}$$

By Lemma 3, the first term of (30) can be obtained as

$$\begin{aligned}&\Lambda\left(U\otimes A\right)x(t)\\ &\quad= \underbrace{\left[NI_n, (N-1)I_n, \ldots, I_n\right]}_{n\times nN}\underbrace{\left(U\otimes A\right)}_{nN\times nN}\\ &\qquad\times\underbrace{\left[x_1(t), \ldots, x_N(t)\right]^T}_{nN\times 1}\\ &\quad= -\sum_{1\leq i<j\leq N} u_{ij}\left(\Lambda_i-\Lambda_j\right)A\left(x_i(t)-x_j(t)\right)\\ &\quad= \sum_{1\leq i<j\leq N}\left(\Lambda_i-\Lambda_j\right)A\left(x_i(t)-x_j(t)\right)\\ &\quad= \sum_{1\leq i<j\leq N}\left(\left(N+1-i\right)I_n\right.\\ &\qquad\qquad\left.-\left(N+1-j\right)I_n\right)A\left(x_i(t)-x_j(t)\right)\\ &\quad= \sum_{1\leq i<j\leq N}\left(j-i\right)A\left(x_i(t)-x_j(t)\right).\end{aligned} \tag{31}$$

Similarly, the other terms of (30) are calculated as

$$\begin{aligned}&-\overline{\sigma}\Lambda\left(U\Gamma_e\otimes I_n\right)x\left(t_k\right)\\ &\quad= \sum_{1\leq i<j\leq N}\left(j-i\right)\left(\overline{\sigma}N\gamma_{ij}I_n\right)\left(x_i\left(t-h(t)\right)-x_j\left(t-h(t)\right)\right),\\ &-\Lambda\left(U\otimes I_n\right)\dot{x}(t)\\ &\quad= -\sum_{1\leq i<j\leq N}\left(j-i\right)I_n\left(\dot{x}_i(t)\right)-\left(\dot{x}_j(t)\right),\\ &\Lambda\left(U\otimes B\right)f\left(Cx(t)\right)\\ &\quad= \sum_{1\leq i<j\leq N}\left(j-i\right)B\left(f\left(Cx_i(t)\right)-f\left(Cx_j(t)\right)\right).\end{aligned} \tag{32}$$

Then, (30) can be rewritten as

$$0 = \Lambda\left(U\otimes I_n\right)\Upsilon\zeta(t) = \sum_{1\leq i<j\leq N}\left(j-i\right)\Upsilon_{ij}\zeta_{ij}(t). \tag{33}$$

Finally, reapplying (ii) and (iii) of Lemma 4 to (26), the following inequalities can be obtained

$$\begin{aligned}&\sum_{1\leq i<j\leq N}\left[\left(j-i\right)\Upsilon_{ij}^{\perp}\right]^T\Xi_{[0]}\left[\left(j-i\right)\Upsilon_{ij}^{\perp}\right]<0,\\ &\sum_{1\leq i<j\leq N}\left[\left(j-i\right)\Upsilon_{ij}^{\perp}\right]^T\Xi_{[h_M]}\left[\left(j-i\right)\Upsilon_{ij}^{\perp}\right]<0.\end{aligned} \tag{34}$$

From (34), if the LMIs (14) satisfy, then the condition (24) subject to (25) holds. This completes our proof.

For comparison, the following corollary is introduced.

Corollary 7. *For a given positive scalar h_M, the node in the system* (1) *under the procotol* (5) *with time-varying sampled data is consented, if there exist matrices $\mathscr{P} = [P_{ij}] \in \mathbb{S}_+^{3n}$, $Q \in$*

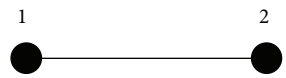

Figure 3: 2-node information flow.

$\mathbb{S}_+^n$, $R \in \mathbb{S}_+^n$, $S \in \mathbb{S}_+^n$, $\mathscr{M} = [M_{ij}] \in \mathbb{R}^{2n\times 2n}$, *and diagonal matrix* $D \in \mathbb{S}_+^{n_y}$ *satisfying the following LMIs for* $1 \le i < j \le N$:

$$\left[(j-i)\,\widetilde{\Upsilon}_{ij}^{\perp}\right]^T \Xi_k \left[(j-i)\,\widetilde{\Upsilon}_{ij}^{\perp}\right] < 0, \quad (k = 1, 2), \tag{35}$$

$$\Omega > 0. \tag{36}$$

Proof. Replacing Υ_{ij} with $\widetilde{\Upsilon}_{ij} = [A \,|\, \sigma d_{ij} N I_n \,|\, 0 \,|\, -I_n \,|\, 0 \,|\, 0 \,|\, B]$ in the proof of Theorem 6 leads to (35). □

4. Numerical Example

In this section, one numerical example will be presented to illustrate the effectiveness of the proposed criteria in this paper.

Consider 2-node information flow drawn in Figure 3 consisted of the Chua's circuit [25] given by

$$\begin{aligned} \dot{x}_{i1}(t) &= \alpha\left(x_{i2}(t) - h\left(x_{i1}(t)\right)\right), \\ \dot{x}_{i2}(t) &= x_{i1}(t) - x_{i2}(t) + x_{i3}(t), \\ \dot{x}_{i3}(t) &= -\beta x_{i2}(t), \quad i = 1, 2 \end{aligned} \tag{37}$$

with the nonlinear function $h(x_{i1}(t)) = m_1 x_{i1}(t) + (1/2)(m_0 - m_1)(|x_{i1}(t) + c| - |x_{i1}(t) - c|)$, where parameters $m_0 = -1/7$, $m_1 = 2/7$, $\alpha = 9$, $\beta = 14.28$, and $c = 1$ and its Lur's form can be rewritten with

$$A = \begin{bmatrix} -\alpha m_1 & \alpha & 0 \\ 1 & -1 & 1 \\ 0 & -\beta & 0 \end{bmatrix}, \qquad B = \begin{bmatrix} -\alpha(m_0 - m_1) \\ 0 \\ 0 \end{bmatrix}, \tag{38}$$

$$C^T = \begin{bmatrix} 1 \\ 0 \\ 0 \end{bmatrix}.$$

For the above system, the maximum interval of $t_{k+1} - t_k$ $(=h_M)$ for fixed coupling strength $\sigma = 1$ is compared between degree and edge betweenness centralities as shown in Table 1. From Table 1, it can be seen that the result with the edge betweenness centrality measure for this example gives larger maximum interval of $t_{k+1} - t_k$ $(=h_M)$ than the one with the degree centrality measure.

Moreover, the elements of matrix Γ_e can be calculated as

$$\begin{aligned} \gamma_{12} &= \sum_{k\neq l} \frac{g_{kl}(e_{12})}{g_{kl}} = \frac{g_{12}(e_{12})}{g_{12}} + \frac{g_{21}(e_{12})}{g_{21}} = \frac{1}{1} + \frac{1}{1} = 2, \\ \gamma_{21} &= \sum_{k\neq l} \frac{g_{kl}(e_{21})}{g_{kl}} = \frac{g_{12}(e_{21})}{g_{12}} + \frac{g_{21}(e_{21})}{g_{21}} = \frac{1}{1} + \frac{1}{1} = 2, \\ \gamma_{11} &= \sum_{j\neq i} \gamma_{1j} = \gamma_{12} = 2, \qquad \gamma_{22} = \sum_{j\neq i} \gamma_{2j} = \gamma_{21} = 2. \end{aligned} \tag{39}$$

However, the system performance with the edge betweenness centrality measure is more poor and needs more protocol input than the one with the degree centrality measure. For comparison between two measure cases, the sampling interval $t_{k+1} - t_k$ $(=h_M)$ is assumed to be 0.4. Figure 4 shows that the states with the responses consent to the same behavior under two measure cases for the given initial states of the nodes $x_1^T(0) = [0.1\ 0.5\text{–}0.7]$ and $x_2^T(0) = [3\ 1\text{–}4]$. In Figure 5, their error trajectories are shown. Here, the case of the edge betweenness centrality measure indicates the poor performance. Thus, it can be confirmed that it is necessary to consider the global information for network structure as mentioned in Remark 1. Their corresponding protocol inputs can be identified in Figure 6. In addition to this, without the protocol, the behaviors of two nodes are different as shown in Figure 7.

5. Conclusions

In this paper, the consensus analysis for nonlinear complex systems under time-varying sampled-data protocol has been conducted. The information for network structure is measured by edge betweenness centrality, which has the global information while the degree centrality has the local one. To achieve this, by constructing the simple Lyapunov-Krasovskii functional, sufficient conditions for guaranteeing asymptotic consensus of such systems have been derived in terms of LMIs. One numerical example has been given to show the usefulness of the proposed model.

Conflict of Interests

The authors declare that there is no conflict of interests regarding the publication of this paper.

Acknowledgments

This research was supported by the Basic Science Research Program through the National Research Foundation of Korea

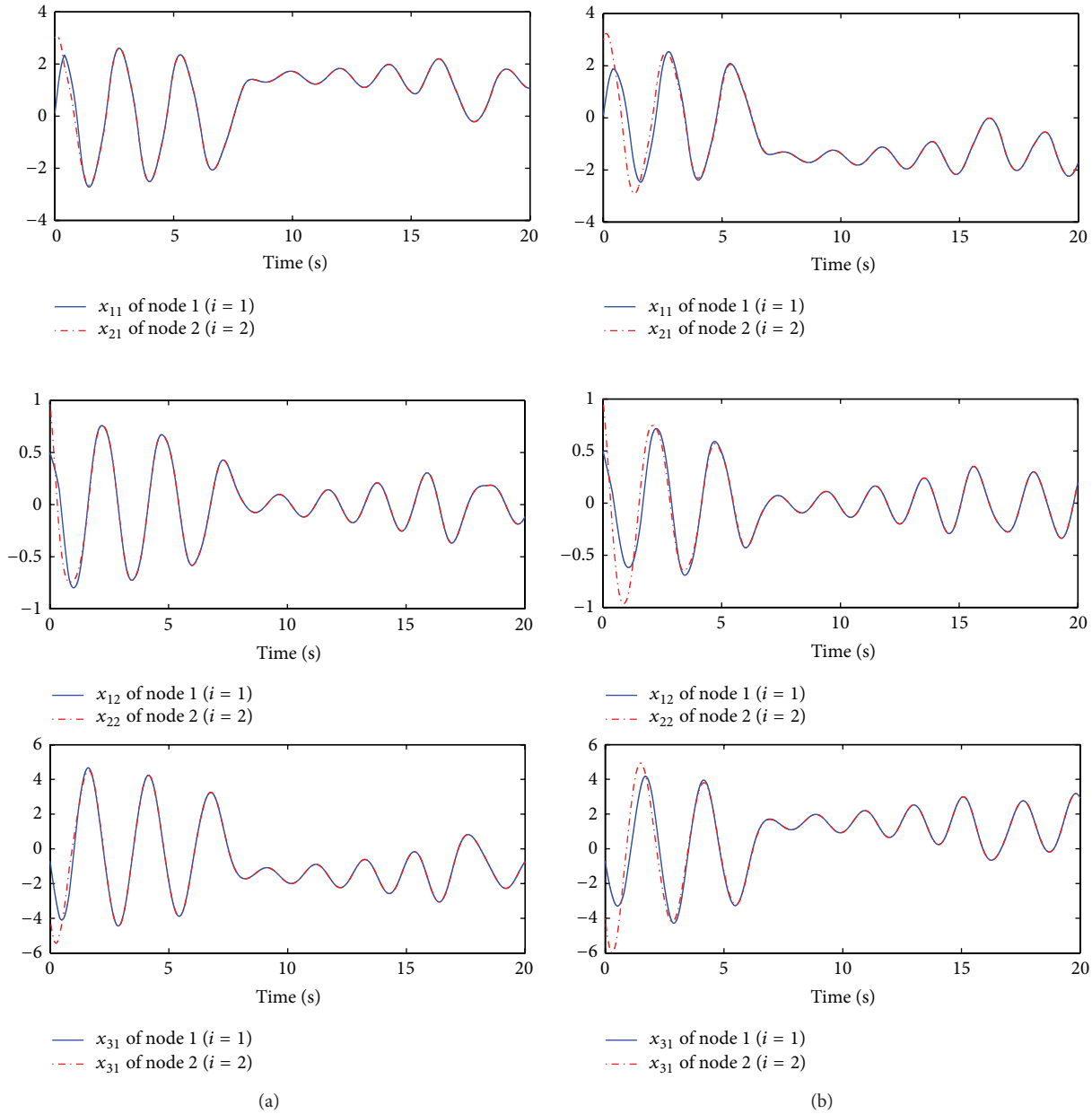

Figure 4: State trajectories of each node: (a) degree and (b) edge.

Table 1: Comparison with fixed coupling strength $\sigma = 1$.

Measures	Methods	Structure	$t_{k+1} - t_k$ $(=h_M)$
Degree centrality	Corollary 7	$^{*}\Gamma_d = \begin{bmatrix} 1 & -1 \\ -1 & 1 \end{bmatrix}$	0.41
Edge betweenness centrality	Theorem 6	$\Gamma_e = \begin{bmatrix} 2 & -2 \\ -2 & 2 \end{bmatrix}$	0.49

*is the Laplacian matrix of graph drawn in Figure 3.

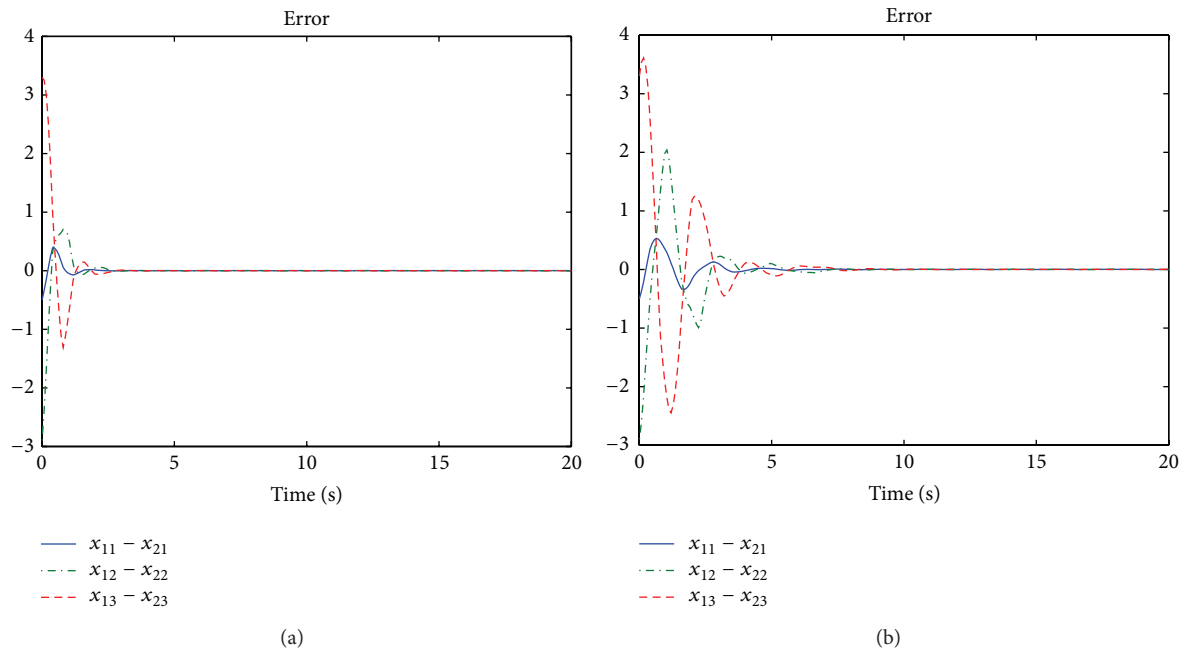

FIGURE 5: Error trajectories of each node: (a) degree and (b) edge.

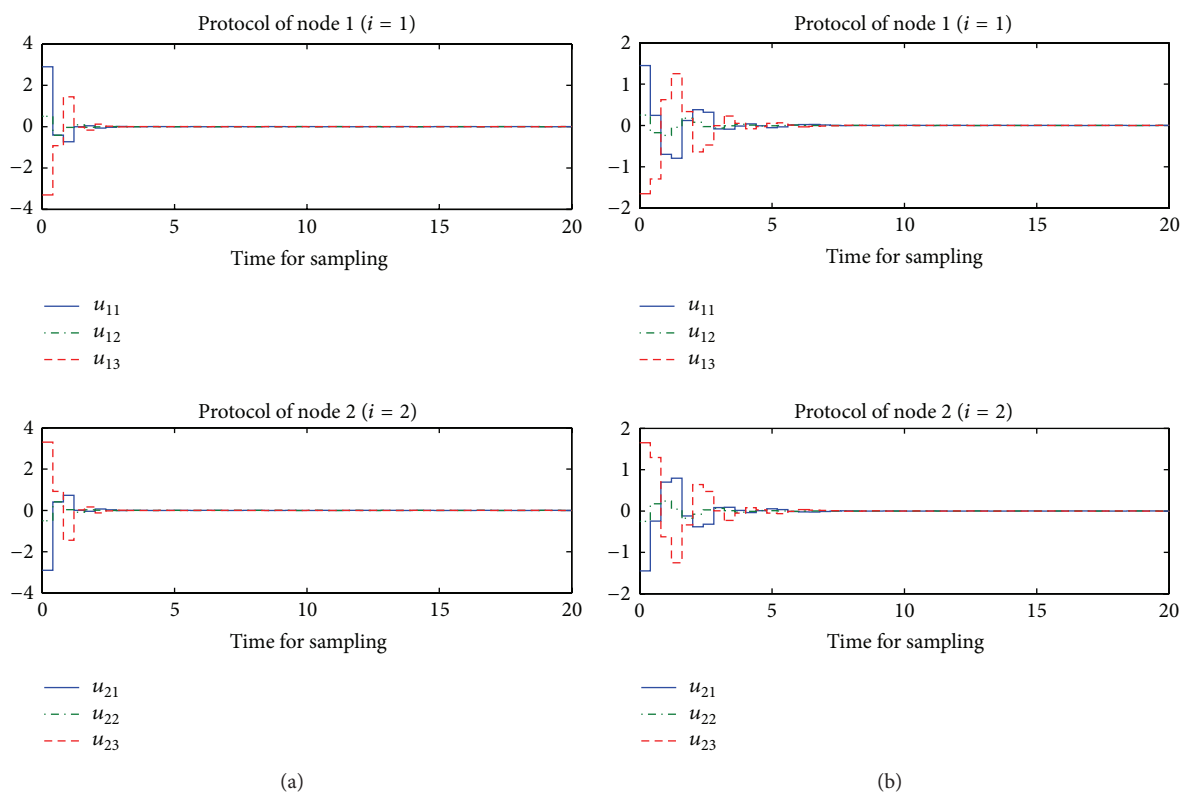

FIGURE 6: Protocol trajectories of each node: (a) degree and (b) edge.

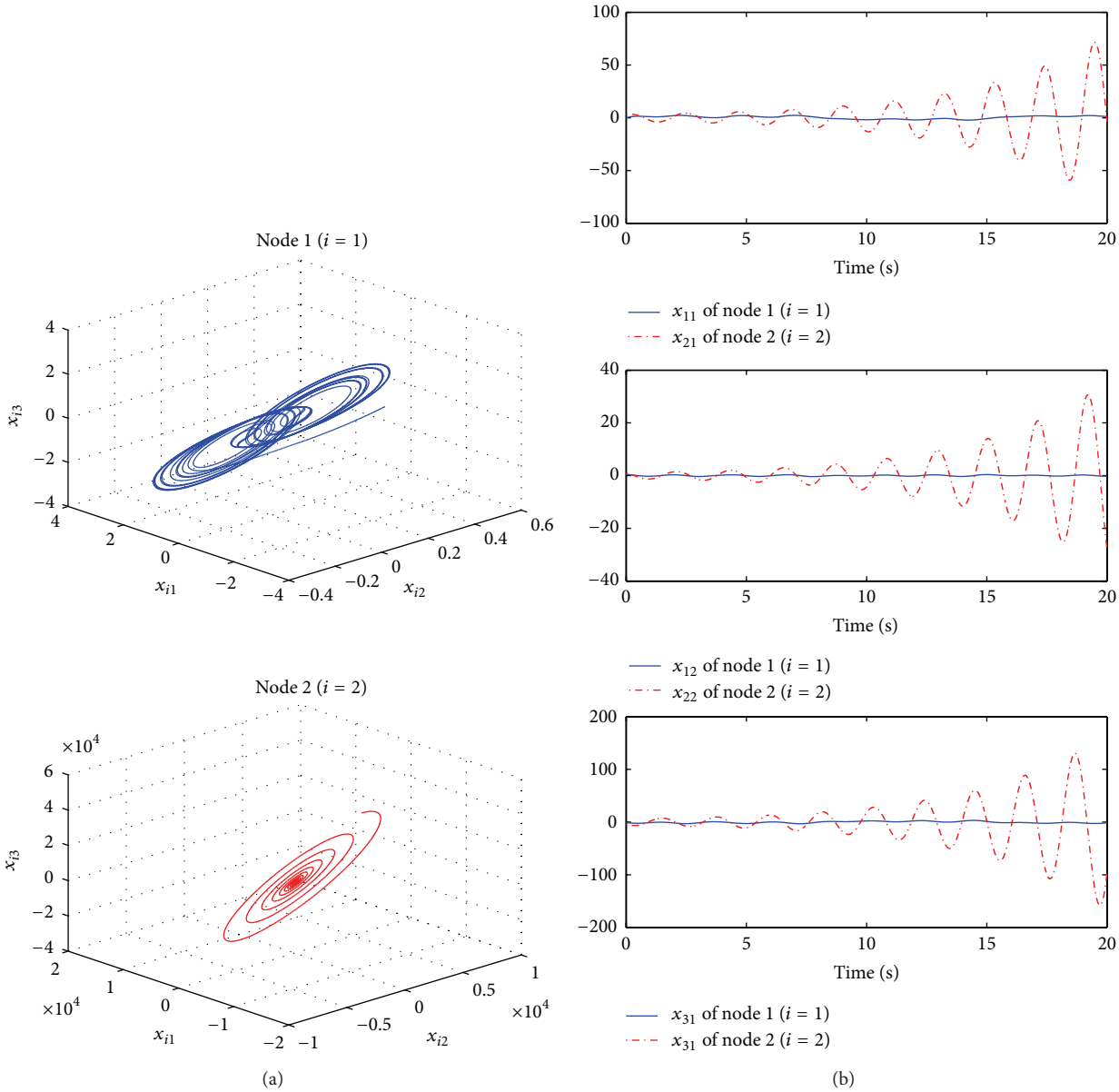

FIGURE 7: Results without the consensus protocol, that is, $u_i(t_k) = 0$: (a) phase and (b) each state.

(NRF) funded by the Ministry of Education, Science and Technology (2008-0062611), and by a Grant of the Korea Healthcare Technology R & D Project, Ministry of Health & Welfare, Republic of Korea (A100054).

References

[1] D. J. Watts and S. H. Strogatz, "Collective dynamics of "small-world" networks," *Nature*, vol. 393, no. 6684, pp. 440–442, 1998.

[2] S. H. Strogatz, "Exploring complex networks," *Nature*, vol. 410, no. 6825, pp. 268–276, 2001.

[3] M. Chavez, D. U. Hwang, A. Amann, H. G. E. Hentschel, and S. Boccaletti, "Synchronization is enhanced in weighted complex networks," *Physical Review Letters*, vol. 94, no. 21, Article ID 218701, 2005.

[4] S. Boccaletti, V. Latora, Y. Moreno, M. Chavez, and D. Hwang, "Complex networks: structure and dynamics," *Physics Reports A: Review Section of Physics Letters*, vol. 424, no. 4-5, pp. 175–308, 2006.

[5] W. Ren and R. W. Beard, "Consensus seeking in multiagent systems under dynamically changing interaction topologies," *IEEE Transactions on Automatic Control*, vol. 50, no. 5, pp. 655–661, 2005.

[6] J. Cao, G. Chen, and P. Li, "Global synchronization in an array of delayed neural networks with hybrid coupling," *IEEE Transactions on Systems, Man, and Cybernetics B: Cybernetics*, vol. 38, no. 2, pp. 488–498, 2008.

[7] J. Qin, H. Gao, and C. Yu, "On discrete-time convergence for general linear multi-agent systems under dynamic topology,"

IEEE Transactions on Automatic Control, vol. 59, no. 4, pp. 1054–1059, 2014.

[8] J. Qin, W. X. Zheng, and H. Gao, "Consensus of multiple second-order vehicles with a time-varying reference signal under directed topology," *Automatica*, vol. 47, no. 9, pp. 1983–1991, 2011.

[9] M. J. Park, O. M. Kwon, J. H. Park, S. M. Lee, and E. J. Cha, "Synchronization criteria for coupled stochastic neural networks with time-varying delays and leakage delay," *Journal of the Franklin Institute*, vol. 349, no. 5, pp. 1699–1720, 2012.

[10] G. F. Franklin, J. D. Powell, and M. Workman, *Digital Control of Dynamic Systems*, Addison-Wesley, Reading, Mass, USA, 1998.

[11] E. Fridman, "A refined input delay approach to sampled-data control," *Automatica*, vol. 46, no. 2, pp. 421–427, 2010.

[12] H. Gao, J. Wu, and P. Shi, "Robust sampled-data H_∞ control with stochastic sampling," *Automatica*, vol. 45, no. 7, pp. 1729–1736, 2009.

[13] T. H. Lee, J. H. Park, S. M. Lee, and O. M. Kwon, "Robust synchronisation of chaotic systems with randomly occurring uncertainties via stochastic sampled-data control," *International Journal of Control*, vol. 86, no. 1, pp. 107–119, 2013.

[14] Y. Gao, L. Wang, G. Xie, and B. Wu, "Consensus of multi-agent systems based on sampled-data control," *International Journal of Control*, vol. 82, no. 12, pp. 2193–2205, 2009.

[15] J. Qin and H. Gao, "A sufficient condition for convergence of sampled-data consensus for double-integrator dynamics with nonuniform and time-varying communication delays," *IEEE Transactions on Automatic Control*, vol. 57, no. 9, pp. 2417–2422, 2012.

[16] Z. Tang, T. Huang, J. Shao, and J. Hu, "Leader-following consensus for multi-agent systems via sampled-data control," *IET Control Theory & Applications*, vol. 5, no. 14, pp. 1658–1665, 2011.

[17] L. C. Freeman, "A set of measure of centrality based on betweenness," *Sociometry*, vol. 40, pp. 35–41, 1977.

[18] M. E. J. Newman and M. Girvan, "Finding and evaluating community structure in networks," *Physical Review E: Statistical, Nonlinear, and Soft Matter Physics*, vol. 69, no. 2, Article ID 026113, 2004.

[19] S. Boyd, L. El Ghaoui, E. Feron, and V. Balakrishnan, *Linear Matrix Inequalities in System and Control Theory*, SIAM, Philadelphia, Pa, USA, 1994.

[20] R. E. Skelton, T. Iwasaki, and K. M. Grigoradis, *A Unified Algebraic Approach to Linear Control Design*, Taylor & Francis, Boca Raton, Fla, USA, 1997.

[21] A. Graham, *Kronecker Products and Matrix Calculus: With Applications*, John Wiley & Sons, New York, NY, USA, 1982.

[22] A. Seuret and F. Gouaisbaut, "Wirtinger-based integral inequality: application to time-delay systems," *Automatica*, vol. 49, no. 9, pp. 2860–2866, 2013.

[23] P. Park, J. W. Ko, and C. Jeong, "Reciprocally convex approach to stability of systems with time-varying delays," *Automatica*, vol. 47, no. 1, pp. 235–238, 2011.

[24] K. Gu, "An integral inequality in the stability problem of time-delay systems," in *Proceedings of the 39th IEEE Confernce on Decision and Control*, pp. 2805–2810, Sydney, Australia, December 2000.

[25] L. O. Chua, M. Komuro, and T. Matsumoto, "The double scroll family," *IEEE Transactions on Circuits and Systems*, vol. 33, no. 11, pp. 1072–1118, 1986.

Hindawi Publishing Corporation
The Scientific World Journal
Volume 2015, Article ID 163234, 9 pages
http://dx.doi.org/10.1155/2015/163234

Research Article

Results for Two-Level Designs with General Minimum Lower-Order Confounding

Zhi Ming Li[1] and Run Chu Zhang[2,3]

[1] *School of Mathematical Sciences, Xinjiang University, Urumqi 830046, China*
[2] *KLAS and School of Mathematics, Northeast Normal University, Changchun 130024, China*
[3] *LPMC and School of Mathematical Sciences, Nankai University, Tianjin 300071, China*

Correspondence should be addressed to Zhi Ming Li; zhimingli525@sina.com

Received 2 June 2014; Accepted 19 November 2014

Academic Editor: Haijun Jiang

The general minimum lower-order confounding (GMC) criterion for two-level design not only reveals the confounding information of factor effects but also provides a good way to select the optimal design, which was proposed by Zhang et al. (2008). The criterion is based on the aliased effect-number pattern (AENP). Therefore, it is very important to study properties of AENP for two-level GMC design. According to the ordering of elements in the AENP, the confounding information between lower-order factor effects is more important than that of higher-order effects. For two-level GMC design, this paper mainly shows the interior principles to calculate the leading elements ${}^{\#}_{1}C_2$ and ${}^{\#}_{2}C_2$ in the AENP. Further, their mathematical formulations are obtained for every GMC 2^{n-m} design with $N = 2^{n-m}$ according to two cases: (i) $5N/16 + 1 \le n < N/2$ and (ii) $N/2 \le n \le N - 1$.

1. Introduction

To find optimal designs in a more elaborate and explicit manner under effect hierarchy principle, Zhang et al. [1] first introduced the aliased effect-number pattern (AENP) and proposed a new criterion of general minimum lower-order confounding (GMC) for two-level regular design. Further, they proved that all the classification patterns conducting the existing criteria, such as maximum resolution (MR) criterion [2], minimum aberration (MA) criterion [3], clear effects (CE) criterion [4], and maximum estimation capacity (MEC) criterion [5], can be expressed as different functions of the AENP so that it can be a basis to unify these criteria.

Through the AENP, we can get a deeper understanding of properties of the above criteria and relationships among them. Zhang and Cheng [6] revealed an exact expression of the average minimum lower-order confounding property of MA design. Hu and Zhang [7] obtained an essential statistical equivalence of MEC design and MA design. From the average least confounding property between lower-order effects, MA designs are most suitable for the situation that all the factors in experiments are treated to be equally important, while GMC design has an individual least confounding property between lower-order effects and possesses the maximum numbers of clear main effects and clear two-factor interactions (2fi's). Because of this, GMC designs can be applied to the experiments which the experimenters have some prior information to the order of the importance factors. In practice, the latter situation more often happens than the former one. Therefore, the study for GMC designs should be significantly important in both theory and application.

Now we review some definitions proposed by Zhang et al. [1]. Let D be a 2^{n-m} design with n factors, m independent defining words, and $N = 2^{n-m}$ runs. We denote the factors by $1, 2, \ldots, n$. An ith-order factor effect is said to be aliased with jth-order factor effects at degree k if it is simultaneously aliased with k jth-order factor effects. The 0th-order effect is the grand mean and 1st-order effect is a main effect.

Let ${}^{\#}_{i}C^{(k)}_{j}(D)$ (written by ${}^{\#}_{i}C^{(k)}_{j}$ for short) be the number of ith-order factor effects that are aliased with k jth-order factor effects. Denote $K_j = \binom{n}{j}$; a set $\{{}^{\#}_{i}C^{(k)}_{j}, 0 \le k \le K_j,$

$0 \le i, j \le n\}$ is called *the aliased effect-number pattern (AENP)* of the design D. The set reflects the overall confounding between factor effects in the design. Define ${}^{\#}_{i}C_j = ({}^{\#}_{i}C_j^{(0)}, {}^{\#}_{i}C_j^{(1)}, \ldots, {}^{\#}_{i}C_j^{(K_j)})$ and a design that sequentially maximizes the vector

$$ {}^{\#}C = \left({}^{\#}_{1}C_2, {}^{\#}_{2}C_2, {}^{\#}_{1}C_3, {}^{\#}_{2}C_3, {}^{\#}_{3}C_2, {}^{\#}_{3}C_3, \ldots\right) \quad (1)$$

is called *a GMC design*, where the ordering of ${}^{\#}_{i}C_j$'s is in accordance with the rule: ${}^{\#}_{i}C_j$ *is before* ${}^{\#}_{u}C_v$ *if either* $\max(i, j) < \max(u, v)$, *or* $\max(i, j) = \max(u, v)$, *with* $i < u$, *or* $\max(i, j) = \max(u, v)$ *with* $i = u$ *and* $j < v$. In order to make main effects or 2fi's estimable, we need to give an assumption: *the interactions involving three or more factors are absent*. Thus, we only study the leading terms ${}^{\#}_{1}C_2$ and ${}^{\#}_{2}C_2$ of AENP for two-level GMC design in this paper.

Zhang et al. [1] listed all two-level GMC designs of 16 and 32 runs, a number of 64-run GMC designs, and obtained the values of ${}^{\#}_{1}C_2$ and ${}^{\#}_{2}C_2$ by computer algorithm. However, the method is not suitable for designs with larger runs. Zhang and Cheng [6] and Chen and Liu [8] provided an important theory for constructing GMC designs. Cheng and Zhang [9] and Li et al. [10] finished the construction of GMC 2^{n-m} designs with $N/4 + 1 \le n \le N - 1$. However, there are few articles that pay attention to calculating the values of elements in the AENP, especially, the confounding information between main effects and 2fi's, or among 2fi's of two-level GMC design.

This paper mainly reveals the interior principles for calculating the values of ${}^{\#}_{1}C_2$ and ${}^{\#}_{2}C_2$ for two-level GMC design. In Section 2, we introduce some notations and obtain useful lemmas to study the lower-order confounding information of two-level GMC designs. Section 3 and Section 4, respectively, obtain values of ${}^{\#}_{1}C_2$ and ${}^{\#}_{2}C_2$ for GMC 2^{n-m} design with resolution $R \ge III$, for $5N/16 + 1 \le n < N/2$ and $N/2 \le n \le N - 1$. Concluding remarks are given in Section 5.

2. Some Notations and Lemmas

Denote $q = n - m$ and $1, 2, \ldots, q$ stand for q independent factors. Let H_q be the set containing all main effects $1, 2, \ldots, q$ and all interactions among them, formed by

$$H_1 = \{1\}, \qquad H_q = \left\{H_{q-1}, q, qH_{q-1}\right\}, \quad (2)$$

where $qH_{q-1} = \{qd: d \in H_{q-1}\}$. By Theorem 2.7.1 of Mukerjee and Wu [11], any 2^{n-m} design D can be represented by an n-subset of H_q; that is, $D \subset H_q$.

Let $T_1 = H_1$ and $T_r = \{r, rH_{r-1}\}$ for $1 < r \le q$. Evidently, $H_q = \cup_{r=1}^{q} T_r$. For $5N/16 + 1 \le n \le N - 1$, Li et al. [10] have gotten that every GMC 2^{n-m} design is constructed by the last n columns of H_q. Therefore, GMC 2^{n-m} designs with $5N/16 + 1 \le n < N/2$ are directly formed by the last n columns of T_q. Denote $S_{qr} = H_q \setminus H_r$ with $1 \le r < q$. For $N/2 \le n \le N - 1$, there exists a number r $(< q)$ so that GMC 2^{n-m} design is formed by the last n columns of $T_r \cup S_{qr}$. Thus, the GMC design can be written by $D_0 \cup S_{qr}$, where D_0 consists of the last $n - (N - 2^r)$ columns of T_r. To get the lower-order confounding information of two-level GMC design, we need to study structure of last n_0 columns of T_r for $r \le q$ and $n_0 \le n$.

Suppose D_0 consists of the last n_0 columns of T_r $(r \le q)$, where $n_0 = \#\{D_0\}$ and $\#A$ denotes the cardinality of a set A. The following example illustrates the structure of D_0.

Example 1. Consider $r = 7$; we select the last n_0 columns of T_7 to construct D_0. Clearly, there are 64 choices besides $D_0 \equiv T_r$. For $1 \le n_0 \le 63$, D_0 is one of the following six forms.

(i) $(u + 1) \cdots 7H_u$ for $1 \le u < 7$.

(ii) $(u + 1) \cdots 7(H_u \setminus H_v)$ for $1 \le v < u < 7$.

(iii) $(u+1) \cdots 7((s+1) \cdots vH_s \cup (H_u \setminus H_v))$ for $1 \le s < v < u < 7$.

(iv) $(u + 1) \cdots 7((s + 1) \cdots v(H_s \setminus H_t) \cup (H_u \setminus H_v))$ for $1 \le t < s < v < u < 7$.

(v) $(u + 1) \cdots 7((s + 1) \cdots v((w + 1) \cdots tH_w \cup (H_s \setminus H_t)) \cup (H_u \setminus H_v))$ for $1 \le w < t < s < v < u < 7$.

(vi) $(u + 1) \cdots 7((s + 1) \cdots v((w + 1) \cdots t(H_w \setminus H_z) \cup (H_s \setminus H_t)) \cup (H_u \setminus H_v))$ for $1 \le z < w < t < s < v < u < 7$.

The above example provides a way to construct D_0. Generally, for any r $(r \le q)$, we consider the construction of D_0 in T_r. Define

$$D_t = H_{i_t} \setminus H_{j_t}, \qquad a_{i_t} = (i_t + 1)(i_t + 2) \cdots j_{t-1}, \qquad 1 \le t \le m, \quad (3)$$

where $1 \le j_m < i_m < j_{m-1} < i_{m-1} < \cdots < j_t < i_t < \cdots < j_1 < i_1 < j_0 = r$. Then, D_0 can be constructed by either of the following cases.

Case 1. One has $D_0 = a_{i_1}(a_{i_2}(\cdots(a_{i_{m-1}}(a_{i_m}D_m \cup D_{m-1}) \cdots) \cup D_2) \cup D_1)$.

Case 2. One has $D_0 = a_{i_1}(a_{i_2}(\cdots(a_{i_{m-1}}(a_{i_m}H_{i_m} \cup D_{m-1}) \cdots) \cup D_2) \cup D_1)$.

In Case 1, the number of elements in D_0 is even since $\#\{D_0\} = \sum_{t=1}^{m}(2^{i_k} - 2^{j_k})$. However, that of D_0 in Case 2 is odd because of $\#\{D_0\} = \sum_{t=1}^{m-1}(2^{i_k} - 2^{j_k}) + 2^{i_m} - 1$.

Consider $D \subset H_q$ and any $\gamma \in H_q$; define

$$B_2(D, \gamma) = \#\{(d_1, d_2): d_1, d_2 \in D,\ d_1 d_2 = \gamma\}, \quad (4)$$

which is the number of 2fi's in D aliased with γ. By the definition of ${}^{\#}_{i}C_j^{(k)}(D)$, it can be easily obtained that

$${}^{\#}_{1}C_2^{(k)}(D) = \#\{\gamma: \gamma \in D, B_2(D, \gamma) = k\}, \quad (5)$$

$${}^{\#}_{2}C_2^{(k)}(D) = (k + 1)\#\left\{\gamma: \gamma \in H_q, B_2(D, \gamma) = k + 1\right\}, \quad (6)$$

where $k = 0, 1, \ldots, K_2$. In order to get the lower-order confounding of D_0 in the above cases, we need to study $B_2(D_t, \gamma)$ for $t \ge 1$.

Lemma 2. *Let D_t be defined in (3) for $t \geq 1$. Then*

$$B_2(D_t,\gamma) = \begin{cases} 2^{i_t-1} - 2^{j_t-1}, & \gamma \in H_{j_t}, \\ 2^{i_t-1} - 2^{j_t}, & \gamma \in H_{i_t} \setminus H_{j_t}, \\ 0, & \gamma \in H_q \setminus H_{i_t}. \end{cases} \tag{7}$$

Proof. For $\gamma \in H_q \setminus H_{i_t}$, we have $B_2(D_t,\gamma) = 0$. If $\gamma \in H_{j_t}$, then

$$B_2(D,\gamma) = \frac{\#\{H_{i_t} \setminus H_{j_t}\}}{2} = 2^{i_t-1} - 2^{j_t-1}. \tag{8}$$

For $\gamma \in H_{i_t} \setminus H_{j_t}$, there are $2^{i_t-1} - 1$ pairs of factors in H_{i_t} so that their interactions are aliased with γ. Among these pairs, there are $2^{j_t} - 1$ pairs with one factor from H_{j_t} and another from $H_{i_t} \setminus H_{j_t}$. Thus,

$$B_2(D_t,\gamma) = \left(2^{i_t-1} - 1\right) - \left(2^{j_t} - 1\right) = 2^{i_t-1} - 2^{j_t}. \tag{9}$$

This completes the proof. □

Next we analyze Case 1 of D_0. For convenience, by (3), denote

$$\mathscr{D}(t) = a_{i_t}\left(\cdots\left(a_{i_{m-1}}\left(a_{i_m}D_m \cup D_{m-1}\right)\cdots\right) \cup D_t\right) \tag{10}$$

for $1 < t \leq m$. Evidently, $\mathscr{D}(t) \subset H_{j_{t-1}}$ and $\mathscr{D}(1) = D_0$ in Case 1. When $d_1 \in \mathscr{D}(t)$ and $d_2 \in D_{t-1}$, we have $d_1 d_2 \in D_{t-1}$. Thus,

$$\#\{(d_1,d_2) : d_1 \in \mathscr{D}(t),\ d_2 \in D_{t-1},\ d_1 d_2 = \gamma\} = \sum_{l=t}^{m} \#\{D_l\} \tag{11}$$

for $\gamma \in D_{t-1}$. Otherwise, the value is zero. Then

$$\#\{(d_1,d_2) : d_1 \in \mathscr{D}(t),\ d_2 \in D_{t-1},\ d_1 d_2 = \gamma\} = \begin{cases} \sum_{l=t}^{m}\left(2^{i_l} - 2^{j_l}\right), & \gamma \in D_{t-1}, \\ 0, & \gamma \notin D_{t-1}. \end{cases} \tag{12}$$

Based on Lemma 2 and (12), we can get the following result for Case 1.

Lemma 3. *Let $D_0 = a_{i_1}(a_{i_2}(\cdots(a_{i_{m-1}}(a_{i_m}D_m \cup D_{m-1})\cdots) \cup D_2) \cup D_1)$. Then*

$$B_2(D_0,\gamma) = \begin{cases} \dfrac{c(m+1)}{2}, & \gamma \in H_{j_m}, \\ c(m+1) - \dfrac{\left(c(t) + 2^{i_t}\right)}{2}, & \gamma \in D_t,\ t = 1,\ldots,m, \\ \dfrac{c(t)}{2}, & \gamma \in H_{j_{t-1}} \setminus H_{i_t},\ t = 2,\ldots,m, \\ 0, & \gamma \in H_q \setminus H_{i_1}, \end{cases} \tag{13}$$

where

$$c(1) = 0, \quad c(t) = \sum_{l=1}^{t-1}\left(2^{i_l} - 2^{j_l}\right), \quad t > 1. \tag{14}$$

Proof. For $1 < l \leq m$, by (10), we have

$$\begin{aligned} &B_2\left(a_{i_l}\left(\mathscr{D}(l) \cup D_{l-1}\right),\gamma\right) \\ &\quad = B_2\left(\mathscr{D}(l) \cup D_{l-1},\gamma\right) \\ &\quad = B_2\left(\mathscr{D}(l),\gamma\right) + B_2\left(D_{l-1},\gamma\right) \\ &\qquad + \#\{(d_1,d_2) : d_1 \in \mathscr{D}(l),\ d_2 \in D_{l-1},\ d_1 d_2 = \gamma\}. \end{aligned} \tag{15}$$

Hence,

$$\begin{aligned} &B_2(D_0,\gamma) \\ &\quad = \sum_{l=1}^{m-2} B_2(D_l,\gamma) + B_2\left(a_{i_m}D_m \cup D_{m-1},\gamma\right) \\ &\qquad + \sum_{l=2}^{m-1} \#\{(d_1,d_2) : d_1 \in \mathscr{D}(l),\ d_2 \in D_{l-1},\ d_1 d_2 = \gamma\} \\ &\quad = \sum_{l=1}^{m} B_2(D_l,\gamma) \\ &\qquad + \sum_{l=2}^{m} \#\{(d_1,d_2) : d_1 \in \mathscr{D}(l),\ d_2 \in D_{l-1},\ d_1 d_2 = \gamma\}. \end{aligned} \tag{16}$$

Put H_r into $2m+1$ incompatible parts: H_{j_m}, D_{l+1}, and $H_{j_l} \setminus H_{i_{l+1}}$ for $l = 0, 1, \ldots, m-1$. Clearly, if $\gamma \in H_q \setminus H_{i_1}$, then $B_2(D_0,\gamma) = 0$. By Lemma 2 and (12), we, respectively, discuss the following cases.

(i) If $\gamma \in H_{j_m}$, then

$$\#\{(d_1,d_2) : d_1 \in \mathscr{D}(l),\ d_2 \in D_{l-1},\ d_1 d_2 = \gamma\} = 0 \tag{17}$$

for $1 < l \leq m-1$. Thus,

$$B_2(D_0,\gamma) = \sum_{l=1}^{m} B_2(D_t,\gamma) = \sum_{l=1}^{m}\left(2^{i_l-1} - 2^{j_l-1}\right). \tag{18}$$

(ii) If $\gamma \in D_t$ with $1 < t \leq m$, one has

$$\begin{aligned} &B_2(D_0,\gamma) \\ &\quad = \sum_{l=1}^{t-1} B_2(D_l,\gamma) + B_2(D_t,\gamma) \\ &\qquad + \#\{(d_1,d_2) : d_1 \in \mathscr{D}(t+1),\ d_2 \in D_t,\ d_1 d_2 = \gamma\} \\ &\quad = \sum_{l=1}^{t-1}\left(2^{i_l-1} - 2^{j_l-1}\right) + \left(2^{i_t-1} - 2^{j_t}\right) \\ &\qquad + \sum_{l=t+1}^{m}\left(2^{i_l} - 2^{j_l}\right) \\ &\quad = \sum_{l=1}^{m}\left(2^{i_l} - 2^{j_l}\right) - \sum_{l=1}^{t-1}\left(2^{i_l-1} - 2^{j_l-1}\right) - 2^{i_t-1}. \end{aligned} \tag{19}$$

(iii) If $\gamma \in H_{j_{t-1}} \setminus H_{i_t}$ for $t > 1$, then

$$B_2(D_0, \gamma) = \sum_{l=1}^{t-1} B_2(D_l, \gamma) = \sum_{l=1}^{t-1} \left(2^{i_l - 1} - 2^{j_l - 1}\right). \quad (20)$$

This completes the proof. □

Lemma 3 shows that the value of $B_2(D_0, \gamma)$ in Case 1 depends on all pairs $\{i_t, j_t\}_{1 \le t \le m}$ which relate to $\#\{D_0\} = \sum_{t=1}^{m}(2^{i_t} - 2^{j_t})$. For instance, take $n_0 = \#\{D_0\} = 42$ that is nearer to the number 2^5 than 2^6; we have

$$n_0 = 2^5 + 2^3 + 2 = \left(2^6 - 2^5\right) + \left(2^4 - 2^3\right) + \left(2^2 - 2\right). \quad (21)$$

Thus $i_1 = 6$, $j_1 = 5$, $i_2 = 4$, $j_2 = 3$, $i_3 = 2$, and $j_3 = 1$. And take $n_0 = 54$ which is closer to the number 2^6 than 2^5; one obtains $n_0 = 2^6 - 2^4 + 6 = 2^6 - 2^4 + 2^3 - 2$. Then $i_1 = 6$, $j_1 = 4$, $i_2 = 3$, and $j_2 = 1$.

Consider Case 2 of D_0. Denote

$$\mathscr{H}(t) = a_{i_t}\left(\cdots\left(a_{i_{m-1}}\left(a_{i_m} H_{i_m} \cup D_{m-1}\right)\cdots\right) \cup D_t\right) \quad (22)$$

for $1 < t \le m$. Clearly, $\mathscr{H}(t) \subset H_{j_{t-1}}$ and $\mathscr{H}(1) = D_0$ in Case 2. For two factors $d_1 \in \mathscr{H}(t)$ and $d_2 \in D_{t-1}$, one has $d_1 d_2 \in D_{t-1}$. Therefore,

$$\#\left\{(d_1, d_2) : d_1 \in \mathscr{H}(t),\ d_2 \in D_{t-1},\ d_1 d_2 = \gamma\right\} = \begin{cases} \sum_{l=t}^{m-1}\left(2^{i_l} - 2^{j_l}\right) + 2^{i_m} - 1, & \gamma \in D_{t-1}, \\ 0, & \gamma \notin D_{t-1}. \end{cases} \quad (23)$$

Specifically, if $t = m$, then

$$\#\left\{(d_1, d_2) : d_1 \in a_{i_m} H_{i_m},\ d_2 \in D_{m-1},\ d_1 d_2 = \gamma\right\} = \begin{cases} 2^{i_m} - 1, & \gamma \in D_{m-1}, \\ 0, & \gamma \notin D_{m-1}. \end{cases} \quad (24)$$

For $m \ge 1$ and $\gamma \in H_{i_m}$, there are $2^{i_m - 1} - 1$ pairs of factors in H_{i_m}, which each interaction is aliased with γ. Then

$$B_2\left(a_{i_m} H_{i_m}, \gamma\right) = B_2\left(H_{i_m}, \gamma\right) = \begin{cases} 2^{i_m - 1} - 1, & \gamma \in H_{i_m}, \\ 0, & \gamma \in H_q \setminus H_{i_m}. \end{cases} \quad (25)$$

Based on the above results, we can obtain the value of $B_2(D_0, \gamma)$ for any $\gamma \in H_q$ in Case 2.

Lemma 4. *Let* $D_0 = a_{i_1}(a_{i_2}(\cdots(a_{i_{m-1}}(a_{i_m} H_{i_m} \cup D_{m-1})\cdots) \cup D_2) \cup D_1)$. *Then*

$$B_2(D_0, \gamma) = \begin{cases} \dfrac{c(m)}{2} + 2^{i_m - 1} - 1, & \gamma \in H_{i_m}, \\ c(m) - \dfrac{\left(c(t) + 2^{i_t}\right)}{2} + 2^{i_m} - 1, & \gamma \in D_t,\ t = 1, \ldots, m-1, \\ \dfrac{c(t)}{2}, & \gamma \in H_{j_{t-1}} \setminus H_{i_t},\ t = 2, \ldots, m, \\ 0, & \gamma \in H_q \setminus H_{i_1}, \end{cases} \quad (26)$$

where $c(t)$ is defined in (14).

Proof. By (22), we obtain

$$\begin{aligned} B_2(D_0, \gamma) &= \sum_{l=1}^{m-1} B_2(D_l, \gamma) + B_2\left(a_{i_m} H_{i_m}, \gamma\right) \\ &\quad + \#\left\{(d_1, d_2) : d_1 \in a_{i_m} H_{i_m},\ d_2 \in D_{m-1},\ d_1 d_2 = \gamma\right\} \\ &\quad + \sum_{l=2}^{m-1} \#\left\{(d_1, d_2) : d_1 \in \mathscr{H}(l),\ d_2 \in D_{l-1},\ d_1 d_2 = \gamma\right\}. \end{aligned} \quad (27)$$

For $\gamma \in H_q \setminus H_{i_1}$, we have $B_2(D_0, \gamma) = 0$. By Lemma 2, (25), and (23), analyze the following cases.

(i) For $\gamma \in H_{i_m}$, we obtain

$$\begin{aligned} B_2(D_0, \gamma) &= \sum_{l=1}^{m-1} B_2(D_l, \gamma) + B_2\left(a_{i_m} H_{i_m}, \gamma\right) \\ &= \sum_{l=1}^{m-1}\left(2^{i_l - 1} - 2^{j_l - 1}\right) + 2^{i_m - 1} - 1. \end{aligned} \quad (28)$$

(ii) For $\gamma \in D_t$ with $1 \le t \le m - 1$, one has

$$\begin{aligned} B_2(D_0, \gamma) &= \sum_{l=1}^{t-1} B_2(D_l, \gamma) + B_2(D_t, \gamma) \\ &\quad + \#\left\{(d_1, d_2) : d_1 \in \mathscr{H}(t+1),\ d_2 \in D_t,\ d_1 d_2 = \gamma\right\} \\ &= \sum_{l=1}^{t-1}\left(2^{i_l - 1} - 2^{j_l - 1}\right) \\ &\quad + \sum_{l=t}^{m-1}\left(2^{i_l} - 2^{j_l}\right) - 2^{i_t - 1} + 2^{i_m} - 1 \\ &= c(m) - \frac{\left(c(t) + 2^{i_t}\right)}{2} + 2^{i_m} - 1. \end{aligned} \quad (29)$$

(iii) For $\gamma \in H_{j_{t-1}} \setminus H_{i_t}$ with $2 \le t \le m$, $B_2(D_0, \gamma) = \sum_{l=1}^{t-1}(2^{i_l - 1} - 2^{j_l - 1})$.

□

In Lemma 4, the value of $B_2(D_0, \gamma)$ is relative to these pairs $\{i_t, j_t\}_{1 < t < m}$ and i_m. For example, consider $n_0 = \#\{D_0\} = 21$. Since $n_0 = (2^5 - 2^4) + (2^3 - 2^2) + 2 - 1$, it yields $i_1 = 5$, $j_1 = 4$, $i_2 = 3$, $j_2 = 2$, and $i_3 = 1$. Taking $n_0 = 29$, we have $n_0 = 2^5 - 3 = 2^5 - 2^2 + 1$; thus $i_1 = 5$, $j_1 = 2$, and $i_2 = 1$.

Lemmas 3 and 4, respectively, obtain the value of $B_2(D_0, \gamma)$ that D_0 consists of the last n_0 columns of T_r $(r \le q)$ for two cases. These results play a key role in calculating ${}^{\#}_{1}C_2$ and ${}^{\#}_{2}C_2$'s for all GMC 2^{n-m} designs with $5N/16 + 1 \le n \le N - 1$. Next sections will, respectively, discuss two-level GMC designs with the factor number n satisfying (i) $5N/16 + 1 \le n < N/2$ or (ii) $N/2 \le n \le N - 1$.

3. GMC 2^{n-m} Designs with $5N/16+1 \le n<N/2$

Li et al. [10] showed all GMC 2^{n-m} designs with $5N/16+1 \le n < N/2$, constructed by the last n columns of T_q. In Section 2, D_0 is constructed by Case 1 or Case 2, which is the last n_0 columns of T_r $(r \le q)$ for $n_0 = \#\{D_0\}$. Therefore, for any GMC 2^{n-m} design D with $5N/16+1 \le n < N/2$, its construction is similar to that of D_0. In (3), take $j_0 = r = q$.

Theorem 5. *Consider GMC 2^{n-m} design*

$$D = a_{i_1}\left(a_{i_2}\left(\cdots\left(a_{i_{m-1}}\left(a_{i_m}D_m \cup D_{m-1}\right)\cdots\right) \cup D_2\right) \cup D_1\right) \tag{30}$$

with $5N/16+1 \le n < N/2$. Then

(a)

$$ {}^{\#}_{1}C_2^{(k)}(D) = \begin{cases} n, & k = 0, \\ 0, & \text{otherwise}, \end{cases} \tag{31}$$

(b)

$$ {}^{\#}_{2}C_2^{(k)}(D) = \begin{cases} \dfrac{n\left(2^{j_m}-1\right)}{2}, & k = \dfrac{n}{2}-1, \\ \left(n - \dfrac{\left(c(t)+2^{i_t}\right)}{2}\right)\left(2^{i_t}-2^{j_t}\right), & k = n - \dfrac{\left(c(t)+2^{i_t}\right)}{2} - 1, \\ & t = 1,\ldots,m, \\ \dfrac{c(t)\left(2^{j_{t-1}}-2^{i_t}\right)}{2}, & k = \dfrac{c(t)}{2}-1,\ t = 2,\ldots,m, \\ 0, & \text{otherwise}, \end{cases} \tag{32}$$

where $c(t)$ is defined in (14).

Proof. Evidently, $n = \sum_{l=1}^{m}(2^{i_l}-2^{j_l})$; we have $c(m+1) = n$. By Lemma 3,

$$B_2(D,\gamma) = \begin{cases} \dfrac{n}{2}, & \gamma \in H_{i_m}, \\ n - \dfrac{\left(c(t)+2^{i_t}\right)}{2}, & \gamma \in D_t,\ t = 1,\ldots,m, \\ \dfrac{c(t)}{2}, & \gamma \in H_{j_{t-1}} \setminus H_{i_t},\ t = 2,\ldots,m, \\ 0, & \gamma \in H_q \setminus H_{i_1}. \end{cases} \tag{33}$$

(a) Since $D \subset H_q \setminus H_{i_1}$, hence by (33) and (5)

$$ {}^{\#}_{1}C_2^{(0)}(D) = \#\{\gamma : \gamma \in D, B_2(D,\gamma) = 0\} = \#\{D\} = n. \tag{34}$$

Otherwise, ${}^{\#}_{1}C_2^{(k)}(D) = 0$ for $k \ne 0$.

(b) Following (33) and (6), we obtain

$$\begin{aligned} {}^{\#}_{2}C_2^{(k)}(D) = {} & (k+1) \\ & \times \Big[\#\left\{\gamma : \gamma \in H_{j_m}, B_2(D,\gamma) = k+1\right\} \\ & + \sum_{t=1}^{m} \#\{\gamma : \gamma \in D_t, B_2(D,\gamma) = k+1\} \\ & + \sum_{t=2}^{m} \#\left\{\gamma : \gamma \in H_{j_{t-1}} \setminus H_{i_t}, B_2(D,\gamma) = k+1\right\} \\ & + \#\left\{\gamma : \gamma \in H_q \setminus H_{i_1}, B_2(D,\gamma) = k+1\right\}\Big]. \end{aligned} \tag{35}$$

If $k = n/2-1$, then

$$ {}^{\#}_{2}C_2^{(k)}(D) = \frac{n\#\left\{H_{j_m}\right\}}{2} = \frac{n\left(2^{j_m}-1\right)}{2}. \tag{36}$$

For $k = n - (c(t)+2^{i_t})/2 - 1$ with $1 \le t \le m$, one has

$$\begin{aligned} {}^{\#}_{2}C_2^{(k)}(D) &= \left(n - \frac{\left(c(t)+2^{i_t}\right)}{2}\right)\#\{D_t\} \\ &= \left(n - \frac{\left(c(t)+2^{i_t}\right)}{2}\right)\left(2^{i_t}-2^{j_t}\right). \end{aligned} \tag{37}$$

And if $k = c(t)/2 - 1$ with $1 < t \le m$, then

$$ {}^{\#}_{2}C_2^{(k)}(D) = \frac{c(t)\#\left\{H_{j_{t-1}} \setminus H_{i_t}\right\}}{2} = \frac{c(t)\left(2^{j_{t-1}}-2^{i_t}\right)}{2}. \tag{38}$$

Otherwise, ${}^{\#}_{2}C_2^{(k)}(D) = 0$. □

For GMC 2^{n-m} design with $5N/16+1 \le n < N/2$, Theorem 5 reveals that the value of ${}^{\#}_{1}C_2$ only depends on the factor number n. However, the value of ${}^{\#}_{2}C_2$ is related to the numbers $\{i_t, j_t\}_{1\le t\le m}$ besides n. We illustrate them via a simple example.

Example 6. Take $q = 5$ and $n = 10$; consider GMC 2^{10-5} design D. Since $n = 2^3+2 = (2^4-2^3)+(2^2-2)$, clearly, we have $i_1 = 4$, $j_1 = 3$, $i_2 = 2$, and $j_2 = 1$. Hence, $2^{i_1}-2^{j_1} = 8$, $2^{i_2}-2^{j_2} = 2$, $2^{j_1}-2^{i_2} = 4$, and $c(1) = 0$, $c(2) = 8$. By Theorem 5, we get

$$\begin{aligned} {}^{\#}_{1}C_2^{(k)}(D) &= \begin{cases} 10, & k = 0, \\ 0, & \text{otherwise}, \end{cases} \\ {}^{\#}_{2}C_2^{(k)}(D) &= \begin{cases} 16, & k = 1, \\ 24, & k = 3, \\ 5, & k = 4, \\ 0, & \text{otherwise}. \end{cases} \end{aligned} \tag{39}$$

Theorem 5 applies to the case that the factor number n of GMC design is even. If n is odd, similar to the proof of Theorem 5, by Lemma 4, one can get the result below.

Theorem 7. *Consider GMC 2^{n-m} design*

$$D = a_{i_1}\left(a_{i_2}\left(\cdots\left(a_{i_{m-1}}\left(a_{i_m}H_{i_m} \cup D_{m-1}\right)\cdots\right) \cup D_2\right) \cup D_1\right) \tag{40}$$

with $5N/16+1 \le n < N/2$. Then

(a)

$$ {}^{\#}_{1}C_2^{(k)}(D) = \begin{cases} n, & k = 0, \\ 0, & otherwise, \end{cases} \tag{41} $$

(b)

$$ {}^{\#}_{2}C_2^{(k)}(D) = \begin{cases} \dfrac{(n-1)\left(2^{i_m}-1\right)}{2}, & k = \dfrac{(n-1)}{2} - 1, \\ \left(n - \dfrac{\left(c(t)+2^{i_t}\right)}{2}\right)\left(2^{i_t} - 2^{j_t}\right), & k = n - \dfrac{\left(c(t)+2^{i_t}\right)}{2} - 1, \\ & t = 1, \ldots, m-1, \\ \dfrac{c(t)\left(2^{j_{t-1}} - 2^{i_t}\right)}{2}, & k = \dfrac{c(t)}{2} - 1,\ t = 2, \ldots, m, \\ 0, & otherwise, \end{cases} \tag{42} $$

where $c(t)$ is defined in (14).

Proof. Note that $n = \sum_{l=1}^{m-1}(2^{i_l} - 2^{j_l}) + 2^{i_m} - 1 = c(m) + 2^{i_m} - 1$. □

Example 8. Let $q = 5$ and $n = 11$; consider GMC 2^{11-6} design D. Here $n = 2^4 - 2^3 + 2^2 - 1$; we have $i_1 = 4$, $j_1 = 3$, and $i_2 = 2$. Thus, $c(2) = 2^{i_1} - 2^{j_1} = 8$ and $2^{j_1} - 2^{i_2} = 4$. Following Theorem 7, it is directly obtained by

$$ {}^{\#}_{1}C_2^{(k)}(D) = \begin{cases} 11, & k = 0, \\ 0, & \text{otherwise}, \end{cases} $$

$$ {}^{\#}_{2}C_2^{(k)}(D) = \begin{cases} 24, & k = 2, \\ 16, & k = 3, \\ 15, & k = 4, \\ 0, & \text{otherwise}. \end{cases} \tag{43} $$

4. GMC 2^{n-m} Designs with $N/2 \le n \le N-1$

In Section 2, we know that any GMC 2^{n-m} design with $N/2 \le n \le N-1$ is constructed by $D_0 \cup S_{qr}$, where D_0 is the last $n - (N - 2^r)$ columns of T_r $(r < q)$. Lemmas 3 and 4 have shown the confounding information of D_0. Next we will study a special design $S_{qr} = H_q \setminus H_r$ $(r < q)$, which consists of the last $N - 2^r$ columns of H_q. Since $r < q$, the factor number of the design S_{qr} satisfies $N - 2^r \ge N/2$. Hence, the design S_{qr} has GMC. By Lemma 2, we directly give the value of $B_2(S_{qr}, \gamma)$ as follows:

$$ B_2\left(S_{qr}, \gamma\right) = \begin{cases} \dfrac{N}{2} - 2^r, & \gamma \in H_q \setminus H_r, \\ \dfrac{N}{2} - 2^{r-1}, & \gamma \in H_r. \end{cases} \tag{44} $$

Next we discuss the values of ${}^{\#}_{1}C_2$ and ${}^{\#}_{2}C_2$ for GMC design S_{qr} with $r < q$.

Theorem 9. *Consider any GMC design $S_{qr} = H_q \setminus H_r$ for $r < q$. Then*

(a)

$$ {}^{\#}_{1}C_2^{(k)}\left(S_{qr}\right) = \begin{cases} N - 2^r, & k = \dfrac{N}{2} - 2^r, \\ 0, & otherwise, \end{cases} \tag{45} $$

(b)

$$ {}^{\#}_{2}C_2^{(k)}\left(S_{qr}\right) = \begin{cases} \left(\dfrac{N}{2} - 2^r\right)\left(N - 2^r\right), & k = \dfrac{N}{2} - 2^r - 1, \\ \left(\dfrac{N}{2} - 2^{r-1}\right)\left(2^r - 1\right), & k = \dfrac{N}{2} - 2^{r-1} - 1, \\ 0, & otherwise. \end{cases} \tag{46} $$

Proof. (a) If $k = N/2 - 2^r$, by (44), then

$$ \begin{aligned} {}^{\#}_{1}C_2^{(k)}\left(S_{qr}\right) &= \#\left\{\gamma : \gamma \in S_{qr}, B_2\left(S_{qr}, \gamma\right) = k\right\} \\ &= \#\left\{S_{qr}\right\} = N - 2^r. \end{aligned} \tag{47} $$

Otherwise, ${}^{\#}_{1}C_2^{(k)}(S_{qr}) = 0$.

(b) For $k \ge 0$, note that

$$ \begin{aligned} {}^{\#}_{2}C_2^{(k)}\left(S_{qr}\right) = {} & (k+1) \\ & \times \left[\#\left\{\gamma : \gamma \in S_{qr}, B_2\left(S_{qr}, \gamma\right) = k+1\right\}\right. \\ & \left. + \#\left\{\gamma : \gamma \in H_r, B_2\left(S_{qr}, \gamma\right) = k+1\right\}\right]. \end{aligned} \tag{48} $$

If $k = N/2 - 2^r - 1$, thus by (44)

$$ {}^{\#}_{2}C_2^{(k)}\left(S_{qr}\right) = \left(\frac{N}{2} - 2^r\right)\#\left\{S_{qr}\right\} = \left(\frac{N}{2} - 2^r\right)\left(N - 2^r\right). \tag{49} $$

Similarly, for $k = N/2 - 2^{r-1} - 1$, we have

$$ {}^{\#}_{2}C_2^{(k)}\left(S_{qr}\right) = \left(\frac{N}{2} - 2^{r-1}\right)\#\left\{H_r\right\} = \left(\frac{N}{2} - 2^{r-1}\right)\left(2^r - 1\right). \tag{50} $$

□

For GMC design S_{qr} $(r < q)$, the values of ${}^{\#}_{1}C_2$ and ${}^{\#}_{2}C_2$ only rely on two numbers N and r. In particular, if $r = q - 1$, then $S_{q(q-1)} = T_q$. By Theorem 9, one has

$$ {}^{\#}_{1}C_2^{(k)}\left(T_q\right) = \begin{cases} \dfrac{N}{2}, & k = 0, \\ 0, & k \ne 0, \end{cases} $$

$$ {}^{\#}_{2}C_2^{(k)}\left(T_q\right) = \begin{cases} \dfrac{N}{4\left(N/2-1\right)}, & k = \dfrac{N}{4}-1, \\ 0, & k \neq \dfrac{N}{4}-1. \end{cases} \tag{51} $$

The next example is used to illustrate this above result.

Example 10. Consider GMC 2^{16-11} design S_{54}. Since $r = 4$ and $N = 32$, one directly gets

$$ {}^{\#}_{1}C_2^{(k)}(D) = \begin{cases} 16, & k = 0, \\ 0, & k \neq 0, \end{cases} \qquad {}^{\#}_{2}C_2^{(k)}(D) = \begin{cases} 120, & k = 7, \\ 0, & k \neq 7. \end{cases} \tag{52} $$

On the other hand, every GMC 2^{n-m} design D with $n \geq N/2$ can be constructed by the form $(D \setminus S_{qr}) \cup S_{qr}$, where $D \setminus S_{qr}$ consists of the last $n-(N-2^r)$ columns of T_r. Then, $D_0 = D \setminus S_{qr}$. Based on Lemma 3 of Li et al. [10], we obtain the relationship of D and D_0 as follows:

$$ B_2(D,\gamma) = \begin{cases} n-\dfrac{N}{2}, & \gamma \in H_q \setminus H_r, \\ B_2\left(D_0,\gamma\right)+\dfrac{N}{2}-2^{r-1}, & \gamma \in H_r. \end{cases} \tag{53} $$

Therefore, we can get the following result.

Theorem 11. *Consider GMC 2^{n-m} design $D = D_0 \cup S_{qr}$ with $r < q$, where $D_0 = a_{i_1}(a_{i_2}(\cdots(a_{i_{m-1}}(a_{i_m}D_m \cup D_{m-1})\cdots)\cup D_2)\cup D_1)$. Then*

(a)

$$ B_2(D,\gamma) = \begin{cases} \dfrac{n}{2}, & \gamma \in H_{j_m}, \\ n-\dfrac{\left(a(t)+2^{i_t}\right)}{2}, & \gamma \in D_t,\ t = 1,\ldots,m, \\ \dfrac{a(t)}{2}, & \gamma \in H_{j_{t-1}} \setminus H_{i_t},\ t = 2,\ldots,m, \\ \dfrac{N}{2}-2^{r-1}, & \gamma \in H_r \setminus H_{i_1}, \\ n-\dfrac{N}{2}, & \gamma \in H_q \setminus H_r, \end{cases} \tag{54} $$

(b)

$$ {}^{\#}_{1}C_2^{(k)}(D) = \begin{cases} N-2^r, & k = n-\dfrac{N}{2}, \\ n-N+2^r, & k = \dfrac{N}{2}-2^{r-1}, \\ 0, & \textit{otherwise}, \end{cases} \tag{55} $$

(c)

$$ {}^{\#}_{2}C_2^{(k)}(D) = \begin{cases} \dfrac{n\left(2^{j_m}-1\right)}{2}, & k = \dfrac{n}{2}-1, \\ \left(n-\dfrac{\left(a(t)+2^{i_t}\right)}{2}\right)\left(2^{i_t}-2^{j_t}\right), & k = n-\dfrac{\left(a(t)+2^{i_t}\right)}{2}-1, \\ & t = 1,\ldots,m, \\ \dfrac{a(t)\left(2^{j_{t-1}}-2^{i_t}\right)}{2}, & k = \dfrac{a(t)}{2}-1, \\ & t = 2,\ldots,m, \\ \left(\dfrac{N}{2}-2^{r-1}\right)\left(2^r-2^{i_1}\right), & k = \dfrac{N}{2}-2^{r-1}-1, \\ \left(n-\dfrac{N}{2}\right)\left(N-2^r\right), & k = n-\dfrac{N}{2}-1, \\ 0, & \textit{otherwise}, \end{cases} \tag{56} $$

where $a(t) = N-2^r+c(t)$ and $c(t)$ is defined in (14).

Proof. (a) By (53) and Lemma 3, note that

$$ c(m+1) = \#\{D_0\} = \sum_{l=1}^{m}\left(2^{i_l}-2^{j_l}\right) = n-N+2^r \tag{57} $$

yields (a).

(b) For $\gamma \in S_{qr}$, by (a), $B_2(D,\gamma) = n-N/2$. If $k = n-N/2$, then

$$ {}^{\#}_{1}C_2^{(k)}(D) = \#\left\{S_{qr}\right\} = N-2^r. \tag{58} $$

Since $D_0 \subset H_r \setminus H_{i_1}$, for $k = N/2-2^{r-1}$, we have

$$ \begin{aligned} {}^{\#}_{1}C_2^{(k)}(D) &= \#\{D_0\} \\ &= \#\left\{\bigcup_{t=1}^{m} D_t\right\} = \sum_{t=1}^{m}\left(2^{i_t}-2^{j_t}\right) = n-N+2^r. \end{aligned} \tag{59} $$

(c) Since

$$ \begin{aligned} {}^{\#}_{2}C_2^{(k)}(D) = {} & (k+1) \\ & \times\Big[\#\left\{\gamma : \gamma \in H_{j_m}, B_2(D,\gamma) = k+1\right\} \\ & + \sum_{t=1}^{m}\#\left\{\gamma : \gamma \in D_l, B_2(D,\gamma) = k+1\right\} \\ & + \sum_{t=2}^{m}\#\left\{\gamma : \gamma \in H_{j_{t-1}} \setminus H_{i_k}, B_2(D,\gamma) = k+1\right\} \\ & + \#\left\{\gamma : \gamma \in H_r \setminus H_{i_1}, B_2(D,\gamma) = k+1\right\} \\ & + \#\left\{\gamma : \gamma \in H_q \setminus H_r, B_2(D,\gamma) = k+1\right\}\Big], \end{aligned} \tag{60} $$

by (a), the result follows. □

When the factor number n of a GMC design satisfying $N/2 \le n \le N-1$ is even, by Theorem 11, we obtain values of the corresponding ${}^{\#}_{1}C_2$ and ${}^{\#}_{1}C_2$. The next example illustrates this point.

Example 12. Let $q = 8$, $r = 7$; consider GMC $2^{154-146}$ design $D = D_0 \cup S_{87}$. Since $n_0 = \#\{D_0\} = 26$ and

$$n_0 = 2^5 - 6 = \left(2^5 - 2^3\right) + \left(2^2 - 2\right), \tag{61}$$

we have $i_1 = 5$, $j_1 = 3$, $i_2 = 2$, and $j_2 = 1$. Thus, $2^{i_1} - 2^{j_1} = 24$, $2^{i_2} - 2^{j_2} = 2$ and $a(1) = N - 2^r + c(1) = 128$, $a(2) = N - 2^r + c(2) = 152$. By (b) and (c) of Theorem 11, one obtains

$$\begin{aligned} {}^{\#}_{1}C_2^{(k)}(D) &= \begin{cases} 128, & k = 26, \\ 26, & k = 64, \\ 0, & \text{otherwise}, \end{cases} \\ {}^{\#}_{2}C_2^{(k)}(D) &= \begin{cases} 3328, & k = 25, \\ 6144, & k = 63, \\ 1776, & k = 73, \\ 456, & k = 75, \\ 77 & k = 76, \\ 0, & \text{otherwise}. \end{cases} \end{aligned} \tag{62}$$

Theorem 13. *Consider GMC 2^{n-m} design $D = D_0 \cup S_{qr}$ with $r < q$, where $D_0 = a_{i_1}(a_{i_2}(\cdots(a_{i_{m-1}}(a_{i_m}H_{i_m} \cup D_{m-1})\cdots) \cup D_2) \cup D_1)$. Then*

(a)

$$B_2(D,\gamma) = \begin{cases} \dfrac{(n-1)}{2}, & \gamma \in H_{i_m}, \\ n - \dfrac{\left(a(t) + 2^{i_t}\right)}{2}, & \gamma \in D_t,\ t = 1,\ldots,m-1, \\ \dfrac{a(t)}{2}, & \gamma \in H_{j_{t-1}} \setminus H_{i_t},\ t = 2,\ldots,m, \\ \dfrac{N}{2} - 2^{r-1}, & \gamma \in H_r \setminus H_{i_1}, \\ n - \dfrac{N}{2}, & \gamma \in H_q \setminus H_r, \end{cases} \tag{63}$$

(b)

$${}^{\#}_{1}C_2^{(k)}(D) = \begin{cases} N - 2^r, & k = n - \dfrac{N}{2}, \\ n - N + 2^r, & k = \dfrac{N}{2} - 2^{r-1}, \\ 0, & \textit{otherwise}, \end{cases} \tag{64}$$

(c)

$$\begin{aligned} &{}^{\#}_{2}C_2^{(k)}(D) \\ &= \begin{cases} \dfrac{(n-1)\left(2^{i_m} - 1\right)}{2}, & k = \dfrac{(n-1)}{2} - 1, \\ \left(n - \dfrac{\left(a(t) + 2^{i_t}\right)}{2}\right)\left(2^{i_t} - 2^{j_t}\right), & k = n - \dfrac{\left(a(t) + 2^{i_t}\right)}{2} - 1, \\ & t = 1,\ldots,m-1, \\ \dfrac{a(t)\left(2^{j_{t-1}} - 2^{i_t}\right)}{2}, & k = \dfrac{a(t)}{2} - 1, \\ & t = 2,\ldots,m, \\ \left(\dfrac{N}{2} - 2^{r-1}\right)\left(2^r - 2^{i_1}\right), & k = \dfrac{N}{2} - 2^{r-1} - 1, \\ \left(n - \dfrac{N}{2}\right)\left(N - 2^r\right), & k = n - \dfrac{N}{2} - 1, \\ 0, & \textit{otherwise}, \end{cases} \end{aligned} \tag{65}$$

where $a(t) = N - 2^r + c(t)$ and $c(t)$ is defined in (14).

Proof. Only prove (a). Since

$$\#\{D_0\} = \sum_{l=1}^{m-1}\left(2^{i_l} - 2^{j_l}\right) + 2^{i_m} - 1 = n - N + 2^r, \tag{66}$$

one has $c(m) = n - (N - 2^r) - (2^{i_m} - 1)$. By (53) and Lemma 4, yields (a). □

The proof of (b) and (c) is similar to those of Theorem 11. The following example serves to show its application.

Example 14. Let $q = 8$, $r = 7$, and $N = 256$ and consider GMC $2^{135-127}$ design $D = D_0 \cup S_{87}$. Since $\#\{D_0\} = 2^3 - 1$, we have $i_1 = 3$. By (b) and (c) of Theorem 13, one gets

$$\begin{aligned} {}^{\#}_{1}C_2^{(k)}(D) &= \begin{cases} 128, & k = 7, \\ 7, & k = 64, \\ 0, & \text{otherwise}, \end{cases} \\ {}^{\#}_{2}C_2^{(k)}(D) &= \begin{cases} 896, & k = 6, \\ 7680, & k = 63, \\ 469, & k = 66, \\ 0, & \text{otherwise}. \end{cases} \end{aligned} \tag{67}$$

5. Concluding Remark

Based on construction of GMC 2^{n-m} designs with $5N/16 + 1 \le n \le N - 1$, we obtain the mathematical formulation to calculate the values of ${}^{\#}_{1}C_2$ and ${}^{\#}_{2}C_2$ in the AENP. These results are very useful to analyze the confounding information among lower-order factors of two-level GMC designs. For GMC 2^{n-m} designs satisfying $n \notin [5N/16 + 1, N - 1]$, some further studies in this direction are in progress.

Conflict of Interests

The authors declare that there is no conflict of interests regarding the publication of this paper.

Acknowledgments

This work was partially supported by the National Natural Science Foundation of China Grants 11171165, 10871104, and 11101074; Scientific Research Program of the Higher Education Institution of XinJiang Grant XJEDU2012S01; and Research Fund for the Doctoral Program of XinJiang University Grant BS130106. The authors are very grateful to the editor, the associate editor, and the referees for their valuable comments which have led to a substantial improvement in the paper.

References

[1] R. C. Zhang, P. Li, S. L. Zhao, and M. Y. Ai, "A general minimum lower-order confounding criterion for two-level regular designs," *Statistica Sinica*, vol. 18, no. 4, pp. 1689–1705, 2008.

[2] G. E. P. Box and J. S. Hunter, "The 2^{k-p} fractional factorial designs part I and II," *Technometrics*, vol. 3, pp. 311–458, 1961.

[3] A. Fries and W. G. Hunter, "Minimum aberration 2^{k-p} designs," *Technometrics*, vol. 22, no. 4, pp. 601–608, 1980.

[4] C. F. J. Wu and Y. Chen, "A graph-aided method for planning two-level experiments when certain interactions are important," *Technometrics*, vol. 34, pp. 162–175, 1992.

[5] D. X. Sun, *Estimation capacity and related topics in experimental designs [Ph. D. thesis]*, University of Waterloo, Waterloo, Canada, 1993.

[6] R. C. Zhang and Y. Cheng, "General minimum lower order confounding designs: an overview and a construction theory," *Journal of Statistical Planning and Inference*, vol. 140, no. 7, pp. 1719–1730, 2010.

[7] J. W. Hu and R. C. Zhang, "Some results on two-level regular designs with general minimum lower-order confounding," *Journal of Statistical Planning and Inference*, vol. 141, no. 5, pp. 1774–1782, 2011.

[8] J. Chen and M. Q. Liu, "Some theory for constructing general minimum lower order confounding designs," *Statistica Sinica*, vol. 21, no. 4, pp. 1541–1555, 2011.

[9] Y. Cheng and R. C. Zhang, "On construction of general minimum lower order confounding 2^{n-m} designs with $N/4+1 \leq n \leq 9N/32$," *Journal of Statistical Planning and Inference*, vol. 140, pp. 2384–2394, 2010.

[10] P. F. Li, S. L. Zhao, and R. C. Zhang, "A theory on constructing 2^{n-m} designs with general minimum lower order confounding," *Statistica Sinica*, vol. 21, no. 4, pp. 1571–1589, 2011.

[11] R. Mukerjee and C. F. J. Wu, *A Modern Theory of Factorial Designs*, Springer, New York, NY, USA, 2006.

Hindawi Publishing Corporation
The Scientific World Journal
Volume 2015, Article ID 497617, 12 pages
http://dx.doi.org/10.1155/2015/497617

Research Article

A Learning Framework of Nonparallel Hyperplanes Classifier

Zhi-Xia Yang,[1,2] Yuan-Hai Shao,[3] and Yao-Lin Jiang[1]

[1] *College of Mathematics and Systems Science, Xinjiang University, Urumqi 830046, China*
[2] *State Key Lab of Biochemical Engineering, Institute of Process Engineering, Chinese Academy of Sciences, Beijing 100190, China*
[3] *Zhijiang College, Zhejiang University of Technology, Hangzhou 310024, China*

Correspondence should be addressed to Yuan-Hai Shao; shaoyuanhai21@163.com

Received 21 June 2014; Revised 19 September 2014; Accepted 19 September 2014

Academic Editor: Qiankun Song

A novel learning framework of nonparallel hyperplanes support vector machines (NPSVMs) is proposed for binary classification and multiclass classification. This framework not only includes twin SVM (TWSVM) and its many deformation versions but also extends them into multiclass classification problem when different parameters or loss functions are chosen. Concretely, we discuss the linear and nonlinear cases of the framework, in which we select the hinge loss function as example. Moreover, we also give the primal problems of several extension versions of TWSVM's deformation versions. It is worth mentioning that, in the decision function, the Euclidean distance is replaced by the absolute value $|w^{\mathrm{T}}x + b|$, which keeps the consistency between the decision function and the optimization problem and reduces the computational cost particularly when the kernel function is introduced. The numerical experiments on several artificial and benchmark datasets indicate that our framework is not only fast but also shows good generalization.

1. Introduction

Classification problem is an important issue in machine learning and data mining, which is mainly comprised of binary and multiclass classification. Support vector machine (SVM), proposed by Burges [1] and Cortes and Vapnik [2], is an excellent tool for classification. In contrast with conventional artificial neural networks (ANNS) which aim at reducing empirical risk, SVM is principled and implements the structural risk minimization (SRM) that minimizes the upper bound of the generalization error [3–5]. Within a few years after its introduction, SVM has been successfully applied to pattern classification and regression estimation like face detection [6, 7], text categorization [8], time series prediction [9], bioinformatics [10], and so forth.

Recently, for binary classification, Mangasarian and Wild [11] proposed the generalized eigenvalue proximal support vector machine (GEPSVM) via two nonparallel hyperplanes. In their approach, the data points of each class are proximal to one of two nonparallel hyperplanes. The nonparallel hyperplanes are determined by eigenvectors corresponding to the smallest eigenvalues of two related generalized eigenvalue problems. Inspired by GEPSVM [11], Jayadeva et al. [12] developed twin SVM (TWSVM) with two nonparallel hyperplanes. However, the two hyperplanes are got by solving two quadratic programming (QP) problems, similar to the standard SVM. Furthermore, TWSVM differs from the standard SVM in fundamental way. In TWSVM, one solves a pair of smaller size QP problems rather than a single QP problem in the standard SVM. Therefore, TWSVM works faster than the standard SVM. Subsequently, there are many extensions for TWSVM including the improvements on TWSVM (TBSVM) [13], the least square TWSVM (LS-TWSVM) [14–17], nonparallel plane proximal classifier (NPPC) [18], smooth TWSVM [19], geometric algorithm [20], and twin support vector regression (TWSVR) [21]. TWSVM was also extended to deal with multiclassification TWSVM [22–24]. More precisely, in [22], TWSVM was extended straight from binary classification to multiclass classification, in which each primal problem covers all patterns except the patterns of the kth class in the constraints for the kth ($k = 1, 2, \ldots, K$) hyperplane. In [23], the authors extended TWSVM based on the idea of "one-versus-rest" (1-v-r) from binary classification to multiclass classification, in which there are two quadratic programming

(QP) problems for each reconstructing binary classification. However, they both have not kept the advantage of TWSVM which has lower computational complexity than that of the standard SVM. In [24], Yang et al. proposed multiple birth SVM (MBSVM) with much lower computational complexity than that of both [22, 23] by solving K smaller size of QP problems for K-class classification; only the empirical risk is considered like TWSVM. However, in TBSVM [13], the structural risk minimization principle is implemented by introducing the regularization term.

In this paper, we propose a novel learning framework of nonparallel hyperplanes support vector machines based on TWSVM and its extension versions, called NPSVMs, which not only provide a unified view for TWSVM and its many extension versions but also can deal with binary and multi-class classification problems. For binary classification, if the loss function is the hinge loss function, then the framework can become TWSVM [12] or TBSVM [13] with different parameters; if the loss function is the square loss function, then the framework is LS-TWSVM [14]; if the loss function is the convex combination of the linear and square loss functions, then the framework is NPPC [18]. Actually, we can also get smooth TWSVM [19] by replacing 2-norm with 1-norm in the framework. However, for multiclass classification, the framework does not directly extend, in which we switch the roles of the patterns of the k-th class and the rest class and replace "min" with "max" in the decision function. Moreover, we only use the absolute value $|w^{\mathrm{T}}x + b|$ rather than the Euclidean distance in the decision function due to the twofold reasons: reducing the computational cost particularly when the kernel function is introduced and making the consistency since it is the corresponding absolute value that appears in the primal problems. Concretely, we discuss the linear and nonlinear cases of the framework, in which we select the hinge loss function as example. Moreover, we also give the primal problems of extensions of LS-TWSVM, 1-norm LS-TWSVM, NPPC, and smooth TWSVM. Finally, the numerical experiments on several artificial and benchmark datasets indicate that our frameworks are not only fast but also show good generalization.

The paper is organized as follows. Section 2 introduces the brief reviews of SVMs. Section 3 proposes our frameworks, in which Section 3.1 discusses the linear framework, Section 3.2 extend into the nonlinear framework, Section 3.3 gives SOR algorithm for solving the hinge NPSVMs, and Section 3.4 discusses several other extension approaches. Finally, Section 4 deals with experimental results and Section 5 contains concluding remarks.

2. Brief Reviews of SVMs

2.1. Twin Support Vector Machine. Given the following training set for the binary classification:

$$\mathrm{T} = \{(x_1, y_1), \ldots, (x_l, y_l)\}, \tag{1}$$

where (x_i, y_i) is the ith data point, the input $x_i \in R^n$ is a pattern, the output $y_i \in \{1, 2\}$ is a class label, $i = 1, \ldots, l$, and l is the number of data points. In addition, let l_1 and l_2 be the number of data points in positive class and negative class, respectively, and $l = l_1 + l_2$. Furthermore, the matrices $A_1 \in R^{l_1 \times n}$ and $A_2 \in R^{l_2 \times n}$ consist of the l_1 inputs of Class 1 and the l_2 inputs of Class 2, respectively.

The gaol of TWSVM [12] is to find two nonparallel hyperplanes in n-dimensional input space:

$$x^{\mathrm{T}} w_1 + b_1 = 0, \tag{2}$$

$$x^{\mathrm{T}} w_2 + b_2 = 0, \tag{3}$$

such that one hyperplane is close to the patterns of one class and far away from the patterns of the other class to some extent. TWSVM is in spirit of GEPSVM [11]. But both of GEPSVM and TWSVM are different from the standard SVM. For TWSVM, each hyperplane is generated by solving a QP problem looking like the primal problem of the standard SVM. The primal problems of TWSVM can be presented as follows:

$$\begin{aligned} \min_{w_1, b_1, \xi_2} \quad & \frac{1}{2} \left\| A_1 w_1 + e_1 b_1 \right\|_2^2 + C_1 e_2^{\mathrm{T}} \xi_2, \\ \text{s.t.} \quad & -\left(A_2 w_1 + e_2 b_1\right) + \xi_2 \geq e_2, \\ & \xi_2 \geq 0; \end{aligned} \tag{4}$$

$$\begin{aligned} \min_{w_2, b_2, \xi_1} \quad & \frac{1}{2} \left\| A_2 w_2 + e_2 b_2 \right\|_2^2 + C_2 e_1^{\mathrm{T}} \xi_1, \\ \text{s.t.} \quad & \left(A_1 w_2 + e_1 b_2\right) + \xi_1 \geq e_1, \\ & \xi_1 \geq 0, \end{aligned} \tag{5}$$

where C_1 and C_2 are nonnegative parameters and e_1 and e_2 are vectors of ones of appropriate dimensions. In the QP problem (4), the objective function tends to keep hyperplane (2) close to the patterns of Class 1 and the constraints require the hyperplane (2) to be at a distance of at least 1 from the patterns of Class 2. The QP problem (5) has similar property. Moreover, we note that the constraints do not contain all patterns in the training set (1) but are determined by only the patterns of one class in both classes. Therefore, in [12], the authors claimed that TWSVM is approximately four times faster than the standard SVM.

Define $G = [A_2 \;\; e_2]$ and $H = [A_1 \;\; e_1]$. It has been shown that when both $G^{\mathrm{T}}G$ and $H^{\mathrm{T}}H$ are positive definites, the Wolfe duals of (4) and (5) are written as follows:

$$\begin{aligned} \max_{\alpha_2} \quad & e_2^{\mathrm{T}} \alpha_2 - \frac{1}{2} \alpha_2^{\mathrm{T}} G \left(H^{\mathrm{T}} H\right)^{-1} G^{\mathrm{T}} \alpha_2, \\ \text{s.t.} \quad & 0 \leq \alpha_2 \leq C_1, \end{aligned} \tag{6}$$

$$\begin{aligned} \max_{\alpha_1} \quad & e_1^{\mathrm{T}} \alpha_1 - \frac{1}{2} \alpha_1^{\mathrm{T}} H \left(G^{\mathrm{T}} G\right)^{-1} H^{\mathrm{T}} \alpha_1, \\ \text{s.t.} \quad & 0 \leq \alpha_1 \leq C_2, \end{aligned} \tag{7}$$

respectively, where α_2 and α_1 are Lagrangian multipliers.

In order to avoid the possible ill-conditioning of $H^{\mathrm{T}}H$ and $G^{\mathrm{T}}G$, TWSVM introduces a term ϵI ($\epsilon > 0$), where I

is an identity matrix of appropriate dimensions. Thus, the nonparallel hyperplanes (2) and (3) can be obtained from the solutions α_1 and α_2 of the QP problems (6) and (7). Consider

$$z_1 = -\left(H^{\mathrm{T}}H + \epsilon I\right)^{-1} G^{\mathrm{T}}\alpha_2, \qquad z_2 = \left(G^{\mathrm{T}}G + \epsilon I\right)^{-1} H^{\mathrm{T}}\alpha_1, \tag{8}$$

where $z_k = \left[w_k^{\mathrm{T}} \;\; b_k\right]^{\mathrm{T}}$, $k = 1, 2$. Moreover, a new pattern $x \in R^n$ is assigned to Class k ($k = 1, 2$), depending on which of the two nonparallel hyperplanes given by (2) and (3) lies closer to; that is,

$$f(x) = \arg\min_{k=1,2} \frac{\left|w_k^{\mathrm{T}}x + b_k\right|}{\left\|w_k\right\|_2}. \tag{9}$$

2.2. Multiple Birth Support Vector Machine. Given the training set

$$\mathrm{T} = \left\{\left(x_1, y_1\right), \ldots, \left(x_l, y_l\right)\right\}, \tag{10}$$

where the input $x_i \in R^n$, $i = 1, \ldots, l$, is the pattern and the output $y_i \in \{1, \ldots, K\}$ is the class label. The task is to seek K hyperplanes,

$$w_k^{\mathrm{T}}x + b_k = 0, \quad k = 1, \ldots, K, \tag{11}$$

and assign the class label according to which hyperplane a new pattern is farthest from.

For convenience, denote the number of data points of the kth class in the training set (10) as l_k and define the following matrixes: the patterns belonging to the kth class are represented by the matrix $A_k \in R^{l_k \times n}$, $k = 1, \ldots, K$. In addition, define the matrix

$$B_k = \left[A_1^{\mathrm{T}}, \ldots, A_{k-1}^{\mathrm{T}}, A_{k+1}^{\mathrm{T}}, \ldots, A_K^{\mathrm{T}}\right]^{\mathrm{T}}; \tag{12}$$

that is, $B_k \in R^{(l-l_k)\times n}$ consists of the patterns belonging to all classes except the kth class, $k = 1, \ldots, K$. The primal problems of MPSVM [24] are comprised of the following K QP problem:

$$\begin{aligned} \min_{w_k, b_k, \xi_k} \quad & \frac{1}{2}\left\|B_k w_k + e_{k1} b_k\right\|^2 + C_k e_{k2}^{\mathrm{T}} \xi_k, \\ \text{s.t.} \quad & \left(A_k w_k + e_{k2} b_k\right) + \xi_k \geq e_{k2}, \quad \xi_k \geq 0, \end{aligned} \tag{13}$$

where $e_{k1} \in R^{(l-l_k)}$ and $e_{k2} \in R^{l_k}$ are the vectors of ones, ξ_k is the slack variable, and $C_k > 0$ is the penalty parameter, $k = 1, \ldots, K$. The dual problem of QP problem (13) is formulated as follows:

$$\begin{aligned} \max_{\alpha_k} \quad & e_{k2}^{\mathrm{T}}\alpha_k - \frac{1}{2}\alpha_k G_k \left(H_k^{\mathrm{T}} H_k\right)^{-1} G_k^{\mathrm{T}}\alpha_k, \\ \text{s.t.} \quad & 0 \leq \alpha_k \leq C_k, \end{aligned} \tag{14}$$

where the penalty parameter $C_k > 0$, $H_k = \left[B_k \;\; e_{k1}\right]$, and $G_k = \left[A_k \;\; e_{k2}\right]$, $k = 1, 2, \ldots, K$. Similarly, in order to avoid the possibility of the ill-conditioning of the matrix $H_k^{\mathrm{T}}H_k$ in some situations, one introduces a regularization term ϵI, where $\epsilon > 0$ is a fixed small scalar and I is the identity matrix with appropriate size.

After getting the solution $\left[w_k^{\mathrm{T}} \;\; b_k\right]^{\mathrm{T}} = -(H_k^{\mathrm{T}}H_k + \epsilon I)^{-1}G_k^{\mathrm{T}}\alpha_k$ to the above QP problem (13) with $k = 1, \ldots, K$, a new pattern $x \in R^n$ is assigned to class k ($k \in \{1, \ldots, K\}$), depending on which of the K hyperplanes given by (11) lies farthest from; that is, the decision function is represented as

$$f(x) = \arg\max_{k=1,\ldots,K} \frac{\left|w_k^{\mathrm{T}}x + b_k\right|}{\left\|w_k\right\|_2}, \tag{15}$$

where $|\cdot|$ is the absolute value.

3. The Framework of Nonparallel Hyperplanes Classifiers

In this section, we propose a learning framework of nonparallel hyperplanes classifier, which gives a unified form for TWSVM and its many extension versions and extend them into multiclass classification problem. We first develop the linear framework and then extend it to nonlinear framework.

3.1. Linear Framework. Given the training set (10), the task is to find K nonparallel hyperplanes:

$$w_k^{\mathrm{T}}x + b_k = 0, \quad k = 1, 2, \ldots, K, \tag{16}$$

one for each class. For obtaining the K unknown hyperplanes, we construct the following standard framework for each unknown hyperplane:

$$\begin{aligned} \min_{w_k, b_k} & \frac{1}{2}\left\|B_k w_k + e_{k2} b_k\right\|_2^2 + \frac{1}{2}C_k^*\left(\left\|w_k\right\|_2^2 + b_k^2\right) \\ & + C_k e_{k1}^{\mathrm{T}} L\left(e_{k1}, A_k w_k + e_{k1} b_k\right), \end{aligned} \tag{17}$$

where the matrix A_k is comprised of the patterns in the kth class, the matrix B_k is defined (12), $C_k^* \geq 0$ and $C_k > 0$ are the parameters, e_{k1} and e_{k2} are vectors of ones of appropriate dimensions, $k = 1, 2, \ldots, K$, and $L(\cdot, \cdot)$ is the loss function (e.g., square loss, hinge loss, etc.). In the optimization problem (17), the first term approximatively minimizes the sum of the squared Euclidean distances from the patterns except for the kth class to hyperplanes; the second term is the Tikhonov regularization term [25] and can implement the structural risk minimization principle like TBSVM [13]; the third term constitutes the loss function which is defined different loss functions corresponding to different models.

For a new pattern $x \in R^n$, we assign to class k ($k = 1, 2, \ldots, K$) according to the following decision function:

$$f(x) = \arg\max_{k=1,2,\ldots,K} \left|w_k^{\mathrm{T}}x + b_k\right|, \tag{18}$$

where $|\cdot|$ is the absolute value. Note that we only use the absolute value $|w^{\mathrm{T}}x + b|$ in the decision function. There are two main reasons: one is that the first term of the optimization problem (17) just minimizes the sum of the square rather

than the sum of square Euclidean distance from the patterns to hyperplanes, so it should keep consistency between the optimization problem and the decision function; another is that it reduces the computational cost particularly when the kernel function is introduced afterwards.

In fact, if $K = 2$, the parameter C_k^* is equal to 0, and the loss function is hinge loss function, that is, $L(1, g(x)) = \max(0, 1-g(x))$, then the optimization problem (17) becomes TWSVM [12]. Moreover, if the parameter $C_k^* > 0$ is alterable, then it is TBSVM [13]. And if the loss function is the square loss function, that is, $L(1, g(x)) = (1 - g(x))^2$, it is LS-TWSVM [14]. And if the loss function is a convex combination of linear and square loss, that is, $L(1, g(x)) = \delta(1 - g(x)) + (1 - \delta)(1 - g(x))^2$, where $\delta \in (0, 1)$, then it is NPPC [18]. Other extension versions of TWSVM also can be contained in the optimization problem (17), for instance, smooth TWSVM, 1-norm LS-TWSVM [17], and so forth, in which we just need to select proper norm or loss function.

More importantly, our framework can solve multiclass classification problem, which is extension of TWSVM, TBSVM, LS-TWSVM, NPPC, and so forth. It should be pointed out that our framework is not straight extension of TWSVM and its deformation versions. Concretely, from the optimization problem (17), we can see that the first term contains the patterns except for those of the kth class and the third term just involves the patterns of the kth class. This strategy cannot lead to significant increase of the complexity of the optimization when the number K of classes increases. We will dwell on in specific algorithm afterwards.

Now, we give the detailed algorithm to the hinge loss function as an example, called hinge NPSVM (HNPSVM). And then the optimization problem (17) is the following formulation with the hinge loss function:

$$\begin{aligned}\min_{w_k,b_k} &\frac{1}{2}\left\|B_k w_k + e_{k2} b_k\right\|_2^2 + \frac{1}{2}C_k^*\left(\left\|w_k\right\|_2^2 + b_k^2\right)\\ &+ C_k e_{k1}^{\mathrm{T}} \max\left(0, e_{k1} - \left(A_k w_k + e_{k1} b_k\right)\right),\end{aligned} \tag{19}$$

where the matrix A_k is comprised of the patterns in the kth class, the matrix B_k is defined (12), $C_k^* \geq 0$ and $C_k > 0$ are the parameters, e_{k1} and e_{k2} are vectors of ones of appropriate dimensions, and $k = 1, 2, \ldots, K$. Actually, the problem is equivalent to the following quadratic programming:

$$\begin{aligned}\min_{w_k,b_k,\xi_k} \quad & \left\|B_k w_k + e_{k2} b_k\right\|_2^2 + \frac{1}{2}C_k^*\left(\left\|w_k\right\|_2^2 + b_k^2\right) + C_k e_{k1}^{\mathrm{T}} \xi_k,\\ \text{s.t.} \quad & \left(A_k w_k + e_{k1} b_k\right) + \xi_k \geq e_{k1}, \quad \xi_k \geq 0,\end{aligned} \tag{20}$$

where the matrix A_k is comprised of the patterns in the kth class, the matrix B_k is defined (12), $C_k^* \geq 0$ and $C_k > 0$ are the parameters, e_{k1} and e_{k2} are vectors of ones of appropriate dimensions, and $k = 1, 2, \ldots, K$.

In fact, for $k = 1, 2, \ldots, K$, we have K QP problems like (20). In particular, when K is equal to 2, that is, $k = 1, 2$, the QP problems (4) and (5) can be obtained as a special case of (20) with $C_k^* = 0$. For simplicity, assume that the number of each class points is almost balanced; namely, the number of the kth class is $l_k = l/K$. Then, note that the constraints just involve the patterns of the kth class, so the complexity of the the problem (20) is no more than $(l_k)^3 = (l/K)^3$. However, if TWSVM is directly extended to multiclass classification case like [22], we will get a different optimization problem, in which the roles of patterns of the kth class and the rest class are switched. Thus, the complexity of the optimization problem will increase significantly and is determined by the patterns except for the patterns of the kth class in the training set (10), which is no more than $((K-1)(l/K))^3$. Obviously, our approach is approximately $(K-1)^3$ times faster than the model in [22]. On the other hand, when the number of each class points is unbalanced, our apprach still is faster than the model in [22] because the complexity of our optimization problem just is decided by the number of the patterns of the kth class rather than the patterns of the rest classes. Therefore, our HNPSVM keeps the computation complexity low.

It is well known that the solution of primal problem (20) is obtained from the solutions of their dual problems. So we now derive their dual problems. The Lagrangian function of the problem (20) is given by

$$\begin{aligned}&L\left(w_k, b_k, \xi_k, \alpha_k, \eta_k\right)\\ &\quad = \frac{1}{2}\left\|B_k w_k + e_{k2} b_k\right\|_2^2 + \frac{1}{2}C_k^*\left(\left\|w_k\right\|_2^2 + b_k^2\right) + C_k e_{k1} \xi_k\\ &\qquad - \alpha_k^{\mathrm{T}}\left(\left(A_k w_k + e_{k1} b_k\right) + \xi_k - e_{k1}\right) - \eta_k^{\mathrm{T}} \xi_k,\end{aligned} \tag{21}$$

where α_k, η_k are nonnegative Lagrange multiplier vectors. The Karush-Kuhn-Tucker (KKT) necessary and sufficient optimality conditions [26] for the QP problem (20) are given by

$$\nabla_{w_k} L = B_k^{\mathrm{T}}\left(B_k w_k + e_{k2} b_k\right) + C_k^* w_k - A_k^{\mathrm{T}} \alpha_k = 0, \tag{22}$$

$$\nabla_{b_k} L = e_{k2}^{\mathrm{T}}\left(B_k w_k + e_{k2} b_k\right) + C_k^* b_k - e_{k1}^{\mathrm{T}} \alpha_k = 0, \tag{23}$$

$$\nabla_{\xi_k} L = C_k e_{k1} - \alpha_k - \eta_k = 0, \tag{24}$$

$$\left(A_k w_k + e_{k1} b_k\right) + \xi_k \geq e_{k1}, \quad \xi_k \geq 0, \tag{25}$$

$$-\alpha_k^{\mathrm{T}}\left(\left(A_k w_k + e_{k1} b_k\right) + \xi_k - e_{k1}\right) = 0, \qquad \eta_k^{\mathrm{T}} \xi_k = 0, \tag{26}$$

$$\alpha_k \geq 0, \qquad \eta_k \geq 0. \tag{27}$$

Since $\eta_k \geq 0$, according to (24), we have

$$0 \leq \alpha_k \leq C_k. \tag{28}$$

Next, from (22) and (23), we can obtain

$$\left(\left[B_k^{\mathrm{T}} \;\; e_k^{\mathrm{T}}\right]\left[B_K \;\; e_k\right] + C_k^* I\right)\left[w_k^{\mathrm{T}} \;\; b_k\right]^{\mathrm{T}} - \left[A_k^{\mathrm{T}} \;\; e_k^{\mathrm{T}}\right]\alpha_k = 0, \tag{29}$$

where I is an identity matrix of appropriate dimensions. Let $v_k = \left[w_k^{\mathrm{T}} \;\; b_k\right]^{\mathrm{T}}$; (29) can be written as

$$\begin{aligned}&\left(H_k^{\mathrm{T}} H_k + C_k I\right) v_k - G_k^{\mathrm{T}} \alpha_k = 0,\\ &\text{or } v_k = \left(H_k^{\mathrm{T}} H_k + C_k I\right)^{-1} G_k^{\mathrm{T}} \alpha_k,\end{aligned} \tag{30}$$

where $H_k = [B_k \;\; e_{k2}]$ and $G_k = [A_k \;\; e_{k1}]$. And then putting (30) into the Lagrangian function (21) and using (22)–(28), we can get the dual problem of the primal problem (20):

$$\begin{aligned} \max_{\alpha_k} \quad & e_{k1}^{\mathrm{T}}\alpha_k - \frac{1}{2}\alpha_k^{\mathrm{T}} H_k \left(G_k^{\mathrm{T}} G_k + C_k^* I\right)^{-1} H_k^{\mathrm{T}} \alpha_k, \\ \text{s.t.} \quad & 0 \le \alpha_k \le C_k, \end{aligned} \tag{31}$$

where $C_k^* > 0$ and $C_k > 0$ are parameters and $k = 1, 2, \ldots, K$. Obviously, if we have the solution of the QP problem (31), then we obtain the K nonparallel hyperplanes (16) by (30).

It is worth mentioning that the parameter C_k^* replaces ϵ as in (8), so C_k^* is no longer a fixed small scalar but a weighting factor which determines the trade-off between the regularization term and the empirical risk in the problem (20). Therefore, the high and low of the value of C_k^* reflects the structure of minimization principle and our HNPSVM includes MBSVM.

3.2. Nonlinear Framework. Similarly, we also extend the linear framework of NPSVMs to nonlinear case. For a K-class classification (10), our goal is to find K kernel-generated hyperplanes:

$$K\left(x, A^{\mathrm{T}}\right) u_k + b_k = 0, \qquad k = 1, \ldots, K, \tag{32}$$

where $A = [A_1, \ldots, A_k]$ and $K(x, A^{\mathrm{T}})$ is an appropriately chosen kernel function.

In order to obtain the K hyperlanes (32), we construct the following framework formulation:

$$\begin{aligned} \min_{u_k, b_k} & \frac{1}{2}\left\|K(B_k^{\mathrm{T}}, A^{\mathrm{T}}) u_k + e_{k2} b_k\right\|_2^2 + \frac{1}{2} C_k^* \left(\|u_k\|_2^2 + b_k^2\right) \\ & + C_k e_{k1}^{\mathrm{T}} L\left(e_{k1}, K\left(A_k^{\mathrm{T}}, A^{\mathrm{T}}\right) u_k + e_{k1} b_k\right), \end{aligned} \tag{33}$$

where the matrix A_k is comprised of the patterns in the kth class, the matrix B_k is defined (12), $C_k^* \ge 0$ and $C_k > 0$ are the parameters, e_{k1} and e_{k2} are vectors of ones of appropriate dimensions, $k = 1, 2, \ldots, K$, and $L(\cdot, \cdot)$ is the loss function (e.g., square loss or hinge loss, etc.). Similarly, as discussed in the last subsection, the problem (33) can be reduced to the nonlinear formulations of the difference approaches (e.g., TWSVM, TBSVM, LS-TWSVM, NPPC, etc.) when the difference loss functions or parameters are selected for $K = 2$.

A new pattern $x \in R^n$ is assigned to the kth class by the following decision functions:

$$f(x) = \arg \max_{k=1,\ldots,K} \left|K\left(x, A^{\mathrm{T}}\right) u_k + b_k\right|, \tag{34}$$

where $|\cdot|$ is the absolute value. Note that, in this decision function (34), we just compute the absolute value rather than Euclidean distance from the pattern x to the hyperplanes. This strategy reduces the complexity of computation because Euclidean distance should be $|K(x, A^{\mathrm{T}}) u_k + b_k| / \sqrt{u_k^{\mathrm{T}} K(A^{\mathrm{T}}, A^{\mathrm{T}}) u_k}$ from the pattern x to the kth hyperplanes. Thus, the decision function (34) not only saves the computation quantity but also keeps the consistency with the first term of the problem (33).

Now, we still select the hinge loss function as example. Then, the problem (33) can be formulated as follows:

$$\begin{aligned} \min_{u_k, b_k, \xi_k} \quad & \frac{1}{2}\left\|K\left(B_k^{\mathrm{T}}, A^{\mathrm{T}}\right) u_k + e_{k2} b_k\right\|_2^2 \\ & + \frac{1}{2} C_k^* \left(\|u_k\|_2^2 + b_k^2\right) + C_k e_{k1}^{\mathrm{T}} \xi_k, \\ \text{s.t.} \quad & \left(K\left(A_k^{\mathrm{T}}, A^{\mathrm{T}}\right) u_k + e_{k1} b_k\right) + \xi_k \ge e_{k1}, \qquad \xi_k \ge 0, \end{aligned} \tag{35}$$

where the matrix A_k is comprised of the patterns in the kth class, the matrix B_k is defined by (12), $C_k^* > 0$ and $C_k > 0$ are parameters, e_{k1} and e_{k2} are vectors of ones of appropriate dimensions, and $k = 1, 2, \ldots, K$. Similarly, derived process with the linear case, its dual problem is formulated as:

$$\begin{aligned} \max_{\alpha_k} \quad & e_{k1}^{\mathrm{T}}\alpha_k - \frac{1}{2}\alpha_k^{\mathrm{T}} R_k \left(S_k^{\mathrm{T}} S_k + C_k^* I\right) R_k^{\mathrm{T}} \alpha_k, \\ \text{s.t.} \quad & 0 \le \alpha_k \le C_k, \end{aligned} \tag{36}$$

where $C_k^* > 0$ and $C_k > 0$ are parameters, $R_k = \left[K(A_k^{\mathrm{T}}, A^{\mathrm{T}}) \;\; e_{k1}\right]$, $S_k = \left[K(B_k^{\mathrm{T}}, A^{\mathrm{T}}) \;\; e_{k2}\right]$, and $k = 1, 2, \ldots, K$. And the augmented vector $z_k = [u_k \;\; b_k]^{\mathrm{T}}$ is given by $z_k = \left(S_k^{\mathrm{T}} S_k + C_k^* I\right)^{-1} R_k^{\mathrm{T}} \alpha_k$.

3.3. SOR Algorithm. In our HNPSVMs, the QP problems (31) and (36) can be rewritten as the following unified forms:

$$\begin{aligned} \min_{\alpha} \quad & \frac{1}{2}\alpha^{\mathrm{T}} Q \alpha - e^{\mathrm{T}} \alpha, \\ \text{s.t.} \quad & 0 \le \alpha \le C, \end{aligned} \tag{37}$$

where $Q \in R^{m \times m}$ is positive definite. For example, the above problem becomes the problem (36), when $Q = R_k(S_k^{\mathrm{T}} S_k + C_k^* I)^{-1} R_k^{\mathrm{T}}$, $C = C_k$.

The above problem (37) can be solved efficiently by the following successive overrelaxation (SOR) algorithm; see [27].

Algorithm 1. SOR for the QP problem (36) is as follows.

(1) Select the parameter $t_k \in (0, 2)$ and the initial value $\alpha_k^0 \in R^{m_k}$.

(2) Suppose that α_k^r is obtained by the r times iterate; compute α_k^{r+1} according to the following iterate formula:

$$\alpha_k^{r+1} = \left(\alpha_k^r - t_k D_k^{-1} \left(Q_k \alpha_k^r - e_{k2} + L_k \left(\alpha_k^{r+1} - \alpha_k^r\right)\right)\right)_\sharp, \tag{38}$$

where $Q = R_k \left(S_k^{\mathrm{T}} S_k + C_k^* I\right)^{-1} R_k^{\mathrm{T}}$. And define $L_k + D_k + L_k^{\mathrm{T}} = Q_k$, where $L_k \in R^{m_k \times m_k}$ and $D_k \in R^{m_k \times m_k}$ are the strictly lower triangular matrix and the diagonal matrix, respectively.

(3) Stop if $\|\alpha_k^{r+1} - \alpha_k^r\|$ is less than some desired tolerance. Else, replace α_k^r by α_k^{r+1} and r by $r+1$ and go to 2.

SOR is an excellent TWSVM solver, because it can process efficiently very large datasets that need not reside in memory. Furthermore, it has been proved that this algorithm converges linearly to a solution in [27, 28]. It should be pointed out that we employ the Sherman-Morrison-Woodbury formula [29] for the inversion of matrix $(S_k^{\mathrm{T}} S_k + C_k^* I)$ and, hence, need only to invert matrix with a lower order l_k, instead of the order l. Further, in practise, if the number of patterns in the kth classe is large, then the rectangular kernel technique [30, 31] can be applied to reduce the dimensionality of our nonlinear classifiers.

3.4. Several Others Approaches. In this section, we briefly give several extension versions based on our framework by selecting different loss function or replacing 2-norm.

First, if the square loss function is chosen, that is, $L(1, g(x)) = (1 - g(x))^2$, then we can get the following formulation from the framework (17):

$$\begin{aligned} \min_{w_k, b_k} \quad & \frac{1}{2}\|B_k w_k + e_{k2} b_k\|_2^2 + \frac{1}{2} C_k^* \left(\|w_k\|_2^2 + b_k^2\right) + C_k \xi_k^{\mathrm{T}} \xi_k, \\ \text{s.t.} \quad & \left(A_k w_k + e_{k1} b_k\right) + \xi_k = e_{k1}, \end{aligned} \tag{39}$$

where the matrix A_k is comprised of the patterns in the kth class and the matrix B_k is defined by (12), $C_k^* > 0$ and $C_k > 0$ are parameters, e_{k1} and e_{k2} are vectors of ones of appropriate dimensions, and $k = 1, 2, \ldots, K$. This is extension version of LS-TWSVM [14].

Second, if we replace 2-norm with 1-norm in the problem (39), then we can get the extension of 1-norm LS-TWSVM [17] as follows:

$$\begin{aligned} \min_{w_k, b_k} \quad & \|B_k w_k + e_{k2} b_k\|_1 + C_k^* \left(\|w_k\|_1 + |b_k|\right) + C_k \|\xi_k\|_1, \\ \text{s.t.} \quad & \left(A_k w_k + e_{k1} b_k\right) + \xi_k = e_{k1}, \end{aligned} \tag{40}$$

where the matrix A_k is comprised of the patterns in the kth class, the matrix B_k is defined by (12), $C_k^* > 0$ and $C_k > 0$ are parameters, e_{k1} and e_{k2} are vectors of ones of appropriate dimensions, and $k = 1, 2, \ldots, K$.

Third, if the loss function is a convex combination of linear and square loss, that is, $L(1, g(x)) = \delta(1 - g(x)) + (1 - \delta)\left(1 - g(x)\right)^2$, where $\delta \in (0, 1)$, then we can obtain extension version of NPPC [18] as follows:

$$\begin{aligned} \min_{w_k, b_k} \quad & \frac{1}{2}\|B_k w_k + e_{k2} b_k\|_2^2 + \frac{1}{2} C_k^* \left(\|w_k\|_2^2 + b_k^2\right) \\ & + C_k \left(\delta e_{k1}^{\mathrm{T}} \xi_k + (1 - \delta) \xi_k^{\mathrm{T}} \xi_k\right), \\ \text{s.t.} \quad & \left(A_k w_k + e_{k1} b_k\right) + \xi_k = e_{k1}, \end{aligned} \tag{41}$$

where the matrix A_k is comprised of the patterns in the kth class, the matrix B_k is defined by (12), $C_k^* > 0$ and $C_k > 0$ are parameters, e_{k1} and e_{k2} are vectors of ones of appropriate dimensions, and $k = 1, 2, \ldots, K$.

Forth, if the square hinge loss function is selected, that is, $L(1, g(x)) = \left(\max\left(0, 1 - g(x)\right)\right)^2$, then we can get the extension version of smooth TWSVM as follows:

$$\begin{aligned} \min_{w_k, b_k, \xi_k} \quad & \|B_k w_k + e_{k2} b_k\|_2^2 + \frac{1}{2} C_k^* \left(\|w_k\|_2^2 + b_k^2\right) + C_k \xi_k^{\mathrm{T}} \xi_k, \\ \text{s.t.} \quad & \left(A_k w_k + e_{k1} b_k\right) + \xi_k \geq e_{k1}, \qquad \xi_k \geq 0, \end{aligned} \tag{42}$$

where the matrix A_k is comprised of the patterns in the kth class, the matrix B_k is defined by (12), $C_k^* > 0$ and $C_k > 0$ are parameters, e_{k1} and e_{k2} are vectors of ones of appropriate dimensions, and $k = 1, 2, \ldots, K$.

These approaches have the same decision function (18) and can be extended into nonlinear case. And their solving methods can construct based on their binary algorithms.

4. Numerical Experiments

In this section, we present experimental results of our binary HNPSVM (BHNPSVM) and multiclass HNPSVM (MHNPSVM) on both artificial and benchmark datasets. In experiments, we focus on the comparison between our methods and some state-of-the-art classification methods, including SVM, GEPSVM, TWSVM, "1-v-1," "1-v-r," and MBSVM. All the classification methods are implemented in MATLAB 7.0 [32] environment on a PC with Intel P4 processor (2.9 GHz) with 1 GB RAM. In order to give the fastest training speed, we employ Libsvm [33] to implement the SVM, "1-v-1," and "1-v-r". Our BHNPSVM and MHNPSVM and TWSVM and MBSVM are implemented using SOR technique; GEPSVM is implemented by simple MATLAB functions like "eig," respectively. As for the problem of selecting parameters, we employ standard 10-fold cross-validation technique [34]. Furthermore, the parameters for all methods are selected from the set $\{2^{-8}, \ldots, 2^8\}$.

4.1. Toy Examples. Firstly, we consider a simple two-dimensional "Cross Planes" dataset as Example 1, which was tested in [11, 13] to indicate that nonparallel hyperplanes classifiers can handle the cross planes dataset much better compared with parallel ones. Now, we show that our BHNPSVM also can handle cross-planes type data well due to use of our decision function. The "Cross Planes" dataset is generated by perturbing points lying on two intersecting lines. Figures 1(a)–1(d) show the dataset and the linear classifiers obtained by SVM, GEPSVM, TWSVM, and our BNPSVM. It is easy to see that the result of our BNPSVM is more reasonable than that of SVM, and better than that of GEPSVM and TWSVM. In addition, we list the accuracy and CPU time for these four classifiers in Table 1. From Table 1, we can see that our BNPSVM obtains the best accuracy while not the slowest computing time.

Secondly, we consider a two-dimensional three-class dataset as Example 2 to show the operating mechanism of our MNPSVM and other multiple-class classifiers. The three-class dataset is generated by perturbing points lying on three

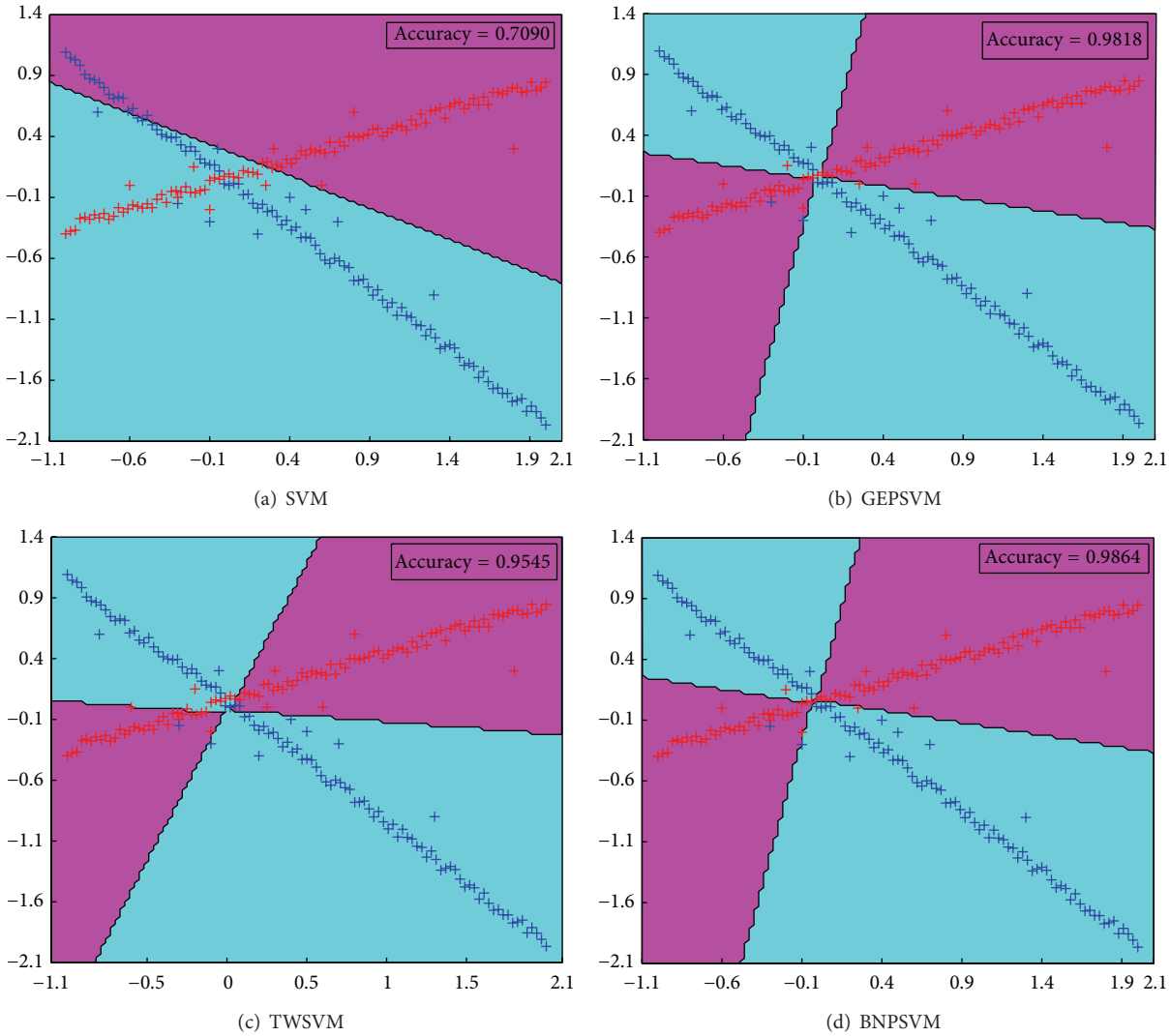

(a) SVM (b) GEPSVM (c) TWSVM (d) BNPSVM

Figure 1: Results of linear SVM, GEPSVM, TWSVM, and BNPSVM on Example 1 dataset.

Table 1: Tenfold testing percentage test set accuracy (%) on example data sets.

Data set	SVM Accuracy % Time (s)	GEPSVM Accuracy % Time (s)	TWSVM Accuracy % Time (s)	BHNPSVM Accuracy % Time (s)
Example 1 (202 × 2)	70.90 0.122	95.45 0.0005	98.18 0.0064	**98.64** 0.0052
Data set	"1-v-1" Accuracy % Time (s)	"1-v-r" Accuracy % Time (s)	MBSVM Accuracy % Time (s)	MHNPSVM Accuracy % Time (s)
Example 2 (330 × 2)	87.33 0.098	86.67 0.0006	89.33 0.0079	**90.67** 0.0095

intersecting lines. Figures 2(a)–2(d) show the dataset and the linear classifiers obtained by "1-v-1," "1-v-r," MBSVM, and MHNPSVM. It is easy to see that the result of MBSVM and MHNPSVM is more reasonable than that of "1-v-1" and "1-v-r." We also list the accuracy and CPU time of Example 2 for these four classifiers in Table 1. From Table 1, we can see that our MHNPSVM obtains the best accuracy in all these two examples, indicating that our MHNPSVM is suitable for both "Cross Planes" and multiclass problems.

4.2. Benchmark Datasets. In order to further compare our methods with others, we examine nine binary-class datasets

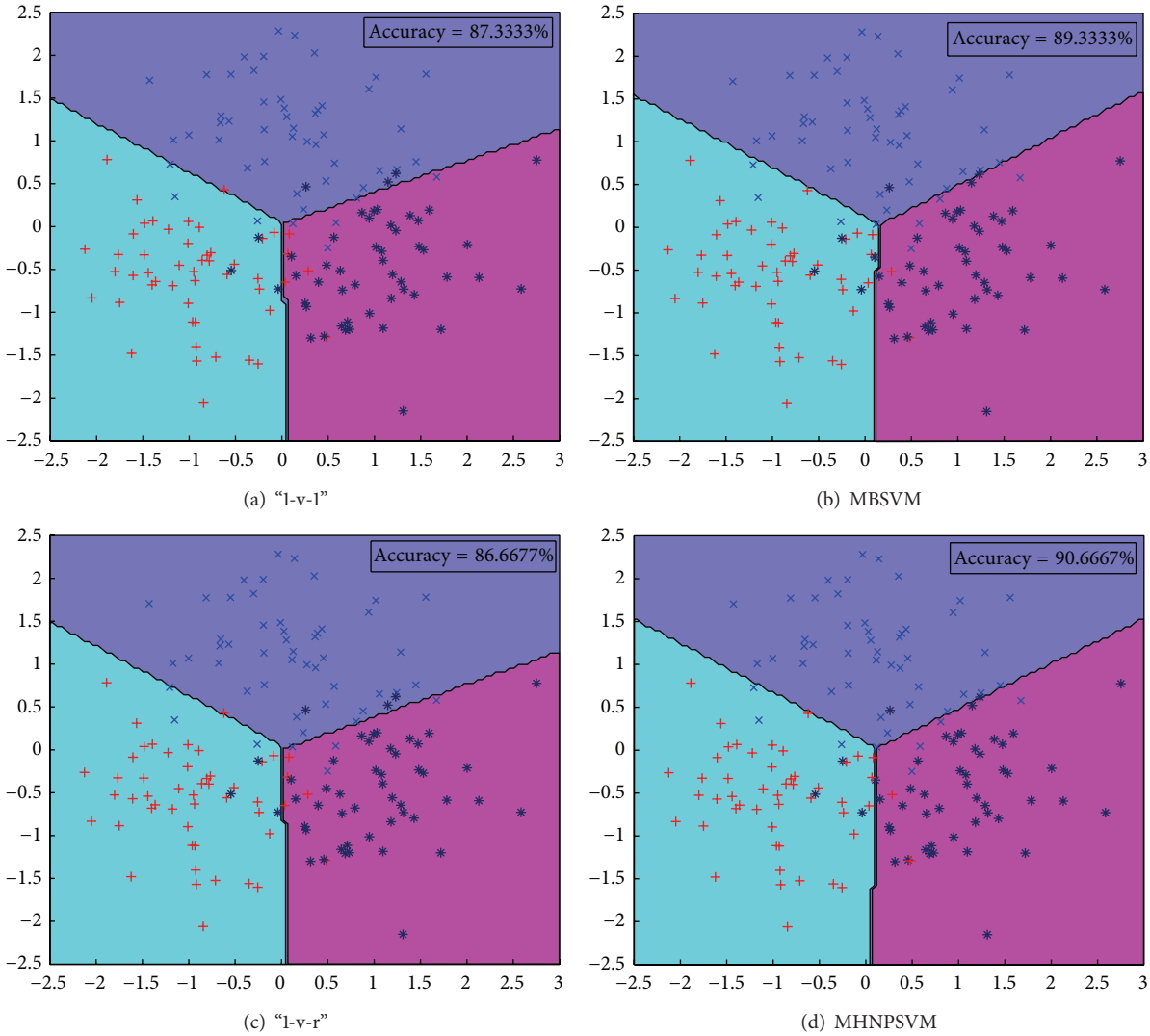

(a) "1-v-1" (b) MBSVM

(c) "1-v-r" (d) MHNPSVM

Figure 2: Results of linear "1-v-1," "1-v-r," MBSVM, and MHNPSVM on Example 2 dataset.

and nine multiclass datasets used by [12, 35], from the UCI Repository of machine learning database [36]. Table 2 gives the details of these eighteen datasets.

In order to compare the behavior of our linear BHNPSVM with SVM, GEPSVM, and TWSVM, the numerical experimental results for binary-class UCI datasets are summarized in Table 3. In Table 3, the classification accuracy and computation time are listed. In Table 3, the best accuracy is shown by bold figures. It is easy to see that most of the accuracies of our linear BHNPSVM are better than linear SVM, GEPSVM, and TWSVM on these datasets. It can also be seen that our BHNPSVM is a little faster than TWSVM and is competitive with SVM (implements by Libsvm). We also list the mean accuracy and mean time for these four classifiers. Our BHNPSVM gains the the highest mean accuracy while faster training speed than TWSVM.

Table 4 is concerned with our kernel BHNPSVM, SVM, GEPSVM, and TWSVM on binary-class UCI datasets. The Gaussian kernel $K(x, x') = e^{-\mu\|x-x'\|^2}$ is used. The kernel parameter μ is also obtained through searching from the range from 2^{-8} to 2^{8}. The training CPU times for these four classifiers are also listed. The results in Table 4 are similar to those appearing in Table 3 and therefore confirm the above conclusion further.

In order to compare the behavior of our MHNPSVM with other multiple-class classifiers, we compare our MHNPSVM with "1-v-1," "1-v-r," and MBSVM, the linear results of numerical experiments on multiclass UCI datasets are summarized in Table 5. In Table 5, the classification accuracy and computation time are listed.

From Table 5, we can see that the accuracy of linear MHNPSVM is significantly better than linear MBSVM on all 9 UCI datasets. We also obtain that MHNPSVM and MBSVM are almost same fast because they both solve two SOR algorithms instead of two QP problems with the same size. In contrast, classification accuracy of "1-v-1" and "1-v-r" is no statistical difference with MHNPSVM for all cases except for vowel dataset, and "1-v-1" and "1-v-r" are a bit lower than

Table 2: The detailed characteristics of the datasets.

Data	#Ins	#Fea	#class	Data	#Ins	#Fea	#class
Hepatitis	155	19	2	Votes	435	16	2
WBPC	198	34	2	Sonar	208	60	2
Heart-statlog	270	13	2	BUPA	345	6	2
Pima-Indian	768	8	2	CMC	1473	9	2
Australian	690	14	2	Iris	150	3	4
Wine	178	3	13	Ecoli	336	8	8
Vowel	528	11	10	Glass	214	6	13
Vehicle	846	4	18	Car	1728	6	4
Segment	2310	7	19	Satimage	4435	6	36

#Ins is the number of the training points; #attributes is the number of attributes; #class is the number of class.

Table 3: Tenfold testing percentage test set accuracy (%) on binary-class UCI data sets for linear classifiers.

Data sets	TWSVM Accuracy % Time (s)	SVM Accuracy % Time (s)	GEPSVM Accuracy % Time (s)	BHNPSVM Accuracy % Time (s)
Hepatitis	82.89 ± 6.30*	84.13 ± 5.58	80.07 ± 5.43	**85.47 ± 1.36***
	0.012	0.012	0.0006	0.0304
BUPA liver	66.40 ± 7.74*	67.78 ± 5.51	61.33 ± 6.26	**69.97 ± 0.56***
	0.840	0.0549	0.0012	0.2143
Heart-statlog	**84.44 ± 6.80**	83.12 ± 5.41	75.37 ± 7.02	**84.44 ± 0.56**
	0.023	0.0281	0.0022	0.1092
Votes	95.85 ± 2.75	95.80 ± 2.65	91.93 ± 3.18	**95.58 ± 2.75**
	0.797	1.1446	0.0039	0.1027
WPBC	**83.68 ± 5.73***	83.30 ± 4.53	76.76 ± 6.67	81.32 ± 1.36*
	0.012	0.0432	0.0002	0.0465
Sonar	77.00 ± 6.10	**80.13 ± 5.43**	73.16 ± 8.33	74.15 ± 1.73
	0.007	0.0946	0.0225	0.007
Australian	85.94 ± 5.84	**88.51 ± 4.85**	80.00 ± 3.99	85.27 ± 3.26
	0.3460	0.2350	0.0029	0.4250
Pima-Indian	73.80 ± 4.97*	**77.34 ± 4.37**	75.47 ± 4.64	77.05 ± 0.48*
	0.121	0.261	0.0016	0.4793
CMC	68.28 ± 2.21*	67.82 ± 2.63	66.76 ± 2.98	**77.86 ± 0.22***
	1.247	0.597	0.0050	1.197
Mean accuracy	79.81	80.88	75.65	**81.23**
Mean time	0.38	0.27	0.004	0.29

* A greater difference between BHNPSVM and TWSVM.

MHNPSVM and MBSVM in average training time. Thus, with the proposed formulation of MHNPSVM allows the classifier to learn better by reducing the generalization errors. However, this improved performance is obtained at the cost of more tuning effort involved. This is because MHNPSVM requires tuning of more parameters than MBSVM.

Table 6 shows the nonlinear MHNPSVM with "1-v-1," "1-v-r," and MBSVM, the results of numerical experiments. In Table 6, the classification accuracy and computation time are listed. The results in Table 6 are similar to those appearing in Table 5; MHNPSVM has better classification accuracy than MBSVM in eight datasets, while MBSVM is better than MHNPSVM in one dataset, and MHNPSVM and MBSVM are much faster than "1-v-1" and "1-v-r", especially when the amount of data increases.

5. Conclusions

In this paper, a general framework of nonparallel hyperplanes support vector machines, termed NPSVMs, are proposed for binary classification and multiclass classification. For binary classification, this framework includes TWSVM and its many deformation versions, for instance, TWSVM, TBSVM, LS-TWSVM, NPPC, and so forth, when different loss functions and parameters are selected. For multiclass classification, we do not directly extend TWSVM and its deformation versions to get the framework, in which we switch the roles of the patterns of the kth class and the rest classes. This strategy does not lead to significant increase of the computation complexity when the number of classes is increasing. Moreover, in the decision function, "min" and Euclidean distance in TWSVM

Table 4: Tenfold testing percentage test set accuracy (%) on binary-class UCI datasets for nonlinear classifiers.

Datasets	TWSVM Accuracy % Time (s)	SVM Accuracy % Time (s)	GEPSVM Accuracy % Time (s)	BHNPSVM Accuracy % Time (s)
Hepatitis	83.39 ± 7.31 0.016	**84.13 ± 6.25** 0.0142	80.00 ± 5.2 0.0035	83.40 ± 3.58 0.0697
BUPA liver	67.83 ± 6.49* 0.033	68.32 ± 7.20 0.0129	63.01 ± 7.46 1.305	**74.24 ± 0.64*** 0.1522
Heart-statlog	82.96 ± 4.67* 0.029	83.33 ± 9.11 0.0250	**86.52 ± 7.36** 0.438	84.04 ± 4.56* 0.1120
Votes	94.91 ± 4.37 0.072	**95.64 ± 7.23** 0.0495	94.5 ± 3.37 0.087	95.21 ± 5.18 0.0152
WPBC	**81.28 ± 5.92** 0.029	80.18 ± 6.90 0.0148	80.07 ± 5.97 0.0043	80.89 ± 1.17 0.0468
Sonar	**89.64 ± 6.11** 0.014	88.93 ± 10.43 0.0781	81.93 ± 4.41 0.020	88.05 ± 1.79 0.2896
Australian	75.8 ± 4.91* 0.420	**85.51 ± 4.85** 0.0425	69.55 ± 5.37 0.334	77.58 ± 2.53* 0.497
Pima-Indian	73.74 ± 5.2* 0.427	76.09 ± 3.58 0.442	74.66 ± 5.00 15.892	**77.70 ± 0.39*** 0.381
CMC	73.95 ± 3.48* 1.708	68.98 ± 3.44 1.755	68.67 ± 3.84 1.042	**78.43 ± 0.13*** 1.920
Mean accuracy	80.39	81.23	77.66	**82.17**
Mean time	0.3053	0.27	2.1251	0.3871

* A greater difference between BHNPSVM and TWSVM.

Table 5: Tenfold testing percentage test set accuracy (%) on multiclass UCI datasets for linear classifiers.

Dataset	1-v-1 Accuracy (%) Time (s)	1-v-r Accuracy (%) Time (s)	MBSVM Accuracy (%) Time (s)	MHNPSVM Accuracy (%) Time (s)
Iris	96.83 ± 1.75 0.025	95.73 ± 3.78 0.014	95.00 ± 4.95 0.009	**96.96 ± 1.12** 0.010
Wine	96.59 ± 1.48 0.058	**97.72 ± 0.74** 0.021	94.77 ± 4.07 0.028	95.88 ± 2.21 0.023
Ecoli	**87.63 ± 0.81** 0.863	86.77 ± 0.87 0.522	85.72 ± 1.02 0.097	86.78 ± 0.75 0.089
Vowel	54.21 ± 2.24 1.459	57.44 ± 3.26 0.580	59.42 ± 4.96* 0.160	**64.60 ± 3.06*** 0.172
Glass	94.16 ± 1.84 1.037	94.42 ± 4.06 0.405	92.80 ± 9.80* 0.183	**95.83 ± 1.04*** 0.105
Vehicle	77.79 ± 2.21 28.11	**78.22 ± 2.10** 10.05	77.59 ± 2.16 2.96	77.13 ± 1.87 2.58
Car	86.78 ± 0.50 16.042	86.72 ± 0.31 13.79	84.09 ± 0.33* 5.92	**87.79 ± 0.91*** 6.05
Segment	91.60 ± 2.428 28.078	**92.54 ± 2.03** 15.26	92.68 ± 1.87 17.04	93.04 ± 2.01 17.55
Satimage	91.80 ± 0.81 60.50	90.20 ± 1.13 32.29	**92.40 ± 2.08** 47.45	91.40 ± 1.49 45.27
Mean accuracy	86.38	86.64	86.05	**87.71**
Mean time	15.13	8.10	8.21	7.98

* A greater difference between MHNPSVM and MBSVM.

Table 6: Tenfold testing percentage test set accuracy (%) on multiclass UCI datasets for nonlinear classifiers.

Dataset	1-v-1 Accuracy (%) Time (s)	1-v-r Accuracy (%) Time (s)	MBSVM Accuracy (%) Time (s)	MHNPSVM Accuracy (%) Time (s)
Iris	**98.93 ± 1.11** 0.0054	97.63 ± 5.46 0.0264	98.12 ± 2.08 0.037	98.74 ± 1.92 0.030
Wine	97.08 ± 3.32 7.294	**97.72 ± 0.86** 4.6504	96.45 ± 1.29 0.592	97.28 ± 0.96 0.523
Ecoli	92.27 ± 1.03 0.382	90.35 ± 0.47 0.0843	91.06 ± 1.45* 0.154	**92.95 ± 0.89*** 0.182
Glass	98.09 ± 1.04 0.692	99.14 ± 0.97 0.1085	98.76 ± 1.22 0.089	**99.24 ± 0.93** 0.092
Vowel	91.37 ± 0.86 1.482	**94.32 ± 0.18** 0.3844	80.42 ± 4.37* 0.623	85.86 ± 4.72* 0.593
Vehicle	81.03 ± 5.73 19.562	82.49 ± 4.26 11.456	82.01 ± 1.33 2.81	**83.57 ± 1.79** 2.50
Car	**88.37 ± 0.55** 3.6571	87.36 ± 0.68 0.9405	85.74 ± 0.33 1.832	86.57 ± 0.46 1.944
Segment	95.15 ± 6.02 128.42	94.65 ± 4.38 91.69	**95.96 ± 4.08** 53.27	95.90 ± 3.29 49.58
Satimage	93.80 ± 1.46 190.27	93.05 ± 1.46 132.47	94.03 ± 1.93 89.05	**94.47 ± 1.58** 88.36
Mean accuracy	92.90	**92.97**	91.39	92.73
Mean time	39.08	26.87	16.50	15.98

* A greater difference between MHNPSVM and MBSVM.

are replaced by "max" and the absolute value $|w^{\mathrm{T}}x+b|$, respectively. The absolute value $|w^{\mathrm{T}}x + b|$ is not only simpler but also more consistent with the primal problems. In particular, we discuss the linear and nonlinear case of the framework with the hinge loss function as example. Moreover, we also give the primal problems of several extensions of TWSVM's deformation versions. The numerical experiments on several artificial and benchmark datasets indicate that our NPSVMs yield comparable generalization performance compared with SVM, GEPSVM, TWSVM, MBSVM, "1-v-1," and "1-v-r". In short, the proposed framework not only includes TWSVM and its many deformation versions but also extends them into multiclass classification under keeping the merit of TWSVM (learning speed).

In the future, we will develop the idea of nonparallel hyperplanes classifiers to other problems such as ordinal regression, multi-instance, and multilabel classification.

Conflict of Interests

The authors declare that there is no conflict of interests regarding the publication of this paper.

Acknowledgments

This work is supported by the National Natural Science Foundation of China (no. 11161045); the Project is sponsored by SRF for ROCS, SEM, and the Open Funding Project of the National Key Laboratory of Biochemical Engineering (no. 2013KF-01) and the Zhejiang Provincial Natural Science Foundation of China (no. Q12A010077).

References

[1] C. J. C. Burges, "A tutorial on support vector machines for pattern recognition," *Data Mining and Knowledge Discovery*, vol. 2, no. 2, pp. 121–167, 1998.

[2] C. Cortes and V. N. Vapnik, "Support-vector networks," *Machine Learning*, vol. 20, no. 3, pp. 273–297, 1995.

[3] C. Nello and S. T. John, *An Introduction to Support Vector Machines and Other Kernel-Based Learning Methods*, Cambridge University Press, Cambridge, Mass, USA, 1st edition, 2000.

[4] N. Deng, Y. Tian, and C. Zhang, *Support Vector Machines: Theory, Algorithms and Extensions*, Chapman & Hall/CRC Data Mining and Knowledge Discovery Series, CRC press, 2013.

[5] V. N. Vapnik, *The Nature of Statistical Learning Theory*, Springer, New York, NY, USA, 1995.

[6] E. Osuna, R. Freund, and F. Girosi, "Training support vector machines: an application to face detection," in *Proceedings of the IEEE Computer Society Conference on Computer Vision and Pattern Recognition*, pp. 130–136, IEEE, San Juan, Puerto Rico, June 1997.

[7] H. Cevikalp, B. Triggs, and V. Franc, "Face and landmark detection by using cascade of classifiers," in *Proceedings of the 10th IEEE International Conference and Workshops on Automatic Face and Gesture Recognition (FG '13)*, pp. 1–7, Shanghai, China, April 2013.

[8] T. Joachims, "Text categorization with support vector machines: learning with many relevant features," in *Machine Learning: ECML-98*, pp. 137–142, 1998.

[9] L. J. Cao, "Support vector machines experts for time series forecasting," *Neurocomputing*, vol. 51, no. 1–4, pp. 321–339, 2003.

[10] Y.-C. Wang, Z.-X. Yang, and N.-Y. Deng, "Support vector machine prediction of enzyme function with conjoint triad feature and hierarchical context," *BMC Systems Biology*, vol. 5, no. 1, article S6, 2011.

[11] O. L. Mangasarian and E. W. Wild, "Multisurface proximal support vector machine classification via generalized eigenvalues," *IEEE Transactions on Pattern Analysis and Machine Intelligence*, vol. 28, no. 1, pp. 69–74, 2006.

[12] Jayadeva, R. Khemchandani, and S. Chandra, "Twin support vector machines for pattern classification," *IEEE Transactions on Pattern Analysis and Machine Intelligence*, vol. 29, no. 5, pp. 905–910, 2007.

[13] Y.-H. Shao, C.-H. Zhang, X.-B. Wang, and N.-Y. Deng, "Improvements on twin support vector machines," *IEEE Transactions on Neural Networks*, vol. 22, no. 6, pp. 962–968, 2011.

[14] M. Arun Kumar and M. Gopal, "Least squares twin support vector machines for pattern classification," *Expert Systems with Applications*, vol. 36, no. 4, pp. 7535–7543, 2009.

[15] M. Arun Kumar, R. Khemchandani, M. Gopal, and S. Chandra, "Knowledge based least squares twin support vector machines," *Information Sciences*, vol. 180, no. 23, pp. 4606–4618, 2010.

[16] Y.-H. Shao, N.-Y. Deng, and Z.-M. Yang, "Least squares recursive projection twin support vector machine for classification," *Pattern Recognition*, vol. 45, no. 6, pp. 2299–2307, 2012.

[17] S. Gao, Q. Ye, and N. Ye, "1-Norm least squares twin support vector machines," *Neurocomputing*, vol. 74, no. 17, pp. 3590–3597, 2011.

[18] S. Ghorai, A. Mukherjee, and P. K. Dutta, "Nonparallel plane proximal classifier," *Signal Processing*, vol. 89, no. 4, pp. 510–522, 2009.

[19] M. A. Kumar and M. Gopal, "Application of smoothing technique on twin support vector machines," *Pattern Recognition Letters*, vol. 29, no. 13, pp. 1842–1848, 2008.

[20] X. Peng, "A ν-twin support vector machine (ν-TSVM) classifier and its geometric algorithms," *Information Sciences*, vol. 180, no. 20, pp. 3863–3875, 2010.

[21] X. Peng, "TSVR: an efficient twin support vector machine for regression," *Neural Networks*, vol. 23, no. 3, pp. 365–372, 2010.

[22] Z. Wang, J. Chen, and M. Qin, "Non-parallel planes support vector machine for multi-class classification," in *Proceedings of the International Conference on Logistics Systems and Intelligent Management (ICLSIM '10)*, vol. 1, pp. 581–585, January 2010.

[23] H. Cong, C. Yang, and X. Pu, "Efficient speaker recognition based on multi-class Twin Support Vector Machines and GMMs," in *Proceedings of the IEEE International Conference on Robotics, Automation and Mechatronics (RAM '08)*, pp. 348–352, September 2008.

[24] Z.-X. Yang, Y.-H. Shao, and X.-S. Zhang, "Multiple birth support vector machine for multi-class classification," *Neural Computing and Applications*, vol. 22, no. 1, pp. 153–161, 2013.

[25] A. N. Tikhonov and V. Y. Arsenin, *Solutions of Ill-Posed Problems*, John Wiley & Sons, New York, NY, USA, 1977.

[26] O. L. Mangasarian, *Non Linear Programming*, SIAM, Philadelphia, Pa, USA, 1994.

[27] O. L. Mangasarian and D. R. Musicant, "Successive overrelaxation for support vector machines," *IEEE Transactions on Neural Networks*, vol. 10, no. 5, pp. 1032–1037, 1999.

[28] I. W.-H. Tsang, A. Kocsor, and J. T.-Y. Kwok, "Large-scale maximum margin discriminant analysis using core vector machines," *IEEE Transactions on Neural Networks*, vol. 19, no. 4, pp. 610–624, 2008.

[29] G. H. Golub and C. F. van Loan, *Matrix Computations*, The John Hopkins University Press, 1996.

[30] Y. J. Lee and O. L. Mangasarian, *Rsvm: Reduced Support Vector Machines*, 2001.

[31] Y.-J. Lee and S.-Y. Huang, "Reduced support vector machines: a statistical theory," *IEEE Transactions on Neural Networks*, vol. 18, no. 1, pp. 1–13, 2007.

[32] *MATLAB*, The MathWorks, 2007, http://www.mathworks.com.

[33] C. C. Chang and C. J. Lin, "LIBSVM: a library for support vector machines," 2001, http://www.csie.ntu.edu.tw/~cjlin/.

[34] R. O. Duda, P. E. Hart, and D. G. Stork, *Pattern Classification*, John Wiley & Sons, New York, NY, USA, 2nd edition, 2001.

[35] C.-W. Hsu and C.-J. Lin, "A comparison of methods for multiclass support vector machines," *IEEE Transactions on Neural Networks*, vol. 13, no. 2, pp. 415–425, 2002.

[36] C. L. Blake and C. J. Merz, "UCI Repository for Machine Learning Databases," 1998, http://www.ics.uci.edu/~mlearn/MLRepository.html.

Hindawi Publishing Corporation
The Scientific World Journal
Volume 2015, Article ID 831396, 9 pages
http://dx.doi.org/10.1155/2015/831396

Research Article

Description and Application of a Mathematical Method for the Analysis of Harmony

Qiting Zuo, Runfang Jin, Junxia Ma, and Guotao Cui

College of Water Conservancy and Environment, Zhengzhou University, No. 100, Science Road, Zhengzhou 450001, China

Correspondence should be addressed to Qiting Zuo; zuoqiting@163.com

Received 18 September 2014; Revised 9 March 2015; Accepted 30 March 2015

Academic Editor: Haibo He

Harmony issues are widespread in human society and nature. To analyze these issues, harmony theory has been proposed as the main theoretical approach for the study of interpersonal relationships and relationships between humans and nature. Therefore, it is of great importance to study harmony theory. After briefly introducing the basic concepts of harmony theory, this paper expounds the five elements that are essential for the quantitative description of harmony issues in water resources management: harmony participant, harmony objective, harmony regulation, harmony factor, and harmony action. A basic mathematical equation for the harmony degree, that is, a quantitative expression of harmony issues, is introduced in the paper: $\mathrm{HD} = ai - bj$, where a is the uniform degree, b is the difference degree, i is the harmony coefficient, and j is the disharmony coefficient. This paper also discusses harmony assessment and harmony regulation and introduces some application examples.

1. Introduction

With the exception of "goodwill competition," living in harmony (in terms of the relationships between people) is recommended, and the resulting community of people living in harmony is often called a "harmony society," "harmony community," "harmony city," "harmony home," and "harmony team." From the point of view of relationships between humans and nature, it is impossible for human beings to dominate nature because people would be forced to live in harmony with nature as a result of a nature counterattack. Therefore, there is no doubt that human beings and nature should be harmonious.

When the word "harmony" is mentioned, it is often associated with the word "games." Game theory is concerned with the behavior of absolutely rational decision makers with unlimited capabilities for reasoning and memorization [1]. Games are defined mathematical objects that consist of a set of players, a set of strategies (i.e., options or moves) that are available to the players, and a specification of the payoff that each player receives for each combination of strategies (i.e., possible outcomes of the game) [2]. Game theory has been used in a variety of fields, and it includes many contents in each field. For example, in water resources research, it reflects in lots of ways, including allocation of water resources [3, 4], water rights [5], water resources development [6], optimal allocation of water resources [7–9], problems of water environment [10], water resources management [11–13], and water conflicts [14, 15]. Game theory is used to represent the "struggle or competition" phenomenon and can be frequently encountered in practice, such as bargaining, offensive and defensive battles, horse racing, and auctions. However, it is insufficient just considering the games. Games can only be used to represent a struggle or competitive phenomenon. In contrast, it is necessary to build a harmony balance in many situations, and game theory cannot be applied for common harmony issues. In addition, there are some extraordinarily difficult problems, such as the "tragedy of the commons" [16, 17], which cannot be solved by game theory alone.

In game theory, "the tragedy of the commons" has been mentioned in the literature through various expressions, but the meaning is basically the same. The "tragedy of the commons" roughly means as follows: if there is a set piece of grassland that is shared by two homes for sheep grazing, the total number of sheep is limited due to the limited grass. From the point of view of the individual, a home that raises more sheep will have a better profit. To maximize his/her profits, each individual attempts to increase his/her number of sheep,

which results in an increasingly high number of total sheep and thus an increasingly excessive use of the grass. This excess leads to grassland degradation and even destruction, that is, the "tragedy of the commons." Therefore, in some cases, it is insufficient to only consider game theory; there is a need to consider harmony issues in these cases. As a result, harmony theory should also be established.

This paper has three objectives: (1) to introduce the concepts of harmony theory and the five essential elements of harmony theory in water resources management based on the above analysis and previous studies [18]; (2) to discuss the mathematical description of harmony theory by proposing a function for the harmony degree, introducing a mathematical approach for the assessment of harmony, and developing a method for harmony regulation; (3) to illustrate the mathematical description of harmony by a series of typical examples.

2. Concepts

Although the word "harmony" is widely used, a unifying concept has not yet been defined. Harmony in this paper is defined as follows: harmony is the action taken to achieve "coordination, accordance, balance, integrity, and adaptation." Because people rely on nature to survive, it is necessary for human society to live in harmony with nature.

The theory and methodology of studies on harmony behavior are termed harmony theory, which is further defined as follows: harmony theory is a method through which various participants work together to achieve harmony. Harmony theory, which is of broad application prospect, is a significant theory that reveals the harmonious relationships in nature and is also a concrete manifestation of dialectical materialism on the assertion of "the coordinated development between humans and nature." Firstly, it should be recognized that "harmony is an important concept in addressing interpersonal relationships and relationships between humans and nature, and it is also a major guarantee and a concrete manifestation to build a harmony society, harmony community, harmony team, and harmony nature." Secondly, it is important to gradually establish the concept of harmony and adhere to the ideological philosophy of harmony. In addition, humans should take the initiative to coordinate the marvelous relationships between people, which is the basis for the coordination of relationships between humans and nature. Furthermore, it is a new theory, and it can provide an appropriate pathway for water resources management in China [19]. The main arguments of harmony theory are the following.

(1) Harmony theory advocates the philosophy that "harmony is the most precious" to address a variety of relationships, and harmony ideology is the cornerstone of harmony theory.

(2) Harmony theory advocates a rational understanding of various contradictions and conflicts existing in various types of relationships, allowing the existence of differences and promoting a harmonious attitude to address various factors of disharmony and problems. Instead of ignoring the disharmony factors, it is necessary to consider all of the harmony factors and disharmony factors.

(3) Harmony theory advocates the concept of harmony between humans and nature and has very pronounced views on the coordinated development of these relationships. It asserts that human beings should take the initiative to coordinate the marvelous relationships among people. There is a possibility to achieve the coordination of the relationships between humans and nature based on this theory.

(4) Harmony theory adheres to the system perspective by promoting system-wide theoretical methods to study the issues of harmonious relationship.

3. Five Factors of Harmony Theory

To obtain a reasonable expression of harmony and a quantitative description of the harmony degree, the following five elements, which are the "five essential factors of harmony theory," need to be defined [18].

(1) Harmony Participant. The term "harmony participant" refers to the parties (generally two or more) involved in the harmony relationship, which are known as "the harmony party." The collection of harmony participants can be represented as $H = \{H_1, H_2, \ldots, H_n\}$, where n is the number of participants in the harmony party, which is also named "n-participant harmony." For a certain harmony party, this variable can be expressed as H_k $(k = 1, 2, \ldots, n)$. For instance, the participants of a harmonious couple are the two spouses, and the harmony participants of a family are all of the family members.

(2) Harmony Objective. This term refers to the target that the harmony participants have to achieve a state of harmony. If not, it is impossible to arrive at a state of harmony. In addition, attaining this goal might only lead to a partial state of harmony. For example, if there are n families sharing a piece of meadow for sheep, it is imperative to ensure that the total number of sheep does not exceed a certain amount (i.e., stocking rate) to avoid grass damage; the certain amount is thus the harmony target of the n households that share a piece of grassland.

(3) Harmony Regulation. This term refers to all of the rules or constraints established by the participants for the purpose of achieving the harmony goals. For example, in order to ensure rationality, a harmony regulation for the abovementioned n households sharing a piece of grassland could be that the amount of the increase in sheep for each household should be proportional to their population. Thus, according to the conditions of these harmony rules, it is appropriate to study harmony problems.

(4) Harmony Factor. This term refers to the factor that should be considered by harmony participants to achieve overall

harmony. Its collection is represented as $F = \{F_1, F_2, \ldots, F_m\}$, where the pth harmony factor is F_p and the total number of factors is m. When $m = 1$, it indicates single-factor harmony, and the harmony factor can be directly expressed as F. If $m \geq 2$, the harmony relationship is called multiple-factor harmony.

(5) Harmony Action. The term "harmony action" refers to the general name of the concrete behavior of the harmony participants for the harmony factors. For example, if n households jointly own a field of grass, the specific action is the quantity of sheep that are raised on that land. The collection of harmony actions taken by the participants in the n-participant harmony and the m harmony factors can be expressed as a matrix:

$$\begin{Bmatrix} A^1{}_1, A^1{}_2, \ldots, A^1{}_n \\ A^2{}_1, A^2{}_2, \ldots, A^2{}_n \\ \vdots \\ A^m{}_1, A^m{}_2, \ldots, A^m{}_n \end{Bmatrix}. \quad (1)$$

A single-factor harmony action is represented as $A = \{A_1, A_2, \ldots, A_n\}$.

4. Calculation of the Harmony Degree

The harmony degree is used for the quantitative expression of the harmony degree [18]. In this section, the harmony degree equation of a given factor (F_p) will be introduced, (i.e, Zuo-harmony degree equation). Then, the calculations of the harmony degree in multifactor harmony and multilevel harmony will be discussed.

4.1. Harmony Degree Equation of a Factor. The harmony degree of a given factor is defined by the following equation:

$$\mathrm{HD}_p = ai - bj, \quad (2)$$

where HD_p is the harmony degree corresponding to a certain factor and $\mathrm{HD}_p \in [0, 1]$. A higher value of HD_p (closer to 1) indicates a higher harmony degree. If the result of (2) shows that $\mathrm{HD}_p < 0$, then HD_p is set to 0.

The variables a and b are the unity degree and the difference degree, respectively. The unity degree a expresses the proportion of harmony participants in accordance with harmony rules with the same goal. The difference degree b is the expression of the proportion of harmony participants with divergent harmony rules and goals. Note that $a \in [0, 1]$, $b \in [0, 1]$, and $a + b \leq 1$. In the presence of "neither unity nor differences" (i.e., "waiver" phenomenon), $a+b < 1$; otherwise, $a + b = 1$. If the harmony actions of a given factor in n-participant harmony are "$A_1, A_2, \ldots, A_n$," it is assumed that the harmony actions of the n-participant harmony with the same target are "$G_1, G_2, \ldots, G_n$"; thus, $a = \sum_{k=1}^{n} G_k / \sum_{k=1}^{n} A_k$. If there is no waiver, then $b = 1 - a$. For example, if the harmony rule is $A_1 : A_2 = 2:1$ and A_1 and A_2 are 100 and 40, respectively, then G_1 and G_2 equal 80 and 40, respectively, $a = (80 + 40)/(100 + 40) = 0.8571$, and $b = 1 - a = 0.1429$. If A_1 and A_2 are 100 and 80, respectively, then G_1 and G_2 equal 100 and 50, respectively, $a = (100 + 50)/(100 + 80) = 0.8333$, and $b = 1 - a = 0.1667$.

The variable i, which is the harmony coefficient, represents the satisfaction degree of the harmony goals and can be determined based on the calculation of the harmony goals, $i \in [0, 1]$. If the harmony goals are absolutely achieved, then $i = 1$. In contrast, if the goals are not achieved, then $i = 0$. The harmony coefficient curve or function can be determined based on the satisfaction degree.

The variable j, which is the disharmony coefficient that reflects the divergent harmony participants, can be calculated and determined according to the difference degree. Note that $j \in [0, 1]$. If the harmony participants are completely opposed, then $j = 1$. In contrast, if the harmony participants are not opposed, then $j = 0$. In all other cases, the value of j is within the range of 0 to 1. The disharmony coefficient curve or function can be determined based on the difference degree; that is, the disharmony coefficient depends on the extent of opposition.

In single-factor harmony (i.e., $m = 1$), the harmony degree equation is expressed as the following equation:

$$\mathrm{HD} = ai - bj. \quad (3)$$

4.2. Harmony Degree Equation for Multifactor Harmony. If there are a number of factors in a harmony problem, a comprehensive multifactor harmony degree should be calculated based on the single-factor harmony degree. This can be accomplished through two methods: weighted average calculation and exponential weighted calculation.

4.2.1. Weighted Average Calculation. Consider the following:

$$\mathrm{HD} = \sum_{p=1}^{m} w_p \mathrm{HD}_p, \quad (4)$$

where HD is the comprehensive harmony degree, $\mathrm{HD} \in [0, 1]$, w_p is the weight of each harmony degree, $w_p \in [0, 1]$, and $\sum_{p=1}^{m} w_p = 1$. The other variables have the same definition as above.

4.2.2. Exponential Weighted Calculation. Consider the following:

$$\mathrm{HD} = \prod_{p=1}^{m} \left(\mathrm{HD}_p\right)^{\beta_p}, \quad (5)$$

where β_p is the index weight of each harmony degree, $\beta_p \in [0, 1]$, and $\sum_{p=1}^{m} \beta_p = 1$. The other variables have the same definition as before.

4.3. Calculation of Multilevel Harmony Degree. There are complex multilevel harmony problems in real life, and a higher-level harmony problem (i.e., a more comprehensive harmony problem) includes or implies a set of lower-level

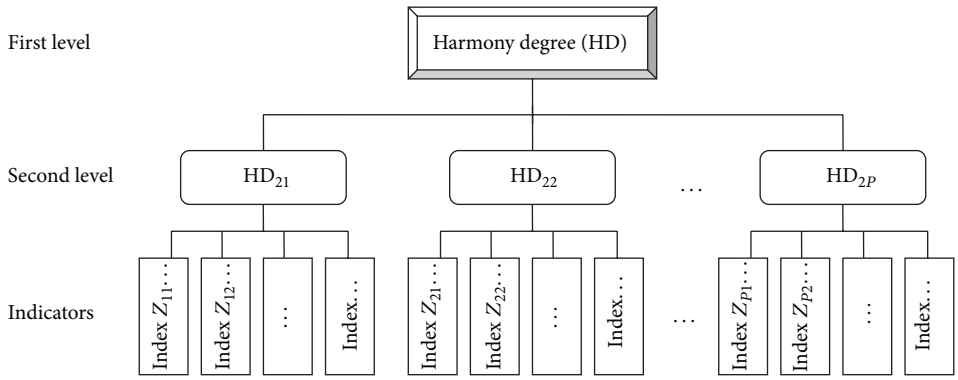

Figure 1: Multilevel harmony index system and harmony degree calculation.

harmony problems (i.e., single harmony problems). Therefore, the calculation of the harmony degree of harmony problems with different levels is essential. Figure 1 shows a harmony problem with two levels. The first level is the highest and the harmony degree is HD, and the second level is a lower level that includes several harmony problems, which are expressed as $\mathrm{HD}_{21}, \mathrm{HD}_{22}, \ldots, \mathrm{HD}_{2P}$ (P is the number of second-level harmony problems). Each lower-level harmony problem has corresponding indexes; that is, the indicators of HD_{21}, HD_{22}, and HD_{2P} are $Z_{11}, Z_{12}, \ldots, Z_{21}, Z_{22}, \ldots$, and $Z_{P1}, Z_{P2}, \ldots$, respectively.

The calculation process of a multilevel harmony problem is as follows. (1) Calculate the harmony degree of the lowest-level harmony problem using the multifactor harmony degree method presented above. (2) Based on the results of step (1), calculate the harmony degree of a higher-level harmony problem in accordance with the weighted average or the exponential weighted method. For instance, as shown in Figure 1, $\mathrm{HD} = \sum_{p=1}^{m} w_p \mathrm{HD}_{2p}$ or $\mathrm{HD} = \prod_{p=1}^{m} (\mathrm{HD}_{2p})^{\beta_p}$. (3) Repeat step (2) until the harmony degrees of the highest-level harmony problem are calculated.

5. Assessment of Harmony

The harmony assessment in water resources management represents the assessment of the harmony degree. This analysis can reflect the overall harmony degree, the present state and level of the harmony degree, and the space-time variation in the harmony degree. Thus, this assessment can provide insight into the evaluation of harmony problems and the development of a harmony strategy. The two main methods for harmony assessment are discussed.

5.1. Evaluation of the Harmony Degree. The evaluation of the harmony degree is a method in which the harmony degree is directly calculated according to certain problems to determine the level of the harmony degree based on its magnitude and to evaluate the calculated harmony degree.

5.2. Multi-Index Comprehensive Evaluation. Multi-index comprehensive evaluation is a method used to characterize the harmony degree synthetically through the establishment of a set of evaluation indexes and criteria. It includes the following three steps: (1) to establish an index system; (2) to determine the evaluation criteria; and (3) to select the evaluation and calculation methods. There are various types of multi-index comprehensive evaluation methods, such as the fuzzy comprehensive evaluation method, the gray comprehensive evaluation method, the analytic hierarchy process method, the set pair analysis method, and the matter element analysis method.

6. Harmony Regulation

Harmony regulation, which is primarily based on the harmony assessment, involves the use of some measures to improve the harmony degree. The primary task of harmony regulation is to advance the harmony degree to ultimately move the harmony problem in a more harmonious direction.

There are two thoughts in harmony regulation. The simple thought is a direct selection in accordance with the magnitude of the harmony degree, that is, "optimal selection method of the harmony action set." The complex thought is to obtain the optimal harmony scheme through the development of harmony regulation models, namely, "optimization-based models of the function of the harmony degree."

6.1. Optimal Selection Method of the Harmony Action Set. The optimal selection method of a harmony action set is to gather all of the harmony actions that meet a certain target (i.e., form a harmony action set) and then select the needed harmony actions (or schemes) from the set (i.e., obtain a concentrated optimal set of harmony actions).

If the harmony degree of the selected harmony action is the maximum centralized harmony degree, then the selected harmony action is considered the optimal harmony action. If it is difficult to obtain the maximum harmony degree, a suboptimal action, which is called a quasi-optimal harmony action, can be used.

Therefore, the key steps of this method are as follows: (1) combine many different schemes (or harmony actions) and calculate the harmony degree for each scheme using the abovementioned harmony degree calculation methods and (2) combine all of the harmony action sets that coincide with

the relevant target values and select the optimal harmony action or the approximately optimal harmony action intensively.

This method has two effects on harmony regulation: (1) the optimization of harmony actions and (2) the optimization of harmony regulation. Through the harmony degree calculation of multiple schemes, access to the maximum or near-maximum harmony degree is easy, which contributes to the optimal scheme selection. However, it would also be easy to select the most favorable harmony regulation by changing a variety of possible options. In fact, sometimes the best harmony rule has a significant effect on the harmony problem.

6.2. Optimization-Based Model of the Function of the Harmony Degree. The development of an optimization model is a common calculation method used in operational research and systems science and has been used widely in practice. A general optimization model consists of an objective function and a set of constraints, and the general form of an optimization model is expressed as follows:

$$Z = \max\left[F(X)\right], \qquad G(X) \le 0, \quad X \ge 0, \tag{6}$$

where X is a decision vector, $F(X)$ is the objective function, the variable Z is the maximum value of the objective function (note that the minimum can be transformed into the maximum by taking the negative of both sides), and $G(X)$ is a set of constraints, which should be written such that the value of each specific constraint is less than or equal to 0 in the equation (if the constraint condition is greater than or equal to 0, it can be transformed to less than or equal to 0 by taking the negative).

This method can be used for the following three conditions.

(1) Establish an optimization model using the harmony degree equation as the objective function. This model is primarily used to identify the optimal harmony action (optimization scheme) under the condition that the harmony degree is the maximum possible value. The normal method for using the harmony degree equation as the objective function is

$$Z = \max\left[\mathrm{HD}(X)\right], \qquad G(X) \le 0, \quad X \ge 0. \tag{7}$$

(2) Construct an optimization model based on the harmony degree as a constraint. This model is primarily used to identify an optimization scheme that ensures that the harmony degree is above a certain limit. This method requires that the harmony degree be not less than a given limit value (set as u_0) and has the following form:

$$Z = \max\left[F(X)\right], \qquad G(X) \le 0, \qquad \mathrm{HD}(X) \geqslant u_0, \qquad X \ge 0. \tag{8}$$

(3) Optimize the harmony regulation. Set up an optimization model that uses the relevant parameters as a variable; that is, set the harmony regulation variable as Y. The general form of the optimization problem is then the following:

$$Z = \max\left[F(X,Y)\right], \qquad G(X,Y) \le 0, \quad X,Y \ge 0. \tag{9}$$

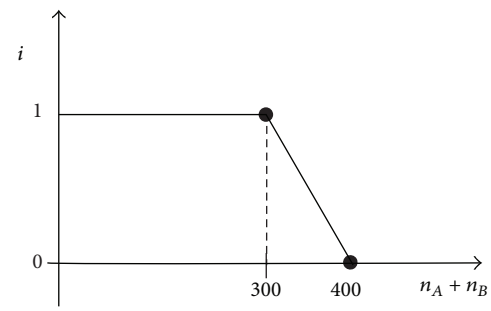

Figure 2: Function of the harmony coefficient i.

7. Application Examples

7.1. Harmony Theory Description of the "Tragedy of the Commons". The "tragedy of the commons," which is a famous example of game theory, cannot be explained well by game theory alone. However, it can be commendably solved using harmony theory.

It is assumed that there is a field of grass that is shared by two families (A and B) for the raising of sheep. Families A and B have 6 and 3 members, respectively. In addition, family A has n_A sheep, and family B has n_B sheep. There is no doubt that a certain amount of grass is essential for all of the sheep to survive, and the total number of sheep has an upper limit.

The relevant assumptions are as follows. The harmony goal of this problem is to ensure that the grassland is controlled such that its grazing capacity is not destroyed. If the normal growth of grass exhibits the general requirement of $n_A + n_B \le 300$, then all of the grass would be destroyed if the number of sheep reaches 400. The harmony regulation is that the number of raised sheep is proportional to the population; that is, $n_A : n_B = 2:1$. Under this condition, it is optimal that families A and B raise 200 and 100 sheep, respectively. However, what is the harmony situation in other cases? Various assumptions are analyzed below.

(1) First, list the function of the harmony coefficient i according to the harmony goals, as shown in Figure 2. Second, determine the function of the disharmony coefficient j, as shown in Figure 3.

According to the harmony regulation that the number of raised sheep is proportional to the population (i.e., $n_A : n_B = 2:1$), the results are as follows. If A owns 200 sheep and B owns 100 sheep, the harmony action of A and B with the same goal is 200 and 100, respectively. Then, $a = (200+100)/(200+100) = 1$ and $b = 0$. In contrast, if A has 200 sheep and B has 160 sheep, the harmony action of A and B with the same goal is still 200 and 100. Then, $a = (200+100)/(200+160) = 0.83$ and $b = 1 - a = 0.17$. If A raises 200 sheep and B raises 60 sheep, the harmony action of A and B with the same goal is 120 and 60. Then, $a = (120+60)/(200+60) = 0.69$ and $b = 1 - a = 0.31$.

Table 1: Harmony degree calculation for various scenarios of the "tragedy of the commons."

Scenario	n_A	n_B	a	b	I	j	HD	Directions
1	200	100	1	0	1	0	1	$n_A : n_B = 2 : 1$ and $n_A + n_B \leq 300$. Optimal action.
2	120	100	0.82	0.18	1	0.18	0.79	Certain "differences" occur.
3	200	80	0.86	0.14	1	0.14	0.84	Certain "differences" occur.
4	200	60	0.69	0.31	1	0.31	0.59	Larger "differences" occur.
5	160	80	1	0	1	0	1	$n_A : n_B = 2 : 1$ and $n_A + n_B \leq 300$. Optimal action.
6	100	50	1	0	1	0	1	$n_A : n_B = 2 : 1$ and $n_A + n_B \leq 300$. Optimal action.
7	200	150	0.86	0.14	0.5	0.14	0.41	Harmony goal is exceeded, and some "differences" occur.
8	250	100	0.86	0.14	0.5	0.14	0.41	Harmony goal is exceeded, and some "differences" occur.
9	300	150	1	0	0	0	0	Harmony goal is significantly exceeded.
10	250	180	0.87	0.13	0	0.13	0	Harmony goal is significantly exceeded, and some "differences" occur.

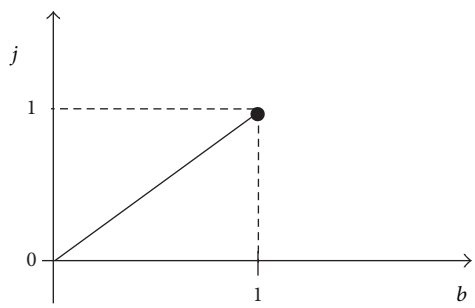

Figure 3: Function of the disharmony coefficient j.

(2) Compare $n_A + n_B$ with the harmony objectives and calculate the harmony coefficient i according to the function of the harmony coefficient i. Similarly, calculate the disharmony coefficient j in accordance with divergence b and its function.

(3) Calculate the harmony degree for several scenarios, as shown in Table 1. The final conclusion is as follows: the optimal harmony action is $n_A : n_B = 2 : 1$ and $n_A + n_B \leq 300$.

The following assumptions were made. If there are no requirements on the harmony regulation, a harmony action is optimal as long as $n_A + n_B \leq 300$ and the harmony degree is 1, which indicates that there are no requirements on the divergence between the harmony participants. If the harmony regulation is $n_A : n_B = 2 : 1$, a harmony action is optimal only when $n_A = 2 \times n_B$ and $n_A + n_B \leq 300$. As shown in Table 1, scenarios 1, 5, and 6 are the optimal harmony actions according to the definition, and scenario 1 is certainly the best scheme with the maximum benefit.

7.2. Optimization of Water Allocation. Transboundary water distribution (regional water allocation) is a very important issue in hydraulic engineering practice. Due to the limit and scarcity of water resources, conflicts appear frequently between regions. As a result, the reasonable distribution of water has long been a difficult issue discussed by the academic community.

Assume that the known study area is divided into three partitions (A, B, and C) and the amount of available water is 764 million cubic meters. In addition, the water diversion proportion is assumed to be 4 : 4 : 2, and the population of the three partitions is 1.49, 1.34, and 0.75 million, respectively, which results in a total population of 3.58 million. Moreover, the average total outputs per cubic meter of water attained by the three partitions are 96, 112, and 105 yuan, respectively.

It is assumed that two harmony factors need to be considered. One is the water distribution harmony factor, which takes the requirements of water resources distribution into account according to the harmony regulation of the proportion of water distribution. The other harmony factor is the benefit harmony factor, which takes the benefit requirements brought by the water resources into consideration in accordance with the harmony regulation of equality in the per capita output.

7.2.1. Function of the Harmony Degree and Harmony Assessment. For the unity degree calculation under the first harmony factor (i.e., water distribution), calculate the unity degree a based on harmony actions G_1, G_2, and G_3 that meet the harmony regulation. As a result, $a = \sum_{k=1}^{n} G_k / \sum_{k=1}^{n} A_k$, where $n = 3$.

To calculate the unity degree for the second harmony factor (i.e., harmony benefit factor), it is assumed that the per capita output of the three partitions is equal; thus, the unity degree a is 1. If these were not equal (x_1, x_2, and x_3 are assumed separately), the unity degree a can be calculated according to the exponential weighted calculation of equal weight with the ratio of each value to the maximum using the following formula:

$$a = \sqrt[3]{\frac{x_1 \times x_2 \times x_3}{[\max(x_1, x_2, x_3)]^3}}. \tag{10}$$

To satisfy the first harmony factor, the total amount of distributed water must be less than the available water resources; that is, the harmony coefficient i equals 1 when this objective is met, and $i = 0$ if this objective is not met. Furthermore, if the influence of the disharmony coefficient is not considered, $j = 0$.

There are no specific harmony objectives for the benefit harmony factor. The harmony coefficient i equals 1, and the disharmony coefficient j is 0.

Table 2: Harmony degree calculation for different schemes of water allocation.

Scheme	Water of partition A (billion m^3)	Water of partition B (billion m^3)	Water of partition C (billion m^3)	Harmony degree of the water diversion harmony factor	Harmony degree of the benefit harmony factor	Multifactor harmony degree
1	3.06	3.06	1.52	0.9948	0.8624	0.9262
2	3.50	2.50	1.64	0.8181	0.9633	0.8877
3	3.40	2.50	1.74	0.8181	0.9171	0.8662
4	3.30	2.50	1.84	0.8181	0.8748	0.8460
5	3.20	2.50	1.94	0.8181	0.8359	0.8269
6	3.10	2.50	2.04	0.8181	0.7998	0.8089
7	3.00	2.50	2.14	0.8181	0.7663	0.7918
8	3.50	2.60	1.54	0.8508	0.9731	0.9099
9	3.40	2.60	1.64	0.8508	0.9666	0.9068
10	3.30	2.60	1.74	0.8508	0.9200	0.8847
11	3.20	2.60	1.84	0.8508	0.8773	0.8639
12	3.10	2.60	1.94	0.8508	0.8380	0.8443
13	3.00	2.60	2.04	0.8508	0.8015	0.8258
14	3.50	2.70	1.44	0.8835	0.9629	0.9223
15	3.40	2.70	1.54	0.8835	0.9752	0.9282
16	3.30	2.70	1.64	0.8835	0.9691	0.9253
17	3.20	2.70	1.74	0.8835	0.9221	0.9026
18	3.10	2.70	1.84	0.8835	0.8790	0.8813
19	3.00	2.70	1.94	0.8835	0.8393	0.8611
20	3.39	2.70	1.55	0.8835	0.9763	0.9288
21	3.38	2.70	1.56	0.8835	0.9775	0.9293
22	3.37	2.70	1.57	0.8835	0.9786	0.9298
23	3.36	2.70	1.58	0.8835	0.9797	0.9304
24	3.35	2.70	1.59	0.8835	0.9808	0.9309
25	3.34	2.70	1.60	0.8835	0.9818	0.9314
26	**3.33**	**2.70**	**1.61**	**0.8835**	**0.9829**	**0.9319**
27	3.32	2.70	1.62	0.8835	0.9790	0.9301
28	3.31	2.70	1.63	0.8835	0.9741	0.9277
29	3.35	2.69	1.60	0.8802	0.9853	0.9313
30	3.34	2.69	1.61	0.8802	0.9839	0.9306
31	3.33	2.69	1.62	0.8802	0.9788	0.9282
32	3.32	2.69	1.63	0.8802	0.9738	0.9259
33	3.31	2.69	1.64	0.8802	0.9689	0.9235
34	3.35	2.71	1.58	0.8868	0.9763	0.9305
35	3.34	2.71	1.59	0.8868	0.9774	0.9310
36	3.33	2.71	1.60	0.8868	0.9784	0.9315
37	3.32	2.71	1.61	0.8868	0.9795	0.9320
38	3.31	2.71	1.62	0.8868	0.9793	0.9319

The multifactor harmony degree (Formula (5)) is calculated taking the two harmony factors into account and using the exponential weighted calculation of equal weights. The results including the final multifactor harmony degree of 38 schemes with different water distributions throughout the three partitions (i.e., harmony actions of this issue) are listed in Table 2.

7.2.2. Optimization of the Harmony Action. In this section, the optimization problem seeks to identify the most optimal harmony action that results in the highest harmony degree. The 38 schemes in Table 2 essentially reflect the process of seeking an optimal harmony behavior. The overall process is the following. First, calculate the multifactor harmony degree (Scheme 1) in accordance with the agreed-upon proportion

Table 3: Optimal harmony action and harmony degree for different schemes of water allocation with varied harmony rules (proportion of water distribution).

Scheme	Water distribution proportion (harmony rules)			Optimal harmony actions (amount of water allocated, billion m^3)			Multifactor harmony degree
	Partition A	Partition B	Partition C	Partition A	Partition B	Partition C	
1	3.36	2.68	1.60	3.35	2.69	1.60	0.9874
2	3.36	2.69	1.60	3.35	2.69	1.60	0.9881
3	3.35	2.68	1.60	3.35	2.69	1.60	0.9883
4	**3.35**	**2.69**	**1.60**	**3.35**	**2.69**	**1.60**	**0.9889**
5	3.34	2.69	1.61	3.34	2.69	1.61	0.9879
6	3.33	2.69	1.62	3.34	2.69	1.61	0.9848
7	3.32	2.69	1.63	3.34	2.69	1.61	0.9818
8	3.31	2.69	1.64	3.34	2.69	1.61	0.9788
9	3.30	2.69	1.65	3.34	2.69	1.61	0.9758
10	3.36	2.70	1.58	3.36	2.69	1.59	0.9871
11	3.35	2.70	1.59	3.35	2.69	1.60	0.9871
12	3.34	2.70	1.60	3.35	2.69	1.60	0.9871
13	3.33	2.70	1.61	3.33	2.70	1.61	0.9871
14	3.34	2.71	1.59	3.33	2.70	1.61	0.9853
15	3.33	2.71	1.60	3.33	2.70	1.61	0.9853

for the water distribution. Second, judge the direction of the water distribution amount for the three partitions that makes the multifactor harmony degree increase and determine an approximate range for the optimal solution (calculated according to a step of 0.1). For example, it is obvious that the harmony degree of Scheme 15 is the maximum from Schemes 2 to 19; in this scheme, the amounts of water allocated to the three partitions are 340, 270, and 154 million m^3. Third, obtain the optimal harmony action, which is represented with scenario 26, in which the amounts of water allocated to the three partitions are 333, 270, and 161 million m^3, respectively, based on changes to the water allocation distribution in scenario 15 (the step size was decreased to 0.01). The harmony degree of scenario 26 is 0.9319, which indicates that this scenario can be described as "basic harmony," that is, approximately complete harmony.

7.2.3. Optimization of the Harmony Rule. In this section, the optimization problem seeks to identify the optimal harmony rule (i.e., water distribution harmony rule) based on changes in the proportion used for the water distribution. In this example, changing the water distribution proportion implies changing the water rules and the calculation methods. The procedures used to calculate the harmony degree are unchanged. The fundamental difference between this and the previous optimization is the changing harmony rules. The harmony regulation used in the previous calculation is a water distribution proportion of 4 : 4 : 2, whereas this proportion is changed in the following analysis.

Table 3 shows the optimal harmony action and harmony degree calculated with changing harmony regulations (i.e., water distribution proportion). The corresponding optimal harmony action and harmony degree can be obtained using similar steps (Table 2); the only difference is that the harmony regulation (water distribution proportion) is changed repeatedly. For example, the harmony rule in Scheme 1 (Table 3) is 3.36 : 2.68 : 1.6, and the corresponding amounts of water allocated to the three partitions are 335, 269, and 160 million cubic meters, respectively. The water distribution proportion was calculated with a step size of 0.01, and some of the calculation results are listed in Table 3. Scheme 4 exhibits the maximum harmony degree of 0.9889 with the optimal harmony rule of 3.35 : 2.69 : 1.60. This maximum harmony degree is significantly larger than that obtained in the previous analysis (Table 2), which demonstrates that the overall level can be improved through the optimization of the harmony regulations.

8. Conclusions

This paper illustrates the widespread existence of harmony relationships and demonstrates that a quantitative study of harmony issues is of great significance for the analysis of various relationships in nature and human society. This is achieved through the introduction of the five essential factors of harmony theory, the calculation of the harmony degree and a harmony assessment, the discussion of harmony regulation issues, and the solution of two application examples.

Through the expositions and the two application examples, some conclusions can be obtained. (1) Harmony issues are common phenomena in nature and human society, and the use of quantitative research is of vital importance. (2) The harmony degree equation is a quantitative expression of harmony issues and a basic mathematical equation used to calculate the dimensions of the harmony degree. A harmony degree HD of 1 indicates complete harmony, whereas HD = 0 indicates absolute disharmony. A value of HD between 0 and 1 indicates changes in the harmony degree from absolute disharmony to complete harmony in accordance with the

quantitative expressions of the harmony degree. (3) The optimal harmony action, the optimal harmony rule, and the best management solution can be obtained mathematically, which provides a theoretical basis for the solutions of many practical problems. (4) As an emerging subdiscipline, harmony theory will aid the scientific understanding and arrangement of harmony issues. Further research on the quantitative expressions and assessment of the harmony degree and the search for optimal harmony regulation strategies will provide additional insight into harmony issues.

Conflict of Interests

The authors declare that there is no conflict of interests regarding the publication of this paper.

Acknowledgments

This research was supported by the National Natural Science Foundation of China (no. 51279183 and no. 51079132), the Major Program of the National Social Science Fund of China (no. 12&ZD215), and Program for Innovative Research Team (in science and technology) in University of Henan Province (13IRTSTHN030).

References

[1] R. Selten, "Reexamination of the perfectness concept for equilibrium points in extensive games," *International Journal of Game Theory*, vol. 4, no. 1, pp. 25–55, 1975.

[2] K. Madani, "Game theory and water resources," *Journal of Hydrology*, vol. 381, no. 3-4, pp. 225–238, 2010.

[3] M. Suzuki and M. Nakayama, "The cost assignment of the cooperative water resource development—a game theoretical approach," *Management Science*, vol. 22, no. 10, pp. 1081–1086, 1976.

[4] L. Wang, L. Fang, and K. W. Hipel, "Water resources allocation: a cooperative game theoretic approach," *Journal of Environmental Informatics*, vol. 2, no. 2, pp. 11–22, 2003.

[5] B. L. William, G. W. Mary, and M. S. Rose, *Linked Models for Indian Water Rights Disputes, Managing Water-Related Conflicts: The Engineer's Role*, American Society of Civil Engineers, 1990.

[6] H. A. Loáiciga, "Analytic game—theoretic approach to groundwater extraction," *Journal of Hydrology*, vol. 297, no. 1–4, pp. 22–33, 2004.

[7] A. Ganji, D. Khalili, and M. Karamouz, "Development of stochastic dynamic Nash game model for reservoir operation. I. The symmetric stochastic model with perfect information," *Advances in Water Resources*, vol. 30, no. 3, pp. 528–542, 2007.

[8] E. S. Homa, R. M. Vogel, M. P. Smith, C. D. Apse, A. Huber-Lee, and J. Sieber, "An optimization approach for balancing human and ecological flow needs," in *Proceedings of the EWRI World Water and Environmental Resources Congress*, pp. 1–12, Anchorage, Alaska, USA, May 2005.

[9] M. Le Bars and P. Le Grusse, "Use of a decision support system and a simulation game to help collective decision-making in water management," *Computers and Electronics in Agriculture*, vol. 62, no. 2, pp. 182–189, 2008.

[10] N. Fraser, *Conflict Analysis: Models and Resolutions*, North-Holland, New York, NY, USA, 1984.

[11] E. Eleftheriadou and Y. Mylopoulos, "Game theoretical approach to conflict resolution in transboundary water resources management," *Journal of Water Resources Planning and Management*, vol. 134, no. 5, pp. 466–473, 2008.

[12] K. R. M. Rajabu, "Use and impacts of the river basin game in implementing integrated water resources management in Mkoji sub-catchment in Tanzania," *Agricultural Water Management*, vol. 94, no. 1–3, pp. 63–72, 2007.

[13] S. Raquel, S. Ferenc, C. Emery Jr., and R. Abraham, "Application of game theory for a groundwater conflict in Mexico," *Journal of Environmental Management*, vol. 84, no. 4, pp. 560–571, 2007.

[14] C.-S. Lee, "Multi-objective game-theory models for conflict analysis in reservoir watershed management," *Chemosphere*, vol. 87, no. 6, pp. 608–613, 2012.

[15] N. Okada, K. W. Hipel, and Y. Oka, "Hypergame analysis of the Lake Biwa conflict," *Water Resources Research*, vol. 21, no. 7, pp. 917–926, 1985.

[16] G. Hardin, "The tragedy of the commons," *Science*, vol. 162, no. 3859, pp. 1243–1248, 1968.

[17] X. Y. Wang and Y. M. Xiao, *Games Theory and Its Applications*, Science Press, Beijing, China, 2008.

[18] Q. T. Zuo, "Mathematical description method and its application of harmony theory," *South-to-North Water Transfers and Water Science & Technology*, vol. 7, no. 4, pp. 129–133, 2009.

[19] Z. Qiting, M. Junxia, and T. Jie, "Chinese water resource management and application of the harmony theory," *Journal of Resources and Ecology*, vol. 4, no. 2, pp. 165–171, 2013.

Hindawi Publishing Corporation
The Scientific World Journal
Volume 2014, Article ID 637865, 7 pages
http://dx.doi.org/10.1155/2014/637865

Research Article

On the Maximum Estrada Index of 3-Uniform Linear Hypertrees

Faxu Li,[1,2] Liang Wei,[3] Jinde Cao,[4,5] Feng Hu,[1,2] and Haixing Zhao[2]

[1] *School of Computer Science, Shaanxi Normal University, Xi'an 710062, China*
[2] *College of Computer, Qinghai Normal University, Xining 810008, China*
[3] *Department of Mathematics, Qinghai Normal University, Xining 810008, China*
[4] *Department of Mathematics, Southeast University, Nanjing 210096, China*
[5] *Department of Mathematics, Faculty of Science, King Abdulaziz University, Jeddah 21589, Saudi Arabia*

Correspondence should be addressed to Haixing Zhao; h.x.zhao@163.com

Received 3 July 2014; Accepted 12 August 2014; Published 28 August 2014

Academic Editor: Jianlong Qiu

For a simple hypergraph H on n vertices, its Estrada index is defined as $EE(H) = \sum_{i=1}^{n} e^{\lambda_i}$, where $\lambda_1, \lambda_2, \ldots, \lambda_n$ are the eigenvalues of its adjacency matrix. In this paper, we determine the unique 3-uniform linear hypertree with the maximum Estrada index.

1. Introduction

Let $G = (V, E)$ be a simple graph, and let n and m be the number of vertices and the number of edges of G, respectively. The characteristic polynomial of a graph G is written as $P(G, \lambda) = \det(\lambda I - A(G))$, where $A(G)$ is the adjacency matrix of G. The eigenvalues of G are the eigenvalues of its adjacency matrix $A(G)$, which are denoted by $\lambda_1, \lambda_2, \ldots, \lambda_n$. A graph-spectrum-based invariant, nowadays named Estrada index, proposed by Estrada in 2000, is defined as [1]

$$EE(G) = \sum_{i=1}^{n} e^{\lambda_i}. \tag{1}$$

Since then, the Estrada index has already found remarkable applications in biology, chemistry, and complex networks [2–5]. Some mathematical properties of the Estrada index, especially bounds for it have been established in [6–15]. For more results on the Estrada index, the readers are referred to recent papers [16–19].

Let $H = (V, \mathscr{E})$ be a simple and finite hypergraph with vertex set $V(G) = \{v_1, v_2, \ldots, v_n\}$ and hyperedge set $\mathscr{E}(G) = \{E_1, E_2, \ldots, E_m\}$. The hypergraph H is called linear if two hyperedges intersect in one vertex at most and also h-uniform if $|E_i| = h$ for each E_i in $\mathscr{E}$, $i = 1, 2, \ldots, m$. An h-uniform hypertree is a connected linear h-hypergraph without cycles. An h-uniform linear hypertree is called 3-uniform linear hypertree if h is equal to 3. Denoted by $\mathcal{S}_m^h$ an h-uniform linear star with m hyperedges. More details on hypergraphs can be found in [20].

Let $A(H)$ denote a square symmetric matrix in which the diagonal elements a_{ij} are zero, and other elements a_{ij} represent the number of hyperedges containing both vertices v_i and v_j (for undirected hypergraphs, $a_{ij} = a_{ji}$). Let $\lambda_1, \lambda_2, \ldots, \lambda_n$ be the eigenvalues of $A(H)$ of H. The subhypergraph centrality of a hypergraph H, firstly put forward by Estrada and Rodríguez-Velázquez in 2006, is defined as [21]

$$\langle C_{SH} \rangle = \frac{1}{n}\sum_{i=1}^{n} C_{SH}(i) = \frac{1}{n}\sum_{i=1}^{n} e^{\lambda_i}. \tag{2}$$

They revealed that the subhypergraph centrality provides a measure of the centrality of complex hypernetworks (social, reaction, metabolic, protein, food web, etc). For convenience, we call the subhypergraph centrality of a hypergraph its Estrada index and define the Estrada index as

$$EE(H) = \sum_{i=1}^{n} e^{\lambda_i}. \tag{3}$$

Thus far, results on the Estrada index of hypergraph seem to be few although the Estrada index of graph has numerous applications. So our main goal is to investigate the Estrada index of 3-uniform linear hypertrees. In this paper,

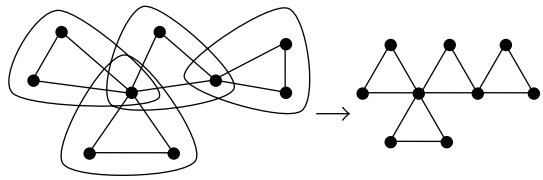

(a) 3-uniform linear hypertree H (b) Completely connected graph of H

Figure 1: A 3-uniform linear hypertree H and its completely connected graph G_H.

we determine the unique 3-uniform linear hypertree with the maximum Estrada index among the set of 3-uniform linear hypertrees.

2. Preliminaries

For a hypergraph H of order n, its completely connected graph, denoted by G_H, is a graph which has the same order and in which two vertices are adjacent if they share one hyperedge. Obviously, G_H is a multigraph. For an h-uniform linear hypergraph H, G_H is a simple graph. According to the definition of adjacency matrix of hypergraph, it is easy to see that both a 3-uniform linear hypertree H and its completely connected graph G_H have the same adjacency matrix; see Figure 1. Then, they have the identical Estrada index. Thus, we investigate the Estrada index of its completely connected graphs instead of the 3-uniform linear hypertrees in this paper.

We use $M_k(G) = \sum_{i=1}^{n} \lambda_i^k$ to denote the kth spectral moment of the graph G. It is well-known [22] that $M_k(G)$ is equal to the number of closed walks of length k in G. Obviously, for any graph G, $M_0(G) = n$, $M_1(G) = 0$, $M_2(G) = 2m$, $M_3(G) = 6t$, and $M_4(G) = 2\sum_{i=1}^{n} d_i^2 - 2m + 8q$, where t, q, and $d_i = d_G(v_i)$ are the number of triangles, the number of quadrangles, and the degree of vertex v_i in graph G, respectively. Then

$$EE(G) = \sum_{i=1}^{n}\sum_{k=0}^{\infty} \frac{\lambda_i^k}{k!} = \sum_{k=0}^{\infty} \frac{M_k(G)}{k!}. \tag{4}$$

For $u, v \in V(G)$, denote by $\mathscr{W}_k(G; u, v)$ the set of (u, v)-walks of length k in G. Obviously, $M_k(G; u, v) = |\mathscr{W}_k(G; u, v)|$. For convenience, let $\mathscr{W}_k(G; u) = \mathscr{W}_k(G; u, u)$ and $M_k(G; u) = M_k(G; u, u)$. Let W be a (u, v)-walk in graph G; we denote by W^{-1} a (v, u)-walk obtained from W by reversing W.

For any two graphs G_1 and G_2, if $M_k(G_1) \geq M_k(G_2)$ for all integers $k > 0$, then $EE(G_1) \geq EE(G_2)$. Moreover, if the strict inequality $M_k(G_1) > M_k(G_2)$ holds for at least one value $k > 0$, then $EE(G_1) > EE(G_2)$.

Denote by $\Gamma(n, m)$ the set of connected graphs on n vertices and m triangles such that any two triangles have a common vertex at most. Apparently, for a 3-uniform linear hypertree H on n vertices and m hyperedges, $G_H \in \Gamma(n, m)$. Now we study the Estrada index of a graph in $\Gamma(n, m)$.

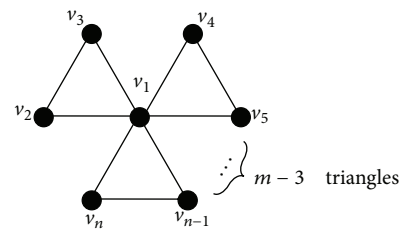

Figure 2: The star S_m^3 on m triangles.

3. Maximum Estrada Index of 3-Uniform Linear Hypertrees

In this section, we determine the maximum value of Estrada index among the set of 3-uniform linear hypertrees.

Lemma 1. *Let S_m^3 be star which is the completely connected graph of $\mathcal{S}_m^3$ with m hyperedges. It is easily found that the star S_m^3 has n vertices labled $v_1, v_2, v_3, \ldots, v_n$ and $m = (n-1)/2$ triangles. Let k be a positive integer; then there is an injection ξ from $\mathscr{W}_k(S_m^3; v_2)$ to $\mathscr{W}_k(S_m^3; v_1)$, and ξ is not surjective for $n \geq 5$, $2 \leq m \leq (n-1)/2$, and $k > 1$, where $\mathscr{W}_k(S_m^3; v_2)$ and $\mathscr{W}_k(S_m^3; v_1)$ are the sets of closed walks of length k of v_2 and v_1 in S_m^3, respectively; see Figure 2.*

Proof. Firstly, we construct a mapping φ from $\mathscr{W}_k(S_m^3; v_2)$ to $\mathscr{W}_k(S_m^3; v_1)$. For $W \in \mathscr{W}_k(S_m^3; v_2)$, let $\varphi(W)$ be the closed walk obtained from W by replacing v_1 by v_2 and v_2 by v_1. Obviously, $\varphi(W) \in \mathscr{W}_k(S_m^3; v_1)$ and φ is a bijection.

Secondly, we construct a mapping ξ from $\mathscr{W}_k(S_m^3; v_2)$ to $\mathscr{W}_k(S_m^3; v_1)$. For $W \in \mathscr{W}_k(S_m^3; v_2)$, we consider the following cases.

Case 1. Suppose W does not pass the edge $v_1 v_t$ for $t \geq 4$; then $\xi(W) = \varphi(W)$.

Case 2. Suppose W passes the edge $v_1 v_t$ for $t \geq 4$. For $W \in \mathscr{W}_k(S_m^3; v_2)$, we may uniquely decompose W into three sections $W_1 W_2 W_3$, where W_1 is the longest (v_2, v_1)-section of W without v_t, W_2 is the internal longest (v_t, v_t')-section of W for $t' \geq 4$, and the last W_3 is the remaining (v_1, v_2)-section of W not containing v_t. We consider the following three subcases.

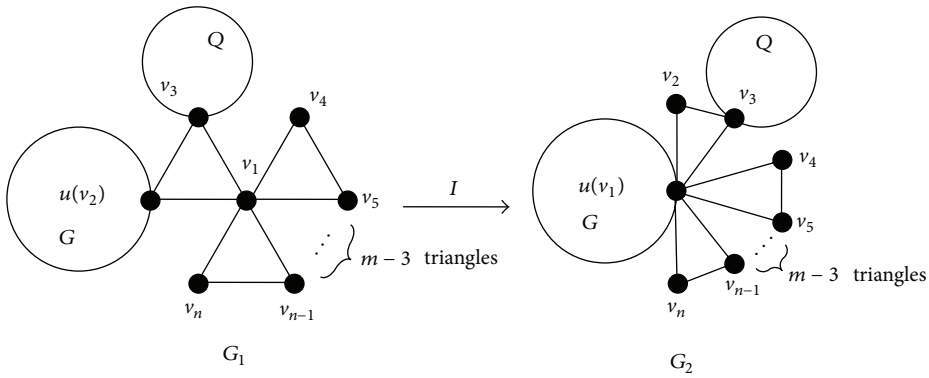

Figure 3: Transformation I.

Case 2.1. If both W_1 and W_3 contain the vertex v_3, we may uniquely decompose W_1 into two sections $W_{11}W_{12}$ and decompose W_3 into two sections $W_{31}W_{32}$, where W_{11} is the shortest (v_2, v_3)-section of W_1, W_{12} is the remaining (v_3, v_1)-section of W_1, W_{31} is the longest (v_1, v_3)-section of W_3, and W_{32} is the remaining (v_3, v_2)-section of W_3.

Let $\xi(W) = \xi(W_{11})\xi(W_{12})\xi(W_2)\xi(W_{31})\xi(W_{32})$, where $\xi(W_{12}) = W_{12}$, $\xi(W_2) = W_2$, $\xi(W_{31}) = W_{31}$, $\xi(W_{11})$ is a (v_1, v_3)-walk obtained from W_{11} replacing v_1 by v_2 and v_2 by v_1, and $\xi(W_{32})$ is a (v_3, v_1)-walk obtained from W_{32} replacing v_1 by v_2 and v_2 by v_1.

Case 2.2. If W_1 contains the vertex v_3 and W_3 does not contain v_3, let $\xi(W) = \xi(W_1)\xi(W_2)\xi(W_3)$, where $\xi(W_2) = W_2$, $\xi(W_1)$ is a (v_1, v_1)-walk obtained from W_1 replacing its first vertex v_2 by v_1v_2, and $\xi(W_3)$ is a (v_1, v_1)-walk obtained from W_3 replacing its last two vertices v_1v_2 by v_1.

Case 2.3. If W_1 does not contain the vertex v_3, let $\xi(W) = \xi(W_1)\xi(W_2)\xi(W_3)$, where $\xi(W_2) = W_2$, $\xi(W_1)$ is a (v_1, v_1)-walk obtained from W_1 replacing its first two vertices v_2v_1 by v_1, and $\xi(W_3)$ is a (v_1, v_1)-walk obtained from W_3 replacing its last vertex v_2 by v_2v_1.

For example, in star S_3^3 on 7 vertices and 3 triangles, $W = v_2v_3v_1v_2v_1v_3v_2$ is a closed walk of length 6 of v_2 not passing the edge v_1v_t. By Case 1, we have

$$\xi(W) = v_1v_3v_2v_1v_2v_3v_1. \tag{5}$$

$W' = v_2v_3v_1v_4v_5v_1v_6v_7v_1v_2$ is a closed walk of length 9 of v_2 passing the edge v_1v_t. By Case 2.2, we get

$$\xi(W') = v_1v_2v_3v_1v_4v_5v_1v_6v_7v_1. \tag{6}$$

$W'' = v_2v_1v_2v_1v_4v_5v_1v_2v_3v_1v_6v_7v_1v_3v_2$ is a closed walk of length 14 of v_2 passing the edge v_1v_t. By Case 2.3, we obtain

$$\xi(W'') = v_1v_2v_1v_4v_5v_1v_2v_3v_1v_6v_7v_1v_3v_2v_1. \tag{7}$$

Obviously, $\xi(W) \in \mathscr{W}_k(S_m^3; v_1)$, ξ is an injective and not a surjective for $n \geq 5$, and $k \geq 1$. □

Lemma 2. *Let u be a nonisolated vertex of a connected graph G. If G_1 and G_2 are the graphs obtained from G by identifying an external vertex v_2 and the center vertex v_1 of the union of $S_m^3 \cup Q$ to u, respectively, where $|V(S_m^3)| = n$, Q is either empty graph or nonempty graph. Then $M_k(G_1) < M_k(G_2)$ for $n \geq 5$ and $k \geq 4$; see Figure 3.*

Proof. Let $\mathscr{W}_k(G_i)$ ($\mathscr{W}_k(G)$, $\mathscr{W}_k(S_m^3 \cup Q)$, resp.) be the set of closed walks of length k of G_i(G, $S_m^3 \cup Q$, resp.) for $i = 1, 2$. Then $\mathscr{W}_k(G_i) = \mathscr{W}_k(G) \cup \mathscr{W}_k(S_m^3 \cup Q) \cup X_i$ is a partition, where X_i is the set of closed walks of length k of G_i; each of them contains both at least one edge in $E(G)$ and at least one edge in $E(S_m^3 \cup Q)$. So $M_k(G_i) = |\mathscr{W}_k(G)| + |\mathscr{W}_k(S_m^3 \cup Q)| + |X_i| = M_k(G) + M_k(S_m^3 \cup Q) + |X_i|$. Thus we need to show the inequality $|X_1| < |X_2|$.

We construct a mapping η from X_1 to X_2 and consider the following four cases.

Case 1. Suppose W is a closed walk starting from $u \in V(G)$ in X_1. For $W \in X_1$, let $\eta(W) = (W - W \cap (S_m^3 \cup Q)) \cup \xi(W \cap (S_m^3 \cup Q))$; that is, $\eta(W)$ is the closed walk in X_2 obtained from W by replacing its every section in $S_m^3 \cup Q$ with its image under the map ξ.

Case 2. Suppose W is a closed walk starting at v_1 in X_1. For $W \in X_1$, we may uniquely decompose W into three sections $W_1W_2W_3$, where W_1 is the longest (v_1, v_2)-section of W without vertices $u_0, \ldots, u_t'' \in V(G)$, W_2 is the internal longest (u_0, u_t'')-section of W (for which the internal vertices are some possible vertices in $V(G_1)$), and W_3 is the remaining (v_2, v_1)-section of W. Let $\eta(W) = \eta(W_1)\eta(W_2)\eta(W_3)$, where $\eta(W_1) = W_1^{-1}$, $\eta(W_3) = W_3^{-1}$, and $\eta(W_2) = (W_2 - W_2 \cap (S_m^3 \cup Q)) \cup \xi(W_2 \cap (S_m^3 \cup Q))$; that is, $\eta(W_2)$ is a (u_0, u_t'')-walk from W_2 by replacing its every section in $S_m^3 \cup Q$ with its image under the map ξ.

Case 3. Suppose W is a closed walk starting from v_3 or $w \in V(Q)$ in X_1. For $W \in X_1$, we may uniquely decompose W into three sections $W_1W_2W_3$, where W_1 is the longest (v_3, v_2) (or (w, v_2))-section of W without vertices $u_0, \ldots, u_t''$, W_2 is the internal longest (u_0, u_t'')-section of W (for which the internal vertices are some possible vertices in $V(G_1)$), and W_3 is the remaining (v_2, v_3) (or (v_2, w))-section of W without vertices $u_0, \ldots, u_t''$. We have three subcases.

Case 3.1. If both W_1 and W_3 do not pass edge v_1v_t, let $\eta(W) = \eta(W_1)\eta(W_2)\eta(W_3)$, where $\eta(W_2) = (W_2 - W_2 \cap (S_m^3 \cup Q)) \cup \xi(W_2 \cap (S_m^3 \cup Q))$, $\eta(W_1)$ is a (v_3, v_1) (or (w, v_1))-walk obtained from W_1 replacing v_1 by v_2 and v_2 by v_1, and $\eta(W_3)$ is a (v_1, v_3) (or (v_1, w))-walk obtained from W_3 replacing v_1 by v_2 and v_2 by v_1.

Case 3.2. If both W_1 and W_3 pass edge v_1v_t, we may anew decompose W into five sections $W_1W_2W_3W_4W_5$, where W_1 is the longest (v_3, v_t) (or (w, v_t))-section of W (which do not contain vertices $u_0, \ldots, u_t''$), W_2 is the second (v_1, v_2)-section of W (for which the internal vertices, if exist, are only possible $v_1, v_2, v_3, w \in V(Q)$), the third W_3 is the internal longest (u_0, u_t'')-section of W (for which the internal vertices are some possible vertices in $V(G_1)$), the fourth W_4 is the longest (v_2, v_1)-section of W (for which the internal vertices, if exist, are only possible $v_1, v_2, v_3, w \in V(Q)$), and the last W_5 is the remaining (v_t', v_3) (or (v_t, w))-section of W. We have three subsubcases.

Case 3.2.1. If both W_2 and W_4 contain the vertex v_3, we may uniquely decompose W_2 into two sections $W_{21}W_{22}$ and W_4 into two sections $W_{41}W_{42}$, where W_{21} is the longest (v_1, v_3)-section of W_2, W_{22} is the remaining shortest (v_3, v_2) of W_2, W_{41} is the shortest (v_2, v_3)-section of W_4, and W_{42} is the remaining longest (v_3, v_1)-section of W_4.

Let $\eta(W) = \eta(W_1)\eta(W_{21})\eta(W_{22})\eta(W_3)\eta(W_{41})\eta(W_{42})\eta(W_5)$, where $\eta(W_1) = W_1$, $\eta(W_{21}) = W_{21}$, $\eta(W_3) = (W_3 - W_3 \cap (S_m^3 \cup Q)) \cup \xi(W_3 \cap (S_m^3 \cup Q))$, $\eta(W_{42}) = W_{42}$ $\eta(W_5) = W_5$, $\eta(W_{22})$ is a (v_3, v_1)-walk obtained from W_{22} replacing v_1 by v_2 and v_2 by v_1, and $\eta(W_{41})$ is a (v_1, v_3)-walk obtained from W_{41} replacing v_1 by v_2 and v_2 by v_1.

Case 3.2.2. If W_2 does not contain the vertex v_3, let $\eta(W) = \eta(W_1)\eta(W_2)\eta(W_3)\eta(W_4)\eta(W_5)$, where $\eta(W_1) = W_1$, $\eta(W_3) = (W_3 - W_3 \cap (S_m^3 \cup Q)) \cup \xi(W_3 \cap (S_m^3 \cup Q))$, $\eta(W_5) = W_5$, $\eta(W_2)$ is a (v_1, v_1)-walk obtained from W_2 replacing its last two vertices v_1v_2 by v_1, and $\eta(W_4)$ is a (v_1, v_1)-walk obtained from W_4 replacing its first vertex v_2 by v_1v_2.

Case 3.2.3. If W_2 contains the vertex v_3 and W_4 does not contain vertex v_3, let $\eta(W) = \eta(W_1)\eta(W_2)\eta(W_3)\eta(W_4)\eta(W_5)$, where $\eta(W_1) = W_1$, $\eta(W_3) = (W_3 - W_3 \cap (S_m^3 \cup Q)) \cup \xi(W_3 \cap (S_m^3 \cup Q))$, $\eta(W_5) = W_5$, $\eta(W_2)$ is a (v_1, v_1)-walk obtained from W_2 replacing its last vertex v_2 by v_2v_1, and $\eta(W_4)$ is a (v_1, v_1)-walk obtained from W_4 replacing its first two vertices v_2v_1 by v_1.

Case 3.3. If W_1 passes edge v_1v_t and W_3 does not pass edge v_1v_t, we may anew decompose W into four sections $W_1W_2W_3W_4$, where W_1 is the longest (v_3, v_t) (or (w, v_t))-section of W (which do not contain vertices $u_0, \ldots, u_t''$), W_2 is the second (v_1, v_2)-section of W (for which the internal vertices, if exist, are only possible $v_1, v_2, v_3, w \in V(Q)$), the third W_3 is the internal longest (u_0, u_t'')-section of W (for which the internal vertices are some possible vertices in $V(G_1)$), and the last W_4 is the longest (v_2, v_3) (or (v_2, w))-section of W (for which the internal vertices, if exist, are only possible $v_1, v_2, v_3, w \in V(Q)$). We consider the following two subsubcases.

Case 3.3.1. If W_2 contains vertex v_3, we may uniquely decompose W_2 into two sections $W_{21}W_{22}$, where W_{21} is the longest (v_1, v_3)-section of W_2 and W_{22} is the remaining shortest (v_3, v_2)-section of W_2.

Let $\eta(W) = \eta(W_1)\eta(W_{21})\eta(W_{22})\eta(W_3)\eta(W_4)$, where $\eta(W_1) = W_1$, $\eta(W_{21}) = W_{21}$, $\eta(W_3) = (W_3 - W_3 \cap (S_m^3 \cup Q)) \cup \xi(W_3 \cap (S_m^3 \cup Q))$, $\eta(W_{22})$ is a (v_3, v_1)-walk obtained from W_{22} replacing v_1 by v_2 and v_2 by v_1, and $\eta(W_4)$ is a (v_1, v_3) (or (v_1, w))-walk obtained from W_4 replacing v_1 by v_2 and v_2 by v_1.

Case 3.3.2. If W_2 does not contain vertex v_3, let $\eta(W) = \eta(W_1)\eta(W_2)\eta(W_3)\eta(W_4)$, where $\eta(W_1) = W_1$, $\eta(W_3) = (W_3 - W_3 \cap (S_m^3 \cup Q)) \cup \xi(W_3 \cap (S_m^3 \cup Q))$, $\eta(W_2)$ is a (v_1, v_1)-walk obtained from W_2 replacing its last two vertices v_1v_2 by v_1, and $\eta(W_4)$ is a (v_1, v_3) (or (v_1, w))-walk obtained from W_4 replacing its first vertex v_2 by v_1v_2.

Case 3.4. If W_1 does not pass edge v_1v_t and W_3 passes edge v_1v_t, we may anew decompose W into four sections $W_1W_2W_3W_4$, where W_1 is the longest (v_3, v_2) (or (w, v_2))-section of W (which do not contain vertices $u_0, \ldots, u_t''$ and must contain vertex v_3), the second W_2 is the internal longest (u_0, u_t'')-section of W (for which the internal vertices are some possible vertices in $V(G_1)$), W_3 is the third (v_2, v_1)-section of W (for which the internal vertices, if exist, are only possible $v_1, v_2, v_3, w \in V(Q)$), and the last W_4 is the longest (v_t, v_3) (or (v_t, w))-section of W. We have two subsubcases.

Case 3.4.1. If W_3 contains vertex v_3, we may uniquely decompose it into two sections $W_{31}W_{32}$, where W_{31} is the shortest (v_2, v_3)-section of W_3 and W_{32} is the remaining longest (v_3, v_1)-section of W_3.

Let $\eta(W) = \eta(W_1)\eta(W_2)\eta(W_{31})\eta(W_{32})\eta(W_4)$, where $\eta(W_2) = (W_2 - W_2 \cap (S_m^3 \cup Q)) \cup \xi(W_2 \cap (S_m^3 \cup Q))$, $\eta(W_{32}) = W_{32}$, $\eta(W_4) = W_4$, $\eta(W_1)$ is a (v_3, v_1) (or (w, v_1))-walk obtained from W_1 replacing v_1 by v_2 and v_2 by v_1, and $\eta(W_{31})$ is a (v_1, v_3)-walk obtained from W_{31} replacing v_1 by v_2 and v_2 by v_1.

Case 3.4.2. If W_3 does not contain vertex v_3, let $\eta(W) = \eta(W_1)\eta(W_2)\eta(W_3)\eta(W_4)$, where $\eta(W_2) = (W_2 - W_2 \cap S_m^3) \cup \xi(W_2 \cap S_m^3)$, $\eta(W_4) = W_4$, $\eta(W_1)$ is a (v_3, v_1) (or (w, v_1))-walk obtained from W_1 replacing its last vertex v_2 by v_2v_1, and $\eta(W_3)$ is a (v_1, v_1)-walk obtained from W_3 replacing its first two vertices v_2v_1 by v_1.

Case 4. Suppose W is a closed walk starting from v_i for $i = 4, 5, 6, \ldots, n$ in X_1. For $W \in X_1$, we may uniquely decompose W into five sections $W_1W_2W_3W_4W_5$, where W_1 is the longest (v_i, v_t)-section of W (which do not contain vertices $u_0, \ldots, u_t''$), W_2 is the second (v_1, v_2)-section of W (for which the internal vertices, if exist, are only possible $v_1, v_2, v_3, w \in V(G)$), the third W_3 is the internal longest (u_0, u_t'')-section of W (for which the internal vertices are some possible vertices in $V(G_1)$), the fourth W_4 is the longest

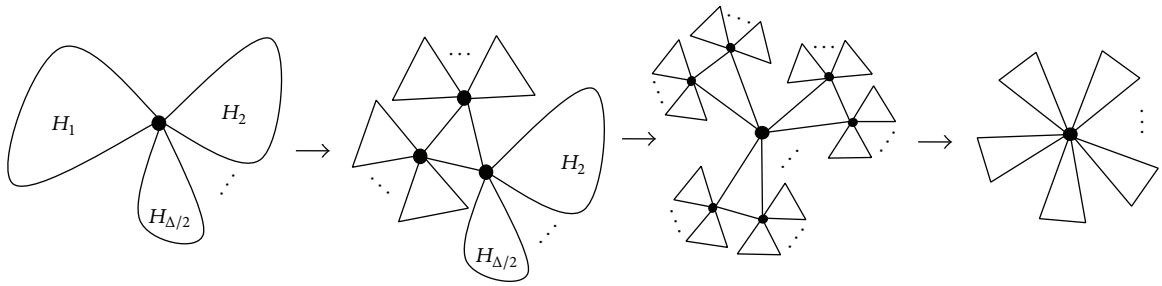

Figure 4: The procedure of transformation.

(v_2, v_1)-section of W (for which the internal vertices, if exist, are only possible $v_1, v_2, v_3, w \in V(G)$), and the last W_5 is the remaining (v_t', v_i)-section of W. We have four subcases.

Case 4.1. If both W_2 and W_4 contain the vertex v_3, we may uniquely decompose W_2 into two sections $W_{21}W_{22}$ and decompose W_4 into two sections $W_{41}W_{42}$, where W_{21} is the longest (v_1, v_3)-section of W_2, W_{22} is the remaining shortest (v_3, v_2) of W_2, W_{41} is the shortest (v_2, v_3)-section of W_4, and W_{42} is the remaining longest (v_3, v_1)-section of W_4.

Let $\eta(W) = \eta(W_1)\eta(W_{21})\eta(W_{22})\eta(W_3)\eta(W_{41})\eta(W_{42})\eta(W_5)$, where $\eta(W_1) = W_1$, $\eta(W_{21}) = W_{21}$, $\eta(W_3) = (W_3 - W_3 \cap (S_m^3 \cup Q)) \cup \xi(W_3 \cap (S_m^3 \cup Q))$, $\eta(W_{42}) = W_{42}\eta(W_5) = W_5$, $\eta(W_{22})$ is a (v_3, v_1)-walk obtained from W_{22} replacing v_1 by v_2 and v_2 by v_1, and $\eta(W_{41})$ is a (v_1, v_3)-walk obtained from W_{41} replacing v_1 by v_2 and v_2 by v_1.

Case 4.2. If W_2 contains the vertex v_3 and W_4 does not contain vertex v_3, let $\eta(W) = \eta(W_1)\eta(W_2)\eta(W_3)\eta(W_4)\eta(W_5)$, where $\eta(W_1) = W_1$, $\eta(W_3) = (W_3 - W_3 \cap (S_m^3 \cup Q)) \cup \xi(W_3 \cap (S_m^3 \cup Q))$, $\eta(W_5) = W_5$, $\eta(W_2)$ is a (v_1, v_1)-walk obtained from W_2 replacing its last vertex v_2 by v_2v_1, and $\eta(W_4)$ is a (v_1, v_1)-walk obtained from W_4 replacing its first two vertices v_2v_1 by v_1.

Case 4.3. If W_2 does not contain the vertex v_3, let $\eta(W) = \eta(W_1)\eta(W_2)\eta(W_3)\eta(W_4)\eta(W_5)$, where $\eta(W_1) = W_1$, $\eta(W_3) = (W_3 - W_3 \cap (S_m^3 \cup Q)) \cup \xi(W_3 \cap (S_m^3 \cup Q))$, $\eta(W_5) = W_5$, $\eta(W_2)$ is a (v_1, v_1)-walk obtained from W_2 by replacing its last two vertices v_1v_2 by v_1, and $\eta(W_4)$ is a (v_1, v_1)-walk obtained from W_4 by replacing its first vertex v_2 by v_1v_2.

For example,

$$\begin{aligned}
&\eta_1\left(u_0u_1\cdots u_rv_2v_3w_1\cdots w_tv_3v_1v_2u_1'\cdots u_s'v_2v_1v_3v_2u_1''\cdots u_t''u_0\right)\\
&= u_0u_1\cdots u_rv_1v_3w_1\cdots w_tv_3v_2v_1u_1'\cdots u_s'v_1v_2v_3v_1u_1''\cdots u_t''u_0,\\
&\eta_1\left(u_0u_1\cdots u_rv_2v_3w_1\cdots w_tv_3v_1v_4v_5v_1v_2u_1'\cdots u_s'v_2v_3v_5v_4v_1v_3v_2u_1''\cdots u_t''u_0\right)\\
&= u_0u_1\cdots u_rv_1v_2v_3w_1\cdots w_tv_3v_1v_4v_5v_1u_1'\cdots u_s'v_1v_3v_5v_4v_1v_3v_1u_1''\cdots u_t''u_0,\\
&\eta_1\left(v_3w_1\cdots w_tv_3v_2u_1\cdots u_rv_2v_1v_5v_4v_1v_2u_1'\cdots u_s'v_2v_1v_3\right)\\
&= v_3w_1\cdots w_tv_3v_1u_1\cdots u_rv_1v_5v_4v_1v_2v_1u_1'\cdots u_s'v_1v_2v_3,\\
&\eta_1\left(v_3v_2v_1v_7v_6v_1v_2v_1v_2u_1\cdots u_rv_2v_1v_4v_5v_1v_3v_2u_1'\cdots u_s'v_2v_1v_7v_6v_1v_2v_3\right)\\
&= v_3v_2v_1v_7v_6v_1v_2v_1u_1\cdots u_rv_1v_4v_5v_1v_3v_2v_1u_1'\cdots u_s'v_1v_2v_1v_7v_6v_1v_2v_3,\\
&\eta_1\left(v_1v_4v_5v_1v_3v_2u_1\cdots u_rv_2v_3v_2v_1v_4v_5v_1v_3v_2u_1'\cdots u_s'v_2v_1\right)\\
&= v_2v_3v_1v_5v_4v_1u_1\cdots u_rv_1v_3v_2v_1v_4v_5v_1v_3v_1u_1'\cdots u_s'v_1v_2,\\
&\eta_1\left(v_4v_5v_1v_3v_2u_1\cdots u_rv_2v_3v_2v_1v_4v_5v_1v_3v_2u_1'\cdots u_s'v_2v_3v_2v_1v_5v_4\right)\\
&= v_4v_5v_1v_3v_1u_1\cdots u_rv_1v_3v_2v_1v_4v_5v_1v_3v_1u_1'\cdots u_s'v_1v_3v_2v_1v_5v_4,
\end{aligned} \tag{8}$$

where $u_0, u_1, \ldots, u_r$, $u_1', \ldots, u_s'$, $u_1'', \ldots, u_t''$ are vertices in G and $w_1, \ldots, w_t$ are vertices in Q.

By Lemma 1, ξ is injective and not surjective. It is easily shown that η is also injective and not surjective. Thus $|X_1| < |X_2|$, $M_k(G_1) < M_k(G_2)$. □

Theorem 3. *Let G_H be an arbitrary graph on n vertices in set $\Gamma(n, m)$, where $n > 5$. Then $EE(G_H) \leq EE(S_m^3)$ with the equality holding if and only if $G_H \cong S_m^3$.*

Proof. Determine a vertex v of the maximum degree Δ as a root in G_H, and let $k \geq 4$ be an integer. Let G_{H_i} be the completely connected graph of 3-uniform linear hypertree H_i attached at v, and let m_i be the number of triangles of G_{H_i} for $i = 1, 2, \ldots, \Delta/2$, respectively. We can repeatedly apply this transformation from Lemma 2 at some vertices whose degrees are not equal to two or $2m_i$ in G_{H_i} till G_{H_i} becomes a star. From Lemma 2, it satisfies that each application of this transformation strictly increases the number of closed walks and also increases Estrada index.

When all G_{H_i} turn into stars, we can again use Lemma 2 at the vertex v as long as there exists at least one vertex whose degree is not equal to two or $2\sum m_i$, further increasing the number of closed walks. In the end of this procedure, we get the star S_m^3. The whole procedure of transformation is shown in Figure 4. □

Lemma 4 (see [20]). *Let v be a vertex of a graph G, $G - \{v\} = G - v$ for $v \in V(G)$, and $\mathscr{C}(v)$ the set of cycles containing v. Consider*

$$P(G,\lambda) = \lambda \cdot P(G - v, \lambda) - \sum_{vw \in E(G)} P(G - v - w, \lambda) - 2\sum_{Z \in \mathscr{C}(v)} P(G - V(Z), \lambda), \tag{9}$$

where $P(G - v - w, \lambda) = 1$ if G is a single edge and $P(G - V(Z), \lambda) = 1$ if G is a cycle.

Now, we calculate $EE(S_m^3)$. Applying Lemma 4, we have

$$P\left(S_m^3, \lambda\right) = (\lambda + 1)^{(n-1)/2}(\lambda - 1)^{(n-3)/2}\left(\lambda^2 - \lambda - n + 1\right). \tag{10}$$

By some simple calculating, we achieve the following eigenvalues:

$$\begin{gathered} \lambda_1 = \lambda_2 = \cdots = \lambda_{(n-1)/2} = -1, \\ \lambda_{(n+1)/2} = \lambda_{(n+3)/2} = \cdots = \lambda_{n-2} = 1, \\ \lambda_{n-1} = \frac{1 - \sqrt{4n-3}}{2}, \qquad \lambda_n = \frac{1 + \sqrt{4n-3}}{2}. \end{gathered} \tag{11}$$

Then, we obtain

$$EE\left(S_m^3\right) = \frac{(n-1)}{2e} + \frac{(n-3)}{2}e + e^{(1+\sqrt{4n-3})/2} + e^{(1-\sqrt{4n-3})/2}. \tag{12}$$

Theorem 3 shows that the star S_m^3 has the maximum Estrada index in set $\Gamma(n, m)$. Thus, according to previous definition, it is easy to show that the 3-uniform star $\mathcal{S}_m^3$ has the maximum Estrada index among the set of 3-uniform linear hypertrees; that is,

$$EE(H) \le EE\left(\mathcal{S}_m^3\right), \tag{13}$$

where

$$EE\left(\mathcal{S}_m^3\right) = \frac{(n-1)}{2e} + \frac{(n-3)}{2}e + e^{(1+\sqrt{4n-3})/2} + e^{(1-\sqrt{4n-3})/2}. \tag{14}$$

Conflict of Interests

The authors declare that there is no conflict of interests regarding the publication of this paper.

Acknowledgments

This work was supported by Program for Changjiang Scholars and Innovative Research Team in University (PCSIRT)(no. ITR1068), Special 973 Program for Key Basic Research of the Ministry of Science and Technology, China (no. 2010CB334708), the National Natural Science Foundation of China (NSFC)(no. 60863006), Scientific Research Foundation of the Department of Science and Technology, Qinghai Province, China (no. 2012-Z-943).

References

[1] E. Estrada, "Characterization of 3D molecular structure," *Chemical Physics Letters*, vol. 319, no. 5-6, pp. 713–718, 2000.

[2] E. Estrada, "Characterization of the folding degree of proteins," *Bioinformatics*, vol. 18, no. 5, pp. 697–704, 2002.

[3] E. Estrada, "Characterization of the amino acid c ontration to the folding degree of proteins," *Proteins*, vol. 54, no. 4, pp. 727–737, 2004.

[4] E. Estrada and J. A. Rodríguez-Velázquez, "Subgraph centrality in complex networks," *Physical Review E: Statistical, Nonlinear, and Soft Matter Physics*, vol. 71, no. 5, 9 pages, 2005.

[5] E. Estrada, J. A. Rodríguez-Velázquez, and M. Randić, "Atomic branching in molecules," *International Journal of Quantum Chemistry*, vol. 106, no. 4, pp. 823–832, 2006.

[6] K. C. Das and S. Lee, "On the Estrada index conjecture," *Linear Algebra and its Applications*, vol. 431, no. 8, pp. 1351–1359, 2009.

[7] H. Deng, "A proof of a conjecture on the Estrada index," *MATCH, Communications in Mathematical and in Computer Chemistry*, vol. 62, no. 3, pp. 599–606, 2009.

[8] Z. Du and B. Zhou, "The Estrada index of trees," *Linear Algebra and Its Applications*, vol. 435, no. 10, pp. 2462–2467, 2011.

[9] Z. Du and B. Zhou, "The Estrada index of unicyclic graphs," *Linear Algebra and Its Applications*, vol. 436, no. 9, pp. 3149–3159, 2012.

[10] Q. Deng and H. Chen, "On extremal bipartite unicyclic graphs," *Linear Algebra and Its Applications*, vol. 444, pp. 89–99, 2014.

[11] A. Ilić and D. Stevanović, "The Estrada index of chemical trees," *Journal of Mathematical Chemistry*, vol. 47, no. 1, pp. 305–314, 2010.

[12] W. Wang and W. Xu, "Graphs with the maximal Estrada indices," *Linear Algebra and its Applications*, vol. 446, pp. 314–328, 2014.

[13] H. Zhao and Y. Jia, "On the Estrada index of bipartite graph," *MATCH: Communications in Mathematical and in Computer Chemistry*, vol. 61, no. 2, pp. 495–501, 2009.

[14] B. Zhou and Z. Du, "Some lower bounds for Estrada index," *Iranian Journal of Mathematical Chemistry*, vol. 1, no. 2, pp. 67–72, 2010.

[15] Z. Zhu, L. Tan, and Z. Qiu, "Tricyclic graph with maximal Estrada index," *Discrete Applied Mathematics*, vol. 162, pp. 364–372, 2014.

[16] Z. Du, "An edge grafting theorem on the Estrada index of graphs and its applications," *Discrete Applied Mathematics*, vol. 161, no. 1-2, pp. 134–139, 2013.

[17] J. A. de la Peña, I. Gutman, and J. Rada, "Estimating the Estrada index," *Linear Algebra and its Applications*, vol. 427, no. 1, pp. 70–76, 2007.

[18] I. Gutman, H. Deng, and S. Radenković, "The Estrada index," in *Applications of Graph Spectra*, D. Cvetković and I. Gutman, Eds., pp. 155–174, Mathematics Institute, Beograd, Serbia, 2011.

[19] J. Liu, X. Pan, and J. Cao, "Some properties on Estrada index of folded hypercubes networks," *Abstract and Applied Analysis*, vol. 2014, Article ID 167623, 6 pages, 2014.

[20] C. Berge, *Graphs and Hypergraphs*, Elsevier, New York, NY, USA, 1973.

[21] E. Estrada and J. A. Rodríguez-Velázquez, "Subgraph centrality and clustering in complex hyper-networks," *Physica A: Statistical Mechanics and Its Applications*, vol. 364, pp. 581–594, 2006.

[22] D. Cvetkoic, M. Doob, and H. Sachs, *Spectra of Graphs. Theory and Application*, vol. 87 of *Pure and Applied Mathematics*, Academic Press, New York, NY, USA, 1980.

Hindawi Publishing Corporation
The Scientific World Journal
Volume 2014, Article ID 490364, 7 pages
http://dx.doi.org/10.1155/2014/490364

Research Article

One Adaptive Synchronization Approach for Fractional-Order Chaotic System with Fractional-Order $1 < q < 2$

Ping Zhou[1,2] and Rongji Bai[1,2]

[1] *Center of System Theory and Its Applications, Chongqing University of Posts and Telecommunications, Chongqing 400065, China*
[2] *Key Laboratory of Network Control and Intelligent Instrument of Ministry of Education, Chongqing University of Posts and Telecommunications, Chongqing 400065, China*

Correspondence should be addressed to Ping Zhou; zhouping@cqupt.edu.cn

Received 19 May 2014; Accepted 11 August 2014; Published 27 August 2014

Academic Editor: Jianquan Lu

Based on a new stability result of equilibrium point in nonlinear fractional-order systems for fractional-order lying in $1 < q < 2$, one adaptive synchronization approach is established. The adaptive synchronization for the fractional-order Lorenz chaotic system with fractional-order $1 < q < 2$ is considered. Numerical simulations show the validity and feasibility of the proposed scheme.

1. Introduction

Fractional-order differential equations can be more accurately described in the real-world physical systems [1–3]. Many fractional-order systems create chaotic attractor. Many fractional-order chaotic attractors have been reported in recent years, for example, the fractional-order Lorenz chaotic attractor [1, 4, 5], the fractional-order Chen chaotic attractor [5], the fractional-order Lu chaotic attractor [2, 4], the fractional-order Chua chaotic attractor [5], the fractional-order Duffing chaotic attractor [6], the fractional-order Rössler chaotic attractor [7, 8], and so on. On the other hand, synchronization of chaotic systems has been given more attention [2, 9–13]. This is due to its applications in the field of engineering and science. Over the last two decades, many scholars have proposed various synchronization schemes. It is well known that many chaotic systems in practical situations are usually with fully or partially unknown parameters. In order to estimate the unknown parameters, a synchronization scheme named adaptive synchronization has been proposed. Now, the adaptive synchronization [13–16] has attracted more and more attention. This is due to its effectiveness in many practical chaos applications.

However, many adaptive synchronization approaches on fractional-order chaotic systems reported previously [2, 9–13] were considered the fractional-order lying in $0 < q < 1$. To the best of our knowledge, there are a few results about adaptive synchronization on fractional-order chaotic systems with fractional-order $1 < q < 2$. In fact, there are many fractional-order systems with fractional-order $1 < q < 2$ in real-world physical systems, for example, the fractional diffusion-wave equation [17], the fractional telegraph equation [18], the time fractional heat conduction equation [19], and so forth. So, an interesting question is how to realize the adaptive synchronization for fractional-order lying in $1 < q < 2$? This question is of practical importance as well as academic significance. In this paper, a positive answer is given for the above question.

Inspired by the above-mentioned discussion, one adaptive synchronization approach for a class of fractional-order chaotic system with $1 < q < 2$ is established. This approach is based on a new stability result of equilibrium point in nonlinear fractional-order systems for fractional-order lying in $1 < q < 2$ [1]. The adaptive synchronization for the fractional-order Lorenz chaotic system with fractional-order $1 < q < 2$ is considered. Numerical simulations show the validity and feasibility of the proposed scheme.

2. Preliminaries and Main Results

In our paper, the qth Caputo derivative for function $g(t)$ is shown as

$$D^q g(t) = \frac{1}{\Gamma(l-q)} \int_0^t \frac{g^{(l)}(\tau)}{(t-\tau)^{q+1-l}} d\tau, \quad l-1 < q < l, \quad (1)$$

where D^q denote the Caputo derivative, l is the smallest integer larger than q, $g^{(l)}(t)$ is the l th derivative in the usual sense, and Γ is the gamma function.

Now, consider the following fractional-order chaotic system:

$$D^q x = f(x) = Mx + n(x), \quad (2)$$

where fractional-order $1 < q < 2$, $x \in R^{n\times 1}$, and $f(x) \in R^{n\times 1}$. $M \in R^{n\times n}$ is a constant matrix. $n(x) \in R^{n\times 1}$ is the nonlinear part of system (2).

The system (2) can be rewritten as follows:

$$D^q x = L\begin{pmatrix} x \\ \sigma_0 \end{pmatrix} + n(x, \sigma_0), \quad (3)$$

where $\sigma_0 \in R$ is the system parameter. $n(x, \sigma_0) \in R^{n\times 1}$ is the nonlinear part, and all the terms with system parameter σ_0 are contained in $n(x, \sigma_0)$. $L \in R^{n\times(n+1)}$ is a constant matrix, and matrix element $L_{i,n+1} = 0$ $(i = 1, 2, \ldots, n)$.

In this paper, we focus on a class of fractional-order chaotic system in which the equation $n(y, \sigma_0) - n(x, \sigma_0) = n_{lp}(x)(y - x) + n_{np}(y - x, x)$ holds. Here, variable $y \in R^{n\times 1}$ is real number. Vector $n_{lp}(x)(y - x)$ and vector $n_{np}(y - x, x)$ are the linear part and nonlinear part with respect to $(y - x)$, respectively. In fact, the nonlinear term $n(x, \sigma_0)$ in many fractional-order chaotic systems meet this equation, for example, the fractional-order Lorenz chaotic system, fractional-order Chen chaotic system, fractional-order Lu chaotic system, fractional-order Rössler chaotic system, the fractional-order Chua's chaotic system and its modified chaotic system, the fractional-order Duffing chaotic system, the fractional-order Arneodo chaotic system, the fractional-order Sprott chaotic system, and so forth.

Next, the adaptive synchronization for fractional-order chaotic system (3) is proposed. Select system (3) as drive system; the response systems with parameter update law are shown as follows:

$$\begin{gathered} D^q y = L\begin{pmatrix} y \\ \sigma \end{pmatrix} + n(y, \sigma) + u(x, y, \sigma), \\ D^q \sigma = \Omega e, \end{gathered} \quad (4)$$

where $y \in R^{n\times 1}$ is state vector, $u(x, y, \sigma) \in R^{n\times 1}$ is a controller, $\Omega \in R^{1\times(n+1)}$ is real constant matrix, and parameter σ is unknown in response system (4). The true value of the "unknown" parameter σ is selected as σ_0. The parameter update law is $D^q\sigma = \Omega e$. The adaptive synchronization errors are $e = (e_1, \ldots, e_n, e_{n+1})^{\mathbf{T}} \in R^{(n+1)\times 1}$, $e_i = (y_i - x_i) \in R$ $(i = 1, 2, \ldots, n)$, and $e_{n+1} = e_\sigma = (\sigma - \sigma_0) \in R$.

Lemma 1 (see [1]). *For the nonlinear part $n(x)$ of systems* (2), *if*

(i) $n(x)|_{x=0} = 0$, $\lim_{x\to 0}(\|n(x)\|/\|x\|) = 0$;

(ii) $\mathrm{Re}[\lambda(M)] < 0$, $-\max[\mathrm{Re}\,\lambda(M)] > [\Gamma(q)]^{1/q}$.

Then, the zero solution of fractional-order chaotic system (2) *is asymptotically stable.*

Based on this lemma, the following main results are given.

Theorem 2. *If the controller is selected as*

$$u(x, y, \sigma) = \left[F - n_{lp}(x)\right] e \quad (5)$$

and the following conditions are satisfied:

(i) $\begin{pmatrix} n_{np}(e,x) \\ 0 \end{pmatrix}\Big|_{e=0} = 0$, $\lim_{e\to 0}(\|\begin{pmatrix} n_{np}(e,x) \\ 0 \end{pmatrix}\|/\|e\|) = 0$ *for any x,*

(ii) $\mathrm{Re}[\lambda\begin{pmatrix} L+F \\ \Omega \end{pmatrix}] < 0$, $-\max[\mathrm{Re}\,\lambda\begin{pmatrix} L+F \\ \Omega \end{pmatrix}] > [\Gamma(q)]^{1/q}$,

then the adaptive synchronization between fractional-order chaotic system (3) *and fractional-order system* (4) *can be arrived, where $n(y, \sigma) - n(x, \sigma_0) = n_{lp}(x)e + n_{np}(e, x)$, $n_{lp}(x) \in R^{n\times(n+1)}$, and $n_{np}(e, x) \in R^{n\times 1}$. $F \in R^{n\times(n+1)}$ is a suitable constant matrix.*

Proof. The error system between systems (4) and (3) can be shown as

$$\begin{gathered} D^q(y - x) = L\left(\begin{pmatrix} y \\ \sigma \end{pmatrix} - \begin{pmatrix} x \\ \sigma_0 \end{pmatrix}\right) + n(y, \sigma) \\ - n(x, \sigma_0) + u(x, y, \sigma). \\ D^q\sigma = \Omega e. \end{gathered} \quad (6)$$

Due to $e = (e_1, \ldots, e_n, e_{n+1})^{\mathbf{T}}$, $e_i = y_i - x_i$ $(i = 1, 2, \ldots, n)$, and $e_{n+1} = e_\sigma = (\sigma - \sigma_0)$, system (6) can be rewritten as

$$\begin{gathered} D^q(y - x) = Le + n(y, \sigma) - n(x, \sigma_0) + u(x, y, \sigma), \\ D^q\sigma = \Omega e. \end{gathered} \quad (7)$$

Using $n(y, \sigma) - n(x, \sigma_0) = n_{lp}(x)e + n_{np}(e, x)$, $D^q\sigma_0 = 0$, and $D^q\sigma = D^q(\sigma - \sigma_0) = D^q e_\sigma$, error system (7) can be changed as

$$\begin{gathered} D^q(y - x) = Le + n_{lp}(x)e + n_{np}(e, x) + u(x, y, \sigma), \\ D^q e_\sigma = \Omega e. \end{gathered} \quad (8)$$

Since $u(x, y, \sigma) = [F - n_{lp}(x)]e$ and $e = (e_1, \ldots, e_n, e_{n+1})^{\mathbf{T}}$, therefore, (8) can be changed as

$$D^q e = \begin{pmatrix} L + F \\ \Omega \end{pmatrix} e + \begin{pmatrix} n_{np}(e, x) \\ 0 \end{pmatrix}. \quad (9)$$

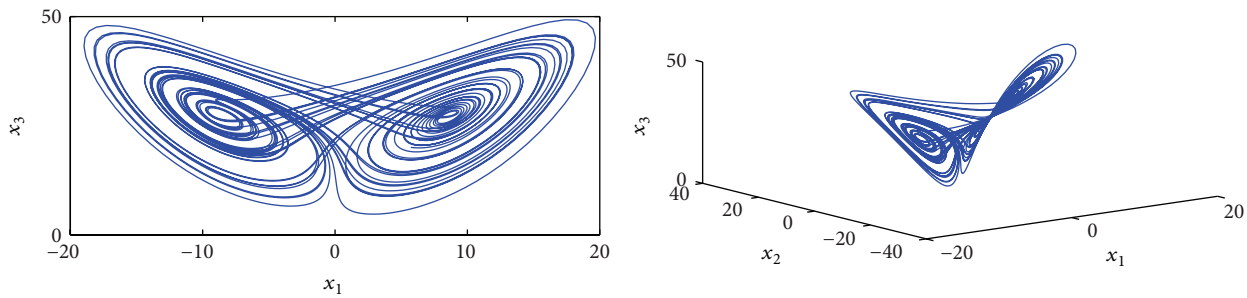

Figure 1: The attractor of fractional-order Lorenz system (12) for $q = 1.05$.

Due to $\left(\begin{smallmatrix} n_{np}(e,x) \\ 0 \end{smallmatrix}\right)\Big|_{e=0} = 0$, $\lim_{e\to 0}(\|\left(\begin{smallmatrix} n_{np}(e,x) \\ 0 \end{smallmatrix}\right)\|/\|e\|) = 0$ for any x, $\mathrm{Re}[\lambda\left(\begin{smallmatrix} L+F \\ \Omega \end{smallmatrix}\right)] < 0$, and $-\max[\mathrm{Re}\,\lambda\left(\begin{smallmatrix} L+F \\ \Omega \end{smallmatrix}\right)] > [\Gamma(q)]^{1/q}$. According to the above-mentioned lemma, the zero solution of fractional-order system (9) is asymptotically stable. So, the following result holds:

$$\lim_{t\to+\infty}\|e\| = 0. \tag{10}$$

It implies the following:

$$\lim_{t\to+\infty}\|y-x\| = 0, \qquad \lim_{t\to+\infty}(\sigma-\sigma_0) = 0. \tag{11}$$

Therefore, the adaptive synchronization between fractional-order chaotic system (3) and fractional-order system (4) can be arrived. The proof is completed. □

3. Illustrative Example

In this section, to show the effectiveness of the adaptive synchronization approach in this paper, the adaptive synchronization for the fractional-order Lorenz chaotic system [4] with fractional-order $1 < q < 2$ is considered. Numerical simulations show the validity and feasibility of the proposed scheme.

The fractional-order Lorenz system is described by

$$\begin{pmatrix} D^q x_1 \\ D^q x_2 \\ D^q x_3 \end{pmatrix} = \begin{pmatrix} a_0(x_2 - x_1) \\ b_0 x_1 - x_2 - x_1 x_3 \\ x_1 x_2 - c_0 x_3 \end{pmatrix}, \tag{12}$$

where a_0, b_0, and c_0 are system parameters. Let $a_0 = 10$, $b_0 = 28$, $c_0 = 8/3$, and $q = 1.05$; the system (12) creates chaotic attractor. The chaotic attractor is shown in Figure 1.

Case 1 (parameter a is unknown in response system). Now, assume the system parameter a in in response system is the unknown parameter. The true value of the "unknown" parameter a is selected as a_0.

The fractional-order Lorenz system (12) can be rewritten as

$$\begin{pmatrix} D^q x_1 \\ D^q x_2 \\ D^q x_3 \end{pmatrix} = \begin{pmatrix} 0 & 0 & 0 & 0 \\ 28 & -1 & 0 & 0 \\ 0 & 0 & -\frac{8}{3} & 0 \end{pmatrix}\begin{pmatrix} x_1 \\ x_2 \\ x_3 \\ a_0 \end{pmatrix} + \begin{pmatrix} a_0(x_2 - x_1) \\ -x_1 x_3 \\ x_1 x_2 \end{pmatrix}, \tag{13}$$

where $a_0 = 10$.

So

$$L = \begin{pmatrix} 0 & 0 & 0 & 0 \\ 28 & -1 & 0 & 0 \\ 0 & 0 & -\frac{8}{3} & 0 \end{pmatrix}. \tag{14}$$

According to Section 2, the response system with unknown parameter a can be given as

$$\begin{pmatrix} D^q y_1 \\ D^q y_2 \\ D^q y_3 \end{pmatrix} = \begin{pmatrix} 0 & 0 & 0 & 0 \\ 28 & -1 & 0 & 0 \\ 0 & 0 & -\frac{8}{3} & 0 \end{pmatrix}\begin{pmatrix} y_1 \\ y_2 \\ y_3 \\ a \end{pmatrix} + \begin{pmatrix} a(y_2 - y_1) \\ -y_1 y_3 \\ y_1 y_2 \end{pmatrix} + \left(F - n_{lp}(x)\right)\begin{pmatrix} e_1 \\ e_2 \\ e_3 \\ e_a \end{pmatrix} \tag{15}$$

and the parameter update law is

$$D^q a = \Omega(e_1 \;\; e_2 \;\; e_3 \;\; e_a)^{\mathrm{T}}. \tag{16}$$

It is easy to obtain the following:

$$\begin{pmatrix} a(y_2 - y_1) \\ -y_1 y_3 \\ y_1 y_2 \end{pmatrix} - \begin{pmatrix} a_0(x_2 - x_1) \\ -x_1 x_3 \\ x_1 x_2 \end{pmatrix} = \begin{pmatrix} -a_0 & a_0 & 0 & x_2 - x_1 \\ -x_3 & 0 & -x_1 & 0 \\ x_2 & x_1 & 0 & 0 \end{pmatrix}\begin{pmatrix} e_1 \\ e_2 \\ e_3 \\ e_a \end{pmatrix} + \begin{pmatrix} e_a(e_2 - e_1) \\ -e_1 e_3 \\ e_1 e_2 \end{pmatrix}. \tag{17}$$

So

$$n_{lp}(x) = \begin{pmatrix} -a_0 & a_0 & 0 & x_2 - x_1 \\ -x_3 & 0 & -x_1 & 0 \\ x_2 & x_1 & 0 & 0 \end{pmatrix},$$
$$n_{np}(e, x) = \begin{pmatrix} e_a(e_2 - e_1) \\ -e_1 e_3 \\ e_1 e_2 \end{pmatrix}. \tag{18}$$

Now, it is easy to verify the following:

$$\begin{aligned} &\frac{\left\| \begin{pmatrix} n_{np}(e,x) \\ 0 \end{pmatrix} \right\|}{\|e\|} \\ &= \sqrt{\frac{e_a^2(e_2 - e_1)^2 + (e_1 e_3)^2 + (e_1 e_2)^2}{e_1^2 + e_2^2 + e_3^2 + e_a^2}} \\ &\le \sqrt{\frac{e_a^2(|e_2| + |e_1|)^2 + (e_1 e_3)^2 + (e_1 e_2)^2}{e_1^2 + e_2^2 + e_3^2 + e_a^2}} \\ &= \sqrt{\frac{e_a^2(|e_2| + |e_1|)^2}{e_1^2 + e_2^2 + e_3^2 + e_a^2} + \frac{(e_1 e_3)^2 + (e_1 e_2)^2}{e_1^2 + e_2^2 + e_3^2 + e_a^2}} \\ &\le \sqrt{\frac{e_a^2(|e_2| + |e_1|)^2}{e_a^2} + \frac{(e_1 e_3)^2 + (e_1 e_2)^2}{e_1^2}} \\ &= \sqrt{(|e_2| + |e_1|)^2 + (e_2)^2 + (e_3)^2}, \\ &\lim_{e \to 0} \frac{\left\| \begin{pmatrix} n_{np}(e,x) \\ 0 \end{pmatrix} \right\|}{\|e\|} \\ &\le \lim_{e \to 0} \sqrt{(|e_2| + |e_1|)^2 + (e_2)^2 + (e_3)^2} = 0, \\ &\left. \begin{pmatrix} n_{np}(e,x) \\ 0 \end{pmatrix} \right|_{e=0} = 0. \end{aligned} \tag{19}$$

Therefore, the first condition in the above-mentioned theorem holds.

Now, choose suitable real constant matrix $\Omega \in R^{1\times n}$ and $F \in R^{n\times(n+1)}$ such that

$$\begin{aligned} &\operatorname{Re}\left[\lambda \begin{pmatrix} L + F \\ \Omega \end{pmatrix}\right] < 0, \\ &-\max\left[\operatorname{Re}\lambda \begin{pmatrix} L + F \\ \Omega \end{pmatrix}\right] > [\Gamma(q)]^{1/q}. \end{aligned} \tag{20}$$

So the second condition in the above-mentioned theorem holds. According to the theorem in Section 2, the adaptive synchronization between drive system (13) and response system (15) with parameter update law (16) can be achieved.

For example, let $F = \begin{pmatrix} -1 & 0 & 0 & 0 \\ -28 & 0 & 0 & 0 \\ 0 & 0 & 0 & 0 \end{pmatrix}$ and $\Omega = \begin{pmatrix} 0 & 0 & 0 & -1 \end{pmatrix}$. So $\begin{pmatrix} L+F \\ \Omega \end{pmatrix} = \begin{pmatrix} -1 & 0 & 0 & 0 \\ 0 & -1 & 0 & 0 \\ 0 & 0 & -8/3 & 0 \\ 0 & 0 & 0 & -1 \end{pmatrix}$. Therefore, $\lambda_i = -1$ $(i = 1, 2, 3)$, $\lambda_4 = -8/3$, and $-\max[\operatorname{Re}\lambda \begin{pmatrix} L+F \\ \Omega \end{pmatrix}] = 1 > [\Gamma(q)]^{1/q} = 0.9722$, respectively. Simulation results are shown in Figure 2. Here, $a(0) = 7$, and all the initial conditions in this paper are $(x_{10}, x_{20}, x_{30}) = (10, 20, 30)$, and $(y_{10}, y_{20}, y_{30}) = (1, 2, 5)$, respectively.

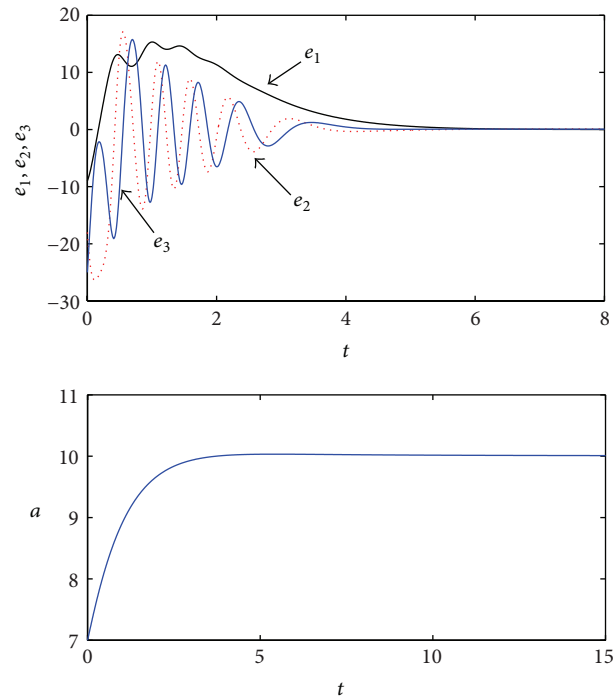

Figure 2: Simulation results of the adaptive synchronization for the fractional-order Lorenz chaotic system.

Case 2 (parameter b is unknown in response system). Now, assume that the system parameter b in response system is the unknown parameter. The true value of the "unknown" parameter b is selected as b_0.

The fractional-order Lorenz system (12) can be rewritten as

$$\begin{pmatrix} D^q x_1 \\ D^q x_2 \\ D^q x_3 \end{pmatrix} = \begin{pmatrix} -10 & 10 & 0 & 0 \\ 0 & -1 & 0 & 0 \\ 0 & 0 & -\frac{8}{3} & 0 \end{pmatrix} \begin{pmatrix} x_1 \\ x_2 \\ x_3 \\ b_0 \end{pmatrix} + \begin{pmatrix} 0 \\ b_0 x_1 - x_1 x_3 \\ x_1 x_2 \end{pmatrix}, \tag{21}$$

where $b_0 = 28$.

So

$$L = \begin{pmatrix} -10 & 10 & 0 & 0 \\ 0 & -1 & 0 & 0 \\ 0 & 0 & -\frac{8}{3} & 0 \end{pmatrix}. \tag{22}$$

According to Section 2, the response system with unknown parameter b can be given as

$$\begin{pmatrix} D^{q_2} y_1 \\ D^{q_2} y_2 \\ D^{q_2} y_3 \end{pmatrix} = \begin{pmatrix} -10 & 10 & 0 & 0 \\ 0 & -1 & 0 & 0 \\ 0 & 0 & -\frac{8}{3} & 0 \end{pmatrix} \begin{pmatrix} y_1 \\ y_2 \\ y_3 \\ b \end{pmatrix} + \begin{pmatrix} 0 \\ by_1 - y_1 y_3 \\ y_1 y_2 \end{pmatrix} + \left(F - n_{lp}(x)\right) \begin{pmatrix} e_1 \\ e_2 \\ e_3 \\ e_b \end{pmatrix} \tag{23}$$

and the parameter update law is

$$D^q b = \Omega (e_1 \;\; e_2 \;\; e_3 \;\; e_b)^{\mathrm{T}}. \tag{24}$$

It is easy to obtain the following:

$$\begin{aligned} &\begin{pmatrix} 0 \\ by_1 - y_1 y_3 \\ y_1 y_2 \end{pmatrix} - \begin{pmatrix} 0 \\ b_0 x_1 - x_1 x_3 \\ x_1 x_2 \end{pmatrix} \\ &= \begin{pmatrix} 0 & 0 & 0 & 0 \\ b_0 - x_3 & 0 & -x_1 & 0 \\ x_2 & x_1 & 0 & 0 \end{pmatrix} \begin{pmatrix} e_1 \\ e_2 \\ e_3 \\ e_b \end{pmatrix} \\ &+ \begin{pmatrix} 0 \\ -e_1 e_3 + e_b e_1 \\ e_1 e_2 \end{pmatrix}. \end{aligned} \tag{25}$$

So

$$\begin{aligned} n_{lp}(x) &= \begin{pmatrix} 0 & 0 & 0 & 0 \\ b_0 - x_3 & 0 & -x_1 & 0 \\ x_2 & x_1 & 0 & 0 \end{pmatrix}, \\ n_{np}(e, x) &= \begin{pmatrix} 0 \\ -e_1 e_3 + e_b e_1 \\ e_1 e_2 \end{pmatrix}. \end{aligned} \tag{26}$$

Now, it is easy to verify the following:

$$\begin{aligned} &\frac{\left\| \left(\begin{smallmatrix} n_{np}(e,x) \\ 0 \end{smallmatrix} \right) \right\|}{\|e\|} \\ &= \sqrt{\frac{(-e_1 e_3 + e_b e_1)^2 + (e_1 e_2)^2}{e_1^2 + e_2^2 + e_3^2 + e_b^2}} \\ &\le \sqrt{\frac{(|e_3| + |e_b|)^2 e_1^2 + (e_1 e_2)^2}{e_1^2 + e_2^2 + e_3^2 + e_b^2}} \\ &\le \sqrt{\frac{(|e_3| + |e_b|)^2 e_1^2 + (e_1 e_2)^2}{e_1^2}} \\ &= \sqrt{(|e_3| + |e_b|)^2 + (e_2)^2}, \end{aligned}$$

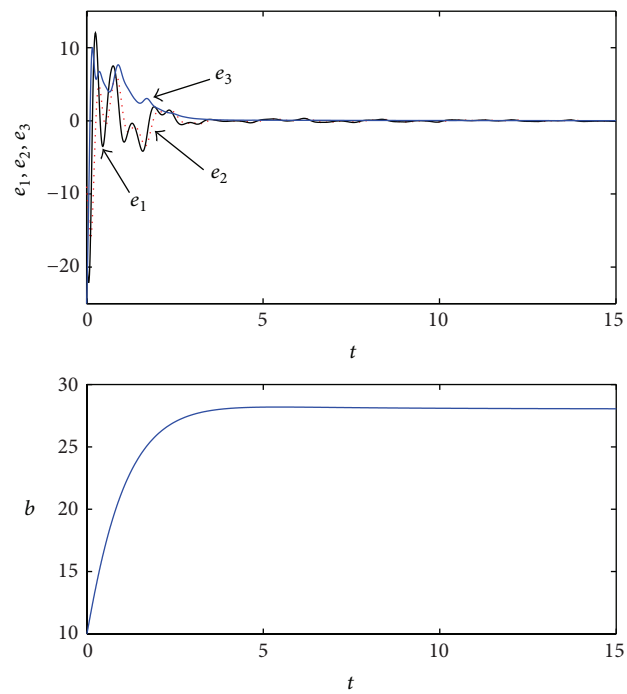

Figure 3: Simulation results of the adaptive synchronization for the fractional-order Lorenz chaotic system.

$$\begin{aligned} &\lim_{e \to 0} \frac{\left\| \left(\begin{smallmatrix} n_{np}(e,x) \\ 0 \end{smallmatrix} \right) \right\|}{\|e\|} \le \lim_{e \to 0} \sqrt{(|e_3| + |e_b|)^2 + (e_2)^2} = 0, \\ &\left(\begin{matrix} n_{np}(e, x) \\ 0 \end{matrix} \right) \Bigg|_{e=0} = 0. \end{aligned} \tag{27}$$

Therefore, the first condition in the above-mentioned theorem holds.

Now, choose suitable real constant matrix $\Omega \in R^{1 \times n}$ and $F \in R^{n \times (n+1)}$ such that

$$\begin{aligned} &\mathrm{Re}\left[\lambda \left(\begin{matrix} L + F \\ \Omega \end{matrix} \right)\right] < 0, \\ &-\max\left[\mathrm{Re}\,\lambda \left(\begin{matrix} L + F \\ \Omega \end{matrix} \right)\right] > [\Gamma(q)]^{1/q}. \end{aligned} \tag{28}$$

So the second condition in the above-mentioned theorem holds. According to the theorem in Section 2, the adaptive synchronization between drive system (21) and response system (23) with parameter update law (24) can be achieved.

For example, let $F = \left(\begin{smallmatrix} 0 & 0 & 0 & 0 \\ -10 & 0 & 0 & 0 \\ 0 & 0 & 0 & 0 \end{smallmatrix} \right)$ and $\Omega = (0 \;\; 0 \;\; 0 \;\; -1)$. So $\left(\begin{smallmatrix} L+F \\ \Omega \end{smallmatrix} \right) = \left(\begin{smallmatrix} -10 & 10 & 0 & 0 \\ -10 & -1 & 0 & 0 \\ 0 & 0 & -8/3 & 0 \\ 0 & 0 & 0 & -1 \end{smallmatrix} \right)$. Therefore, $\lambda_{\pm} = -5.5 \pm 8.9303\,j$, $\lambda_3 = -8/3$, $\lambda_4 = -1$, and $-\max[\mathrm{Re}\,\lambda \left(\begin{smallmatrix} L+F \\ \Omega \end{smallmatrix} \right)] = 1 > [\Gamma(q)]^{1/q} = 0.9722$, respectively. Simulation results are shown in Figure 3. Here, $b(0) = 10$.

Case 3 (parameter c is unknown in response system). Now, assume that the system parameter c in response system is

the unknown parameter. The true value of the "unknown" parameter c is selected as c_0.

The fractional-order Lorenz system (12) can be rewritten as

$$\begin{pmatrix} D^q x_1 \\ D^q x_2 \\ D^q x_3 \end{pmatrix} = \begin{pmatrix} -10 & 10 & 0 & 0 \\ 28 & -1 & 0 & 0 \\ 0 & 0 & 0 & 0 \end{pmatrix} \begin{pmatrix} x_1 \\ x_2 \\ x_3 \\ c_0 \end{pmatrix} + \begin{pmatrix} 0 \\ -x_1 x_3 \\ x_1 x_2 - c_0 x_3 \end{pmatrix}. \tag{29}$$

So

$$L = \begin{pmatrix} -10 & 10 & 0 & 0 \\ 28 & -1 & 0 & 0 \\ 0 & 0 & 0 & 0 \end{pmatrix}. \tag{30}$$

According to Section 2, the response system is given as

$$\begin{pmatrix} D^q y_1 \\ D^q y_2 \\ D^q y_3 \end{pmatrix} = \begin{pmatrix} -10 & 10 & 0 & 0 \\ 28 & -1 & 0 & 0 \\ 0 & 0 & 0 & 0 \end{pmatrix} \begin{pmatrix} y_1 \\ y_2 \\ y_3 \\ c \end{pmatrix} + \begin{pmatrix} 0 \\ -y_1 y_3 \\ y_1 y_2 - c y_3 \end{pmatrix} + \left(F - n_{lp}(x)\right) \begin{pmatrix} e_1 \\ e_2 \\ e_3 \\ e_c \end{pmatrix} \tag{31}$$

and the parameter update law is

$$D^q c = \Omega \begin{pmatrix} e_1 & e_2 & e_3 & e_c \end{pmatrix}^{\mathrm{T}}. \tag{32}$$

It is easy to obtain the following:

$$\begin{aligned} &\begin{pmatrix} 0 \\ -y_1 y_3 \\ y_1 y_2 - c y_3 \end{pmatrix} - \begin{pmatrix} 0 \\ -x_1 x_3 \\ x_1 x_2 - c_0 x_3 \end{pmatrix} \\ &= \begin{pmatrix} 0 & 0 & 0 & 0 \\ -x_3 & 0 & -x_1 & 0 \\ x_2 & x_1 & -c_0 & -x_3 \end{pmatrix} \begin{pmatrix} e_1 \\ e_2 \\ e_3 \\ e_c \end{pmatrix} \\ &+ \begin{pmatrix} 0 \\ -e_1 e_3 \\ e_1 e_2 - e_c e_3 \end{pmatrix}. \end{aligned} \tag{33}$$

So

$$\begin{aligned} n_{lp}(x) &= \begin{pmatrix} 0 & 0 & 0 & 0 \\ -x_3 & 0 & -x_1 & 0 \\ x_2 & x_1 & -c_0 & -x_3 \end{pmatrix}, \\ n_{np}(e, x) &= \begin{pmatrix} 0 \\ -e_1 e_3 \\ e_1 e_2 - e_c e_3 \end{pmatrix}. \end{aligned} \tag{34}$$

Now, it is easy to verify the following:

$$\begin{aligned} &\frac{\left\| \begin{pmatrix} n_{np}(e,x) \\ 0 \end{pmatrix} \right\|}{\|e\|} \\ &= \sqrt{\frac{(e_1 e_2 - e_c e_3)^2 + (e_1 e_3)^2}{e_1^2 + e_2^2 + e_3^2 + e_c^2}} \\ &\le \sqrt{\frac{(|e_1|\,|e_2| + |e_c|\,|e_3|)^2 + (e_1 e_3)^2}{e_1^2 + e_2^2 + e_3^2 + e_c^2}} \\ &= \left(\frac{2|e_1|\,|e_2|\,|e_3|\,|e_c|}{e_1^2 + e_2^2 + e_3^2 + e_c^2} + \frac{(e_c e_3)^2}{e_1^2 + e_2^2 + e_3^2 + e_c^2} + \frac{(e_1 e_2)^2 + (e_1 e_3)^2}{e_1^2 + e_2^2 + e_3^2 + e_c^2} \right)^{1/2} \\ &\le \sqrt{\frac{2|e_1|\,|e_2|\,|e_3|\,|e_c|}{e_1^2 + e_2^2 + e_3^2 + e_c^2} + \frac{(e_c e_3)^2}{e_c^2} + \frac{(e_1 e_2)^2 + (e_1 e_3)^2}{e_1^2}} \\ &= \sqrt{\frac{2|e_1|\,|e_2|\,|e_3|\,|e_c|}{e_1^2 + e_2^2 + e_3^2 + e_c^2} + 2e_3^2 + e_2^2} \\ &\le \sqrt{\frac{2|e_1|\,|e_2|\,|e_3|\,|e_c|}{2|e_1|\,|e_2| + 2|e_3|\,|e_c|} + 2e_3^2 + e_2^2} \\ &= \sqrt{\left(\frac{1}{|e_3|\,|e_c|} + \frac{1}{|e_1|\,|e_2|} \right)^{-1} + 2e_3^2 + e_2^2}, \\ &\lim_{e \to 0} \frac{\left\| \begin{pmatrix} n_{np}(e,x) \\ 0 \end{pmatrix} \right\|}{\|e\|} \\ &\le \lim_{e \to 0} \sqrt{\left(\frac{1}{|e_3|\,|e_c|} + \frac{1}{|e_1|\,|e_2|} \right)^{-1} + 2e_3^2 + e_2^2} = 0, \\ &\left. \begin{pmatrix} n_{np}(e,x) \\ 0 \end{pmatrix} \right|_{e=0} = 0. \end{aligned} \tag{35}$$

Therefore, the first condition in the above-mentioned theorem holds.

Now, choose suitable real constant matrix $\Omega \in R^{1\times n}$ and $F \in R^{n\times(n+1)}$ such that

$$\begin{aligned} &\mathrm{Re}\left[\lambda \begin{pmatrix} L + F \\ \Omega \end{pmatrix} \right] < 0, \\ &-\max\left[\mathrm{Re}\,\lambda \begin{pmatrix} L + F \\ \Omega \end{pmatrix} \right] > [\Gamma(q)]^{1/q}. \end{aligned} \tag{36}$$

So, the second condition in the above-mentioned theorem holds. According to the theoremin Section 2, the adaptive synchronization between drive system (29) and response system (31) with parameter update law (32) can be achieved.

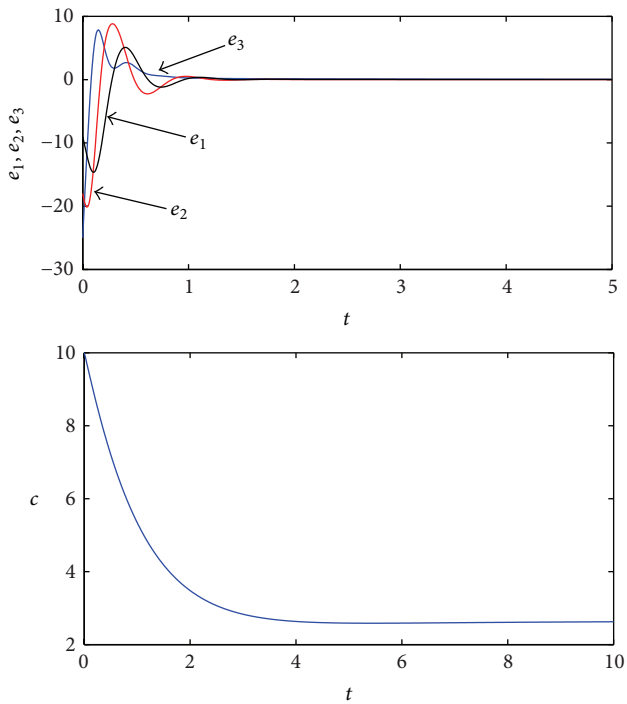

FIGURE 4: Simulation results of the adaptive synchronization for the fractional-order Lorenz chaotic system.

For example, let $F = \begin{pmatrix} 0 & 0 & 0 & 0 \\ -38 & 0 & 0 & 0 \\ 0 & 0 & -1 & 0 \end{pmatrix}$ and $\Omega = \begin{pmatrix} 0 & 0 & 0 & -1 \end{pmatrix}$. So $\begin{pmatrix} L+F \\ \Omega \end{pmatrix} = \begin{pmatrix} -10 & 10 & 0 & 0 \\ -10 & -1 & 0 & 0 \\ 0 & 0 & -1 & 0 \\ 0 & 0 & 0 & -1 \end{pmatrix}$. Therefore, $\lambda_i = -1$ $(i = 1, 2)$, $\lambda_{\pm} = -5.5 \pm 8.9303j$, and $-\max[\operatorname{Re}\lambda\begin{pmatrix} L+F \\ \Omega \end{pmatrix}] = 1 > [\Gamma(q)]^{1/q} = 0.9722$, respectively. Simulation results are shown in Figure 4. Here, $c(0) = 10$.

4. Conclusions

One adaptive synchronization scheme for a class of fractional-order chaotic system with fractional-order $1 < q < 2$ is suggested in this paper. This synchronization approach is based on a new stability result of equilibrium point in nonlinear fractional-order systems for fractional-order lying in $1 < q < 2$. In order to verify the effectiveness of the adaptive synchronization approach, the adaptive synchronization for the fractional-order Lorenz chaotic system with fractional-order $1 < q < 2$ is considered. Numerical simulations show the validity and feasibility of the proposed scheme. The current results in this paper can be extended to several unknown parameters of the fractional-order chaotic systems. Moreover, this synchronization approach can be applied to other fractional-order chaotic systems.

Conflict of Interests

The authors declare that there is no conflict of interests regarding the publication of this paper.

References

[1] L. Chen, Y. He, Y. Chai, and R. Wu, "New results on stability and stabilization of a class of nonlinear fractional-order systems," *Nonlinear Dynamics*, vol. 75, no. 4, pp. 633–641, 2014.

[2] R. Hilfer, *Applications of Fractional Calculus in Physics*, World Scientific, Singapore, 2000.

[3] M. Naber, "Time fractional Schrödinger equation," *Journal of Mathematical Physics*, vol. 45, no. 8, pp. 3339–3352, 2004.

[4] I. Grigorenko and E. Grigorenko, "Chaotic dynamics of the fractional Lorenz system," *Physical Review Letters*, vol. 91, Article ID 034101, 2003.

[5] P. Zhou, R. Ding, and Y. X. Cao, "Multi drive-one response synchronization for fractional-order chaotic systems," *Nonlinear Dynamics*, vol. 70, no. 2, pp. 1263–1271, 2012.

[6] Z. M. Ge and C. Y. Ou, "Chaos in a fractional order modified Duffing system," *Chaos, Solitons and Fractals*, vol. 34, no. 2, pp. 262–291, 2007.

[7] D. Cafagna and G. Grassi, "Hyperchaos in the fractional-order Roμssler system with lowest-order," *International Journal of Bifurcation and Chaos*, vol. 19, no. 1, pp. 339–347, 2009.

[8] P. Zhou and F. Yang, "Hyperchaos, chaos, and horseshoe in a 4D nonlinear system with an infinite number of equilibrium points," *Nonlinear Dynamics*, vol. 76, no. 1, pp. 473–480, 2014.

[9] J. C. Sprott, *Chaos and Time-Series Analysis*, Oxford University Press, Oxford, UK, 2003.

[10] G. R. Chen and X. Dong, "From chaos to order perspectives," in *Methodologies and Applications*, World scientific, Singapore, 1998.

[11] X. Y. Wang and J. M. Song, "Synchronization of the fractional order hyperchaos Lorenz systems with activation feedback control," *Communications in Nonlinear Science and Numerical Simulation*, vol. 14, no. 8, pp. 3351–3357, 2009.

[12] P. Zhou and W. Zhu, "Function projective synchronization for fractional-order chaotic systems," *Nonlinear Analysis: Real World Applications*, vol. 12, no. 2, pp. 811–816, 2011.

[13] R. Zhang and S. Yang, "Adaptive synchronization of fractional-order chaotic systems via a single driving variable," *Nonlinear Dynamics*, vol. 66, no. 4, pp. 831–837, 2011.

[14] L. L. Li and J. D. Cao, "Cluster synchronization in an array of coupled stochastic delayed neural networks via pinning control," *Neurocomputing*, vol. 74, no. 5, pp. 846–856, 2011.

[15] J. Q. Lu and J. D. Cao, "Adaptive synchronization in tree-like dynamical networks," *Nonlinear Analysis: Real World Applications*, vol. 8, no. 4, pp. 1252–1260, 2007.

[16] J. Q. Lu and J. D. Cao, "Adaptive synchronization of uncertain dynamical networks with delayed coupling," *Nonlinear Dynamics*, vol. 53, no. 1-2, pp. 107–115, 2008.

[17] F. Mainardi, "The fundamental solutions for the fractional diffusion-wave equation," *Applied Mathematics Letters*, vol. 9, no. 6, pp. 23–28, 1996.

[18] L. Beghin and E. Orsingher, "The telegraph process stopped at stable-distributed times and its connection with the fractional telegraph equation," *Fractional Calculus & Applied Analysis*, vol. 6, no. 2, pp. 187–204, 2003.

[19] W. Zhang, X. Cai, and S. Holm, "Time-fractional heat equations and negative absolute temperatures," *Computers & Mathematics with Applications*, vol. 67, no. 1, pp. 164–171, 2014.

Hindawi Publishing Corporation
The Scientific World Journal
Volume 2014, Article ID 713541, 8 pages
http://dx.doi.org/10.1155/2014/713541

Research Article

A Novel Chaotic Map and an Improved Chaos-Based Image Encryption Scheme

Xianhan Zhang[1] and Yang Cao[2,3]

[1] *Department of Mathematics, Southeast University, Nanjing 210096, China*
[2] *Department of Mechanical Engineering, The University of Hong Kong, Pokfulam, Hong Kong*
[3] *College of Telecommunications and Information Engineering, Nanjing University of Posts and Telecommunications, Nanjing 210003, China*

Correspondence should be addressed to Yang Cao; caoyeacy@hku.hk

Received 12 June 2014; Accepted 3 July 2014; Published 20 July 2014

Academic Editor: Qiankun Song

In this paper, we present a novel approach to create the new chaotic map and propose an improved image encryption scheme based on it. Compared with traditional classic one-dimensional chaotic maps like Logistic Map and Tent Map, this newly created chaotic map demonstrates many better chaotic properties for encryption, implied by a much larger maximal Lyapunov exponent. Furthermore, the new chaotic map and Arnold's Cat Map based image encryption method is designed and proved to be of solid robustness. The simulation results and security analysis indicate that such method not only can meet the requirement of imagine encryption, but also can result in a preferable effectiveness and security, which is usable for general applications.

1. Introduction

With the discovery of a series of chaotic maps such as Tent Map [1, 2] and Logistic Map [3], researchers and scholars have been able to apply them into a variety of fields. The knowledge of chaotic maps is perhaps one of the most significant achievements in nonlinear science. Since 1980s, researches on chaos theory have been overlapping and mixing up with other subjects, in the meanwhile promoting their further developments. The fields that take advantage of knowledge concerning chaos range greatly from math and astronomy to music and art. Besides, the most famous magazines in the world such as Nature and Scientific American once published a great deal of discoveries and progresses in chaos theory [4]. Therefore, it is reasonable to judge that chaos has been becoming a universal language between these important subjects.

If we are to further classify the applications of the chaos in different categories, chaos analysis [5] and chaos synthesis [6] will be the answer. As for the former, based on complex manual work and natural system, we tend to find some hidden rules inside of them. One example is the prediction towards time series [7–10]. For the latter, by using manually produced chaotic system, we are inclined to discover some possible functions contained within the chaotic dynamics [11–13].

In addition, some likely applications of the chaos are listed below. First, combining neural network and chaos, we utilize chaotic status of intermediate processes to let networks avoid the partial minimum point. And hence it guarantees global optimum according to [14]. Second, the chaos theory has already been used in high-speed searching process. Last but not least, chaotic maps are widely applied in secure communication which is carefully studied in [13, 15]. We could not only use chaotic signals to encrypt the information needed to be secure but also decipher encrypted one as well according to [16–18]. Also, researches regarding these aspects are known to have already been put in the national defense plan of China.

Despite the fact that the fields that call for chaotic maps range greatly, one thing they share in common is that they all need the chaotic features of chaotic maps. In other words, the feature that a simple initial point and a given value of the parameter could completely control the whole process is what we need. As a matter of fact, chaotic maps are quite sensitive to the initial point, which means even a very slight change in

the value of initial point would result in a dramatic change of the sequence produced by the chaotic map. However, at present, only a limited number of one-dimensional chaotic maps (e.g., Tent Map and Logistic Map) are introduced. Also, their properties are somehow limited and may no longer satisfy our needs. Too often our methods of encryption and engineering projects are merely based on these simple chaotic maps. Without new and better chaotic maps, our applications will remain unchanged and might get stuck in the future. This may lead to an urgent need for more and better chaotic maps.

In this paper, a new one-dimensional chaotic map is first introduced, and we use the maximal Lyapunov exponent [19–21] to determine how well the map performs. In addition, we later prove that this new chaotic map actually exhibits a larger maximal Lyapunov exponent, indicating better properties of the chaotic map. What is more is that a new algorithm based on this new chaotic map is used in image encryption, providing a brand new way to encrypt images. Compared with previous ways to encrypt image, it not only utilizes the excellent chaotic property of the newly discovered map itself but also entails another classical map: Arnold's Cat Map [22–24], through which coordinates of the target image's grey value matrix will be changed to another. Lastly, a security analysis is accomplished by plotting histogram of the image's grey values and calculating information entropy [25]. Without any knowledge as to how many times the target image is iterated, it is next to impossible to decrypt the encrypted image. Therefore, the safety of the image is largely strengthened and guaranteed. Now we discuss this new chaotic map and how to use it to encrypt images in detail in the following.

2. Design and Analysis to the New Chaotic Map

In this section, we first discuss the definition of "maximal Lyapunov exponent." Then, we plot the Lyapunov spectrum of the two traditional one-dimensional chaotic maps. Next, a new chaotic map is introduced. Lastly, a comparison between the new chaotic map and two traditional maps is carefully made.

2.1. Maximal Lyapunov Exponent

2.1.1. Definition of the Lyapunov Exponent. According to statements in [19, 26], Lyapunov exponent λ usually represents the features of a chaotic system, named after the great Russian mathematician Lyapunov.

For discrete system (maps or fixed point iterations) $x_n = f(x_{n-1})$ and for an orbit starting with x_0, the Lyapunov exponent can be defined as follows:

$$\lambda(x_0) = \lim_{n\to\infty} \frac{1}{n} \sum_{i=1}^{\infty} \ln \left| f'(x_i) \right|. \quad (1)$$

It is common to refer to the largest λ defined by (1) as the maximal Lyapunov exponent because it determines a notion of predictability for a chaotic system.

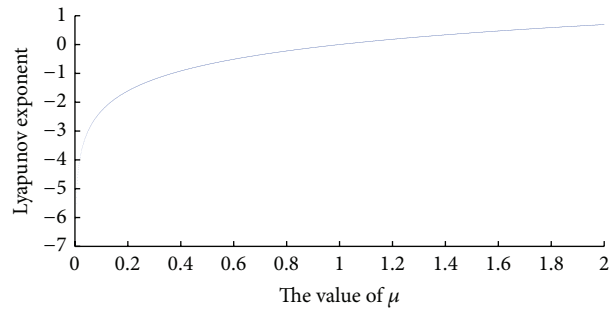

Figure 1: Lyapunov exponent spectrum of Tent Map.

2.1.2. Properties of Maximal Lyapunov Exponent (MLE). A positive λ is usually taken as an indication that the system is basically chaotic. Besides, it is also apparently true that the larger MLE is, the more chaotic the map is. And this means a better chaotic map according to [20].

Remark 1. Lyapunov exponent, as an important exponent to test the property of chaotic map, is widely used in the world of chaos. Actually, from the definition equation (1), we could clearly find out that Lyapunov is an average value of $\ln|f'(x)|$. Since $|f'(x)|$ is the indicating parameter that measures the variation speed for $f(x)$, Lyapunov exponent, the average value of $\ln|f'(x)|$ is bound to reflect the chaotic properties of $f(x)$. Thus, maximal Lyapunov exponent can largely expresses the overall performance of chaotic maps.

Next, we begin with calculating the MLE and plotting the Lyapunov exponent spectrum for two typical one-dimensional maps, Tent Map and Logistic Map.

2.2. Tent Map. In mathematics, according to [1], Tent Map with parameter μ is a real-valued function $f(\mu)$ defined by

$$f(\mu) = \mu \min\{x, 1-x\}; \quad \mu \in (0,2). \quad (2)$$

Thus, we can obtain the Lyapunov exponent spectrum of Tent Map, which is shown in Figure 1.

In addition, we could calculate the MLE for Tent Map, which is 0.6931 (when $\mu \to 2$), indicating that the map itself is chaotic.

2.3. Logistic Map. Logistic Map [27, 28] is a polynomial mapping of degree 2 that exhibits chaotic behavior. The Logistic Map equation is given by

$$x_{n+1} = \mu x_n (1 - x_n). \quad (3)$$

When the variable μ is given different value, ranging from 2 to 4, through formula (1), we could plot Lyapunov exponent of Logistic Map as well. That is shown in Figure 2.

It is obviously shown in Figure 2 that, when $\mu \to 4$, MLE of Tent Map is reached. Through calculating, maximal Lyapunov exponent of the Logistic Map is 0.6785.

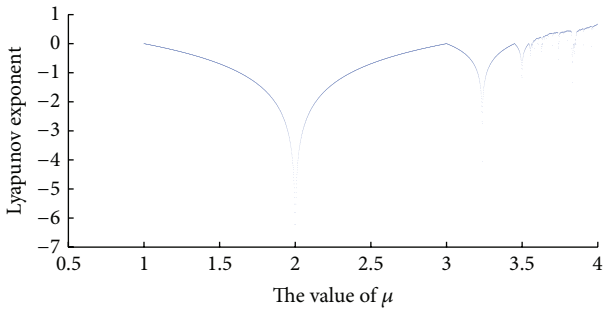

Figure 2: Lyapunov exponent spectrum of Logistic Map.

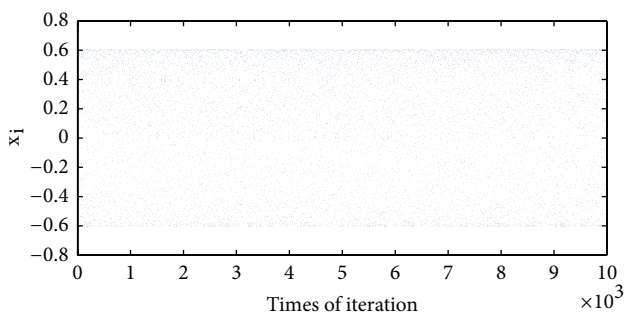

Figure 3: Scattered 10000 points gained from the new chaotic map.

2.4. A New Chaotic Map. When we replace "x" with "$1-2|x|$" in Logistic Map, formula (4) will be attained:

$$x_{n+1} = 2\mu\left|x_n\right|\left(1-2\left|x_n\right|\right); \quad \left(-1 < x_n < 1\right). \tag{4}$$

If we choose $x_0 = 0.4$ as the initial point of the map and the parameter $\mu = 2.4140$, after 10000 times of iterations, we will get the randomly scattered image of the map in Figure 3 when we plot every x_i $(i = 1, 2, \ldots)$.

Remark 2. It is clearly displayed in Figure 3 that the sequence generated from the new chaotic map ranges from -0.6 to 0.6, while, in Tent Map and Logistic map, it is a little larger, ranging from -1 to 1. However, this does not matter that much, since we consider the range that they share in common, which is $-0.6 < x_n < 0.6$.

In order to see if the map is a chaotic map and, if yes, how good the map is, similarly, we also use the maximal Lyapunov exponent to see that, starting with $x_0 = 0.4$ and iterating 2000 times. Hence, Figure 4 will be yielded.

As is shown in Figure 4, when $\mu = 2.4140$, the MLE of the new chaotic map reaches beyond 1, to be exact, 1.0742.

Next, we combine the three Lyapunov exponent spectrums given above together and Figure 5 is the result.

Remark 3. Just like what we have discussed in Section 2.1, a larger maximal Lyapunov exponent indicates not only a stronger sensitivity to the initial point but also it also indicates that the chaotic system itself is "more chaotic." In other words, the chaotic map with larger MLE is of better quality. It is demonstrated above that the MLE of the two most typical chaotic maps (2) and (3) all end below 1, which are apparently

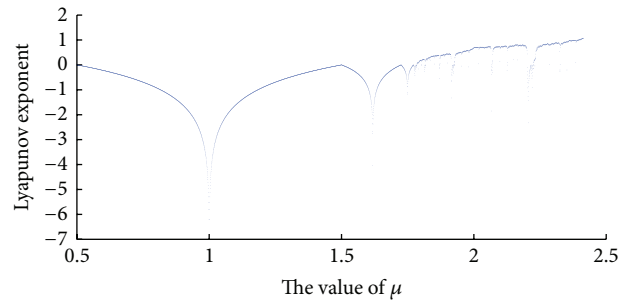

Figure 4: Lyapunov exponent spectrum of the new map.

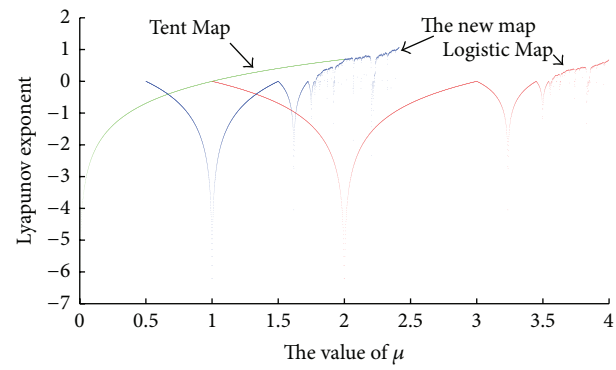

Figure 5: Lyapunov exponent spectrum comparison with three chaotic maps.

smaller than the new map (4). The MLE of the new chaotic map, as expected, has reached beyond 1. Therefore, the new map (4) is supposed to bear the potential to perform more effectively in engineering or encryption process than the two classic ones (2) and (3) mentioned above.

3. Application on Image Encryption

3.1. Encryption Scheme. In this section, we are about to take one step further, applying the new map on image encryption.

Now, we begin introducing an image encryption algorithm based on the map we have just constructed.

Step 1. For given initial point x_0 and the parameter μ, we could simply use the new map (4) to produce a sequence $m_k \in (-0.6, 0.6)$ $(k = 1, 2, \ldots)$. Consider

$$m_{n+1} = 2\mu\left|m_n\right|\left(1-2\left|m_n\right|\right) \quad \left(-0.6 < m_n < 0.6\right). \tag{5}$$

Then, in order to make $|x_k|$ reach closely 1, we choose $x_k = (5/3)m_k$; $(k = 1, 2, \ldots)$.

Step 2. Next, we transform decimal numbers x_k to the form of binary numbers, and consequently we will get x'_k. After that, we choose the first 8 figures after the decimal point of x'_k to form a new binary number, B_k.

To put in the language of math, that is:

$$x'_k = \sum_{v=0}^{\infty} a_{k,v} 2^{-(v+1)}; \quad a_{k,v} = 0 \text{ or } 1.$$

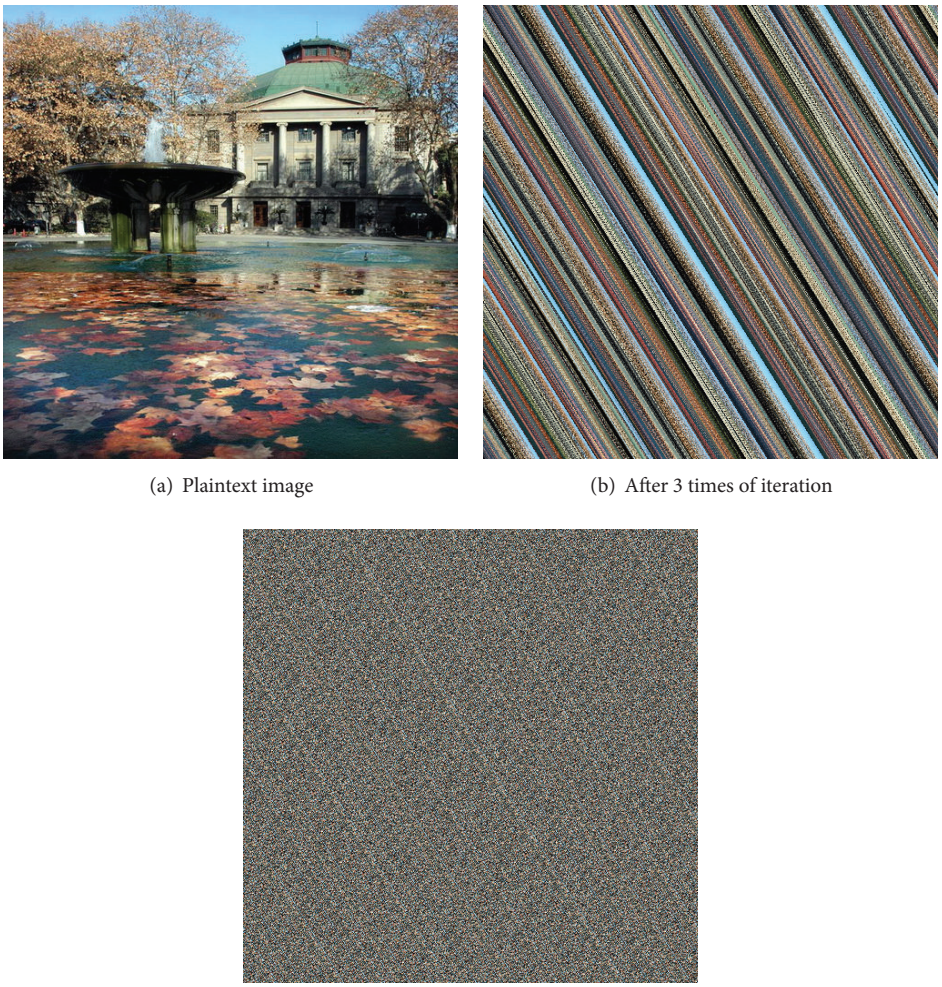

(a) Plaintext image

(b) After 3 times of iteration

(c) After 6 times of iteration

Figure 6: Sample experiment based on Arnold's Cat Map.

$$x'_k = \sum_{v=0}^{7} a_{k,v} 2^{-(v+1)} = 2^{-8} \sum_{0}^{7} a_{k,v} 2^{7-v} = 2^{-8} B_{k;}$$
$$B_k = a_{k,v} 2^{7-v}. \tag{6}$$

Thus, for each x_k, there is a unique B_k corresponding to it. Obviously, B_k is formed by the first 8 numbers after the decimal point of x'_k. In this way, we could obtain the original chaotic sequence in the form of binary numbers with 8 places. Similar approaches have been discussed in [29].

Remark 4. Binary numbers with 8 places have three major advantages that are listed below. First of all, it corresponds well with (R, G, B), which is the gray values' row vector of each point in an image. R refers to red, G refers to green, and B refers to blue. In fact, they all range from 0 to 255. And, hence, if they are written into binary forms, 8-place binary numbers will be exactly what we get. Therefore this step provides convenience to the following steps. Secondly, computers have always been using binary numbers to operate. Thus binary numbers tend to make calculation efficient and time-saving. Thirdly, as per what we have discussed in Section 2.1, the sequence generated by the chaotic map is basically random and therefore this will lead the binary numbers to be random as well due to the transmission of randomness.

Step 3. Suppose that the pixel of the target image is $m \times n$, and then we put B_k produced in Step 1 into a matrix AA with the size $m \times n$. In other words, from left to right and from up to down, each B_k is assigned to a unique, particular position in matrix AA.

Step 4. For point (i, j) from the plaintext image we have its grey value vector (R, G, B) written in binary form. In order to build a connection between the grey value matrix of the plaintext image and the chaotic sequence matrix AA, it is reasonable to think of the XOR operation ($\oplus$), the definition of which is given below in accordance with [30]:

$$\begin{aligned} 1 \oplus 0 &= 1; \qquad 1 \oplus 1 = 0. \\ 0 \oplus 0 &= 0; \qquad 0 \oplus 1 = 1. \end{aligned} \tag{7}$$

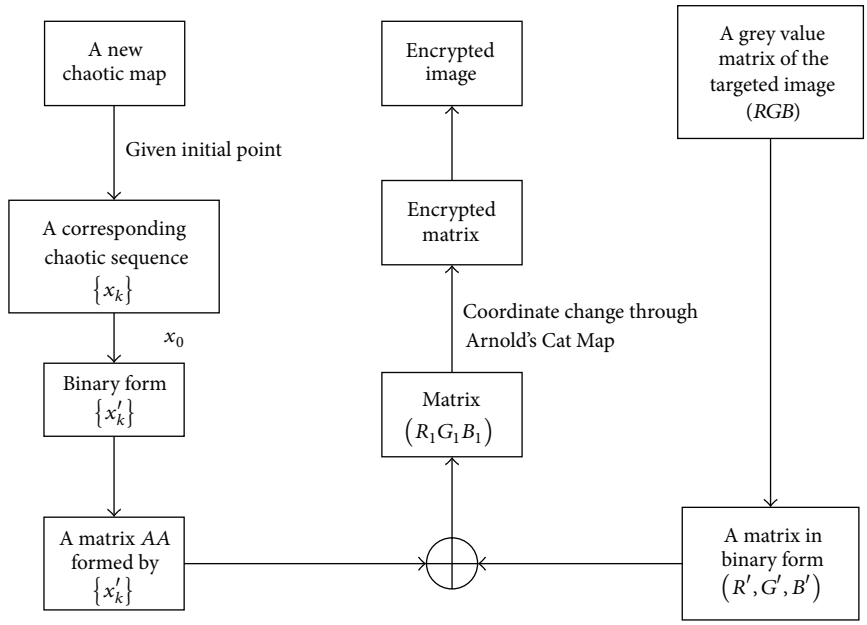

Figure 7: Proposed encryption scheme.

Thus, we use XOR to "make a mess." For point (i, j) from the plaintext image, we also extract $\mathrm{AA}(i, j)$ from AA, which is made up with the chaotic sequence generated. Next, we do XOR operation as follows:

$$\begin{aligned} R_1 &= R \oplus \mathrm{AA}(i, j). \\ G_1 &= G \oplus \mathrm{AA}(i, j). \\ B_1 &= B \oplus \mathrm{AA}(i, j). \end{aligned} \tag{8}$$

Step 5. In Step 6, we make a change to the coordinate of (i, j). To be exact, let $\binom{i}{j}$ be the starting column vector, which is $\binom{X_0}{Y_0}$, and then iterate a given "k" times with formula (9) according to [23, 24]

$$\begin{pmatrix} X_{n+1} \\ Y_{n+1} \end{pmatrix} = \begin{pmatrix} a & b \\ c & d \end{pmatrix} \begin{pmatrix} X_n \\ Y_n \end{pmatrix} \bmod m, \quad (ad - bc = 1). \tag{9}$$

After iteration of a given "k" times, we will obtain a new coordinate for point (i, j) in the plaintext image, and we mark it as (i', j'). This is one of the most famous coordinate change maps, the Arnold's Cat Map. Lastly, we assign the value of (R_1, G_1, B_1) from (i, j) to (i', j'). (Tips: "mod" in the formula means complementation, if the plaintext image is of the size $x_a \times y_a$ (the pixel value); $m = \max\{x_a, y_a\}$.) A sample experiment has been provided in Figure 6.

Remark 5. There exists actually a slight defect of Step 5, due to the fact that, after a special number of iteration times, the image could simply be restored as in the beginning according to [22]. As Arnold's Cat Map is defined, it is a periodic map, and this property leads to an unsafe encryption. Therefore, it is very significant to choose a proper value of "k," the number of times of iterations to prevent the image from being restored.

Remark 6. Along with defects, there are also huge advantages. First, only a few times of iteration are enough to guarantee the thorough change of the picture. Without knowing the times of iteration, it takes next to forever to decipher the image, as you could see as follows. Second, "mod" guarantees that the size of the image will be exactly the same if the picture is square-sized. Lastly, there is no denial that it is easy to recover the original image using some fundamental knowledge from algebra. Elaborate discussion will be in Section 3.2.

Step 6. Repeat Steps 3–5 for every point in the target plaintext image, and use these processed grey values to form an encrypted image.

3.2. Decryption Scheme

Step 1. Read the encrypted image, and then write its grey value into a three-dimensional matrix.

Step 2. According to Step 6 in encryption, we could simply do the opposite: start with (i', j') in the encrypted image, use the formula listed below, and iterate "k" times as well:

$$\begin{pmatrix} X_{n+1} \\ Y_{n+1} \end{pmatrix} = \frac{1}{ad - bc} \begin{pmatrix} d & -b \\ -c & a \end{pmatrix} \begin{pmatrix} X_n \\ Y_n \end{pmatrix} \bmod m \quad (ad - bc = 1). \tag{10}$$

(a) Plaintext image (b) Ciphered image

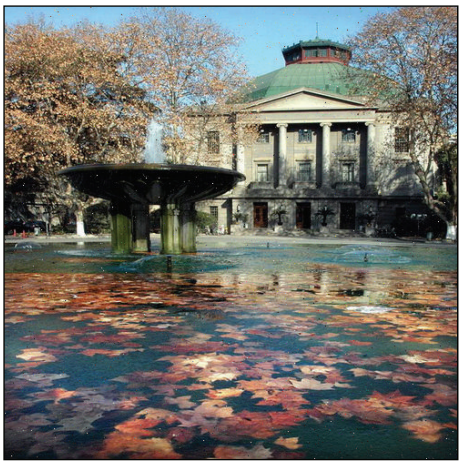

(c) Restored image

Figure 8: Simulation results.

The definition of "m" is the same as the one mentioned above, and thus we attain the original coordinate of (i, j).

Step 3. See Steps 1 and 2 in the encryption part.

Step 4. In order to restore changes from Step 5, just do XOR operation with (R_1, G_1, B_1) in points (i, j) and $\mathrm{AA}(i, j)$ again. Hence, (R, G, B) is obtained. That is,

$$\begin{aligned} R &= R_1 \oplus \mathrm{AA}(i, j). \\ G &= G_1 \oplus \mathrm{AA}(i, j). \\ B &= B_1 \oplus \mathrm{AA}(i, j). \end{aligned} \tag{11}$$

Step 5. Use (R, G, B) of every point to form the original image. Hence, restoration of the plaintext image is accomplished.

3.3. Overall Process of Image Encryption. Statements mentioned above yield the encryption scheme listed in Figure 7.

3.4. Simulation Results. Take the image of Figure 8(a) as a sample to test the algorithm mentioned above and the plaintext image, encrypted image, and restored image are given in Figure 8.

4. Security Analysis

In this section, by plotting the histogram and calculating the so-called "information entropy," we test the security qualities of the proposed method in Section 2.

4.1. Histogram Analysis. There is no denying that a well-ciphered image should provide no chances for the attackers to decrypt through statistics analysis. On the one hand, the grey level of the plaintext image in Figure 8(a) is somehow similar to normal distribution in accordance with Figure 9(a) and this would bring about vulnerabilities to decryption. On the other hand, the ciphered image in Figure 8(b), though not perfectly average on each value between 1 and 256, is somehow subjected to uniform distribution according to Figure 9(b), which undoubtedly adds up difficulty for the attacker to decrypt according to [16].

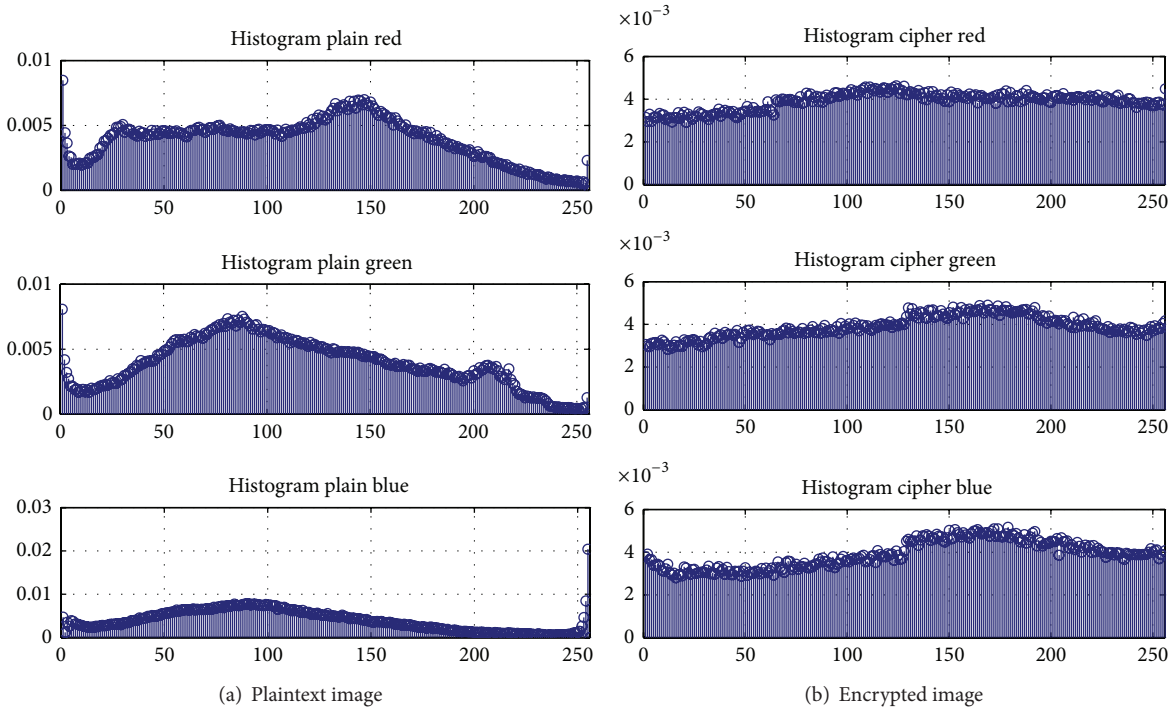

Figure 9: Histogram analysis results.

4.2. Information Entropy. According to the thesis in [25], the value of information entropy typically expresses the feature of randomness. Its definition is given by

$$H(m) = -\sum p(m_i) \log_2 \frac{1}{p(m_i)}, \tag{12}$$

where "m" refers to message and $p(m_i)$ represents the chances of appearance of the ith message. As for images, $p(m_i)$ stands for the probability of a particular grey value (R, G, B). Under this circumstance, $H(m)$ is also called "image entropy." The entropy of a perfectly encrypted image should, in ideal case, approach 24, since $3 \times \log_2 256 = 24$ (3 means 3 color planes) according to [14, 31]. The entropy $H(m) = 23.9616$ is yielded through calculating, which is extremely close to 24. Therefore it can be inferred that the encrypted image is almost random. In this way, we tend to believe that the safety of the image is largely promoted and ensured.

Remark 7. As the result of the entropy shows, $H(m)$ is perfectly close to 24, which is an ideal entropy for a randomly encrypted image. And this result in turn proves the excellent chaotic properties of the new chaotic map. What is more is that the comparison between the histograms of the plaintext image and the encrypted image shows that the new chaotic map actually makes grey values distribute uniformly, which convinces us of the fact the new chaotic map is of robust quality.

5. Conclusion

In this paper, a new chaotic map with better chaotic properties has been proposed. To step further, a comparison with traditional one-dimensional chaotic maps has been made as well through their maximal Lyapunov exponent spectrums, which proves the new chaotic map's marvelous application prospect. In addition, it has been applied on image encryption. Along with Arnold's Cat Map, it could successfully produce a ciphered image based on original plaintext image. Steps and the proposed scheme to encrypt a targeted image and decrypt a ciphered image have been given. What is more is that the results of encryption and decryption simulation have been provided. At last, security reliability towards this algorithm has been discussed. As a result, this method is of excellent quality and robustness and turns to be theoretical unbreakable by convention attacks without any knowledge to the values of the starting point and parameters. Yet, to seek perfectness, a safe conveyance of the parameter still remains to be a problem. That is, when the attacker gains the parameter value and initial point value, a whole system can break down easily. Thus a safe transmission of keys may be our next direction to study.

Conflict of Interests

The authors declare that there is no conflict of interests regarding the publication of this paper.

References

[1] T. Yoshida, H. Mori, and H. Shigematsu, "Analytic study of chaos of the tent map: band structures, power spectra, and critical behaviors," *Journal of Statistical Physics*, vol. 31, no. 2, pp. 279–308, 1983.

[2] L. Shan, H. Qiang, J. Li, and Z. Wang, "Chaotic optimization algorithm based on Tent map," *Control and Decision*, vol. 20, no. 2, pp. 179–182, 2005.

[3] L. Kocarev and G. Jakimoski, "Logistic map as a block encryption algorithm," *Physics Letters A*, vol. 289, no. 4-5, pp. 199–206, 2001.

[4] M. Gutzwiller, "Quantum chaos," *Scientific American*, vol. 266, pp. 26–32, 1992.

[5] C. Chang-Jian and C. Chen, "Bifurcation and chaos analysis of a flexible rotor supported by turbulent long journal bearings," *Chaos, Solitons and Fractals*, vol. 34, no. 4, pp. 1160–1179, 2007.

[6] I. Zelinka, G. Chen, and S. Celikovsky, "Chaos synthesis by evolutionary algorithms," in *Evolutionary Algorithms and Chaotic Systems*, pp. 345–382, Springer, 2010.

[7] J. Zhang and X. Xiao, "Predicting chaotic time series using recurrent neural network," *Chinese Physics Letters*, vol. 17, no. 2, pp. 88–90, 2000.

[8] M. Han, J. Xi, S. Xu, and F. Yin, "Prediction of chaotic time series based on the recurrent predictor neural network," *IEEE Transactions on Signal Processing*, vol. 52, no. 12, pp. 3409–3416, 2004.

[9] M. Ye and X. Wang, "Chaotic time series prediction using least squares support vector machines," *Chinese Physics*, vol. 13, no. 4, pp. 454–458, 2004.

[10] D. S. K. Karunasinghe and S. Liong, "Chaotic time series prediction with a global model: artificial neural network," *Journal of Hydrology*, vol. 323, no. 1–4, pp. 92–105, 2006.

[11] W. Zhang, "Global and chaotic dynamics for a parametrically excited thin plate," *Journal of Sound and Vibration*, vol. 239, no. 5, pp. 1013–1036, 2001.

[12] J. G. Lu, "Chaotic dynamics and synchronization of fractional-order Arneodo's systems," *Chaos, Solitons and Fractals*, vol. 26, no. 4, pp. 1125–1133, 2005.

[13] O. M. Kwon, J. H. Park, and S. M. Lee, "Secure communication based on chaotic synchronization via interval time-varying delay feedback control," *Nonlinear Dynamics*, vol. 63, no. 1-2, pp. 239–252, 2011.

[14] D. Yang, G. Li, and G. Cheng, "On the efficiency of chaos optimization algorithms for global optimization," *Chaos, Solitons and Fractals*, vol. 34, no. 4, pp. 1366–1375, 2007.

[15] R. Luo and Y. Wang, "Finite-time stochastic combination synchronization of three different chaotic systems and its application in secure communication," *Chaos*, vol. 22, no. 2, Article ID 023109, 2012.

[16] Y. Cao, "A new hybrid chaotic map and its application on image encryption and hiding," *Mathematical Problems in Engineering*, vol. 2013, Article ID 728375, 13 pages, 2013.

[17] J. Guo, Z. Lü, and L. Zhang, "Breaking a chaotic encryption based on henon map," in *Proceedings of the 3rd International Symposium on IEEE Information Processing (ISIP '10)*, pp. 169–171, Qingdao, China, October 2010.

[18] M. Naeemabadi, N. Chomachar, M. Zabihi, B. S. Ordoubadi, M. Khalilzadeh, and M. S. Ordoubadi, "Encryption based on variable chaotic key for wireless medical data transmission," in *Proceedings of the 5th International Conference on Application of Information and Communication Technologies (AICT '11)*, pp. 1–5, IEEE, 2011.

[19] M. T. Rosenstein, J. J. Collins, and C. J. de Luca, "A practical method for calculating largest Lyapunov exponents from small data sets," *Physica D: Nonlinear Phenomena*, vol. 65, no. 1-2, pp. 117–134, 1993.

[20] H. Kantz, "A robust method to estimate the maximal Lyapunov exponent of a time series," *Physics Letters A*, vol. 185, no. 1, pp. 77–87, 1994.

[21] M. Setare and D. Momeni, "Geodesic stability for Kehagias-Sfetsos black hole in Hořava-lifshitz gravity via Lyapunov exponents," *International Journal of Theoretical Physics*, vol. 50, pp. 106–113, 2011.

[22] F. Faure, S. Nonnenmacher, and S. de Bièvre, "Scarred eigenstates for quantum cat maps of minimal periods," *Communications in Mathematical Physics*, vol. 239, no. 3, pp. 449–492, 2003.

[23] L. Zhang, X. Liao, and X. Wang, "An image encryption approach based on chaotic maps," *Chaos, Solitons & Fractals*, vol. 24, no. 3, pp. 759–765, 2005.

[24] C. Çokal and E. Solak, "Cryptanalysis of a chaos-based image encryption algorithm," *Physics Letters. A*, vol. 373, no. 15, pp. 1357–1360, 2009.

[25] S. M. Pincus, "Approximate entropy as a measure of system complexity," *Proceedings of the National Academy of Sciences of the United States of America*, vol. 88, no. 6, pp. 2297–2301, 1991.

[26] A. Wolf, J. B. Swift, H. L. Swinney, and J. A. Vastano, "Determining Lyapunov exponents from a time series," *Physica D: Nonlinear Phenomena*, vol. 16, no. 3, pp. 285–317, 1985.

[27] E. A. Jackson and A. Hübler, "Periodic entrainment of chaotic logistic map dynamics," *Physica D: Nonlinear Phenomena*, vol. 44, no. 3, pp. 407–420, 1990.

[28] S. C. Phatak and S. S. Rao, "Logistic map: a possible random-number generator," *Physical Review E*, vol. 51, no. 4, pp. 3670–3678, 1995.

[29] L. M. Leibowitz, "A simplified binary arithmetic for the Fermat number transform," *IEEE Transactions on Acoustics, Speech, and Signal Processing*, vol. 24, no. 5, pp. 356–359, 1976.

[30] J.-W. Han, C.-S. Park, D.-H. Ryu, and E.-S. Kim, "Optical image encryption based on XOR operations," *Optical Engineering*, vol. 38, no. 1, pp. 47–54, 1999.

[31] W. Yu and J. Cao, "Cryptography based on delayed chaotic neural networks," *Physics Letters A: General, Atomic and Solid State Physics*, vol. 356, no. 4-5, pp. 333–338, 2006.